

**DISSERTATION**

**IN VIVO AND IN VITRO**

**CHARACTERISATION OF MAP1S FUNCTION**

angestrebter akademischer Titel:  
Doktorin der Naturwissenschaften (Dr. rer. nat)

Verfasserin: Mag. Ilse Kalny  
Matrikelnummer: 9700130  
Dissertationsgebiet: A 091 441, Genetik-Mikrobiologie  
Betreuer: Univ. Prof. Friedrich Propst



## Acknowledgements

At this place I would like to thank all who supported me during my PhD studies and contributed to this work.

This work was financed by the FWF, Wings of life, and the University of Vienna.

Special thanks go to Univ. Prof. Dr. Friedrich Propst for giving me the opportunity to carry out my PhD work in his group, for his supervision, support, and critical discussions.

Thanks go to Arabella, Jazek and Christian for helping me with generating mice, and to Irmi and Univ. Prof. Dr. Hans Lassmann for histological analysis. I am also grateful to Gerlinde and Elisabeth for being always helpful.

Many thanks go to all now and former colleagues from the Department of Molecular Cell Biology, especially to my lab colleagues Alzbeta, Doro, Waltraud, Ewa and Luise (in order of appearance) for creating an excellent working atmosphere and for many productive discussions about science and beyond.

I am grateful to all members of "BPWMCA" and the "girls club" for their friendship and all the fun we had!

Thanks to all my friends and former working colleagues Sigrid, Ulli, Irene B, Irene L, Gerlinde, Andi, Chantal, Birgit and Sibylle for their friendship, (scientific) discussions and support.

I would also like to thank my family who taught me to believe in myself.

Finally, I wish to thank my partner, Franz, for supporting me in every possible way, for always encouraging me, for his understanding and love.



# Table of contents

Table of contents.....	5
List of figures and tables .....	7
ABSTRACT .....	9
ZUSAMMENFASSUNG .....	11
INTRODUCTION.....	13
THE CYTOSKELETON .....	13
Intermediate filaments.....	13
Actin filaments.....	15
Microtubules.....	17
MICROTUBULE ASSOCIATED PROTEINS .....	19
MAP1 family proteins .....	20
MAP1A and MAP1B.....	21
MAP1B Gene Targeting studies.....	24
The role of MAP1B in human diseases .....	27
MAP1S.....	29
Putative functions of MAP1S.....	30
AIMS OF THE THESIS.....	34
PART I – POSTTRANSLATIONAL MODIFICATIONS OF MAP1S IN	
COMPARISON TO MAP1A AND MAP1B .....	35
RESULTS.....	36
Homotypic and heterotypic complexes of MAP1 proteins.....	36
The potential S-nitrosylation of MAP1S and its influence on microtubule binding compared to other MAP1 proteins.....	41
The influence of S-nitrosylation on the formation of an additional LC isoform .....	48
Posttranslational cleavage of MAP1S.....	50
The influence of S-nitrosylation on the posttranslational cleavage of MAP1S .....	53
N-ε-acetylation of MAP1 proteins .....	54
DISCUSSION.....	56
Homotypic and heterotypic complexes of MAP1 proteins.....	56
The potential S-nitrosylation of MAP1S and its influence on microtubule binding compared to other MAP1 proteins.....	57
The influence of S-nitrosylation on the formation of an additional LC isoform .....	59
The influence of nNOS activity on posttranslational cleavage of MAP1S .....	61
N-ε-acetylation of MAP1 proteins .....	62
PART II – GENERATION AND FIRST ANALYSIS OF MAP1S KNOCKOUT	
MICE .....	64
RESULTS.....	65
The conditional knockout strategy .....	65
Generation of conditional MAP1S knockout mice.....	67

General examination of homozygous knockout mice .....	73
Histological analysis.....	74
The expression pattern of MAP1A and MAP1B in the brain of MAP1S knockout mice .....	77
MAP1S knockout DRGNs .....	78
MAP1S knockout Schwann cells.....	80
MAP1S knockout fibroblasts .....	81
Cellcycle phase distribution in MAP1S knockout fibroblasts .....	82
Cell migration in MAP1S knockout fibroblasts.....	83
DISCUSSION .....	88
General examination and histological analysis of MAP1S knockout mice.....	88
MAP1S knockout DRGNs and Schwann cells .....	91
Cell cycle phase distribution in MAP1S knockout fibroblasts .....	92
Cell migration in MAP1S knockout fibroblasts.....	94
MATERIALS AND METHODS.....	99
Commonly used buffers.....	99
DNA METHODS .....	99
DNA manipulation and preparation .....	99
Agarose gel .....	99
Preparation of rubidium chloride competent bacteria and transformation	100
Isolation of genomic DNA from cells and mouse tails.....	100
Polymerase chain reaction (PCR) .....	101
Southern Blot analysis.....	102
Cloning of the MAP1S conditional knockout targeting vector .....	103
PROTEIN METHODS .....	104
Preparation of cell extracts.....	104
Preparation of tissue extracts .....	105
Purification of microtubule proteins .....	105
Determination of protein concentration.....	106
Pulse-chase labeling of adherent cells with <sup>35</sup> S methionine and <sup>35</sup> S cysteine .....	106
Immunoblotting.....	107
Co-Immunoprecipitation .....	107
Blot overlay assay .....	108
CELL CULTURE, IMMUNOFLUORESCENCE MICROSCOPY .....	108
Maintenance of cell lines .....	108
Transfection of mammalian cells using FuGENE6 .....	109
Activation and inhibition of nitrosylation in cultured cells .....	110
Immunofluorescence microscopy of cells.....	110
Isolation and cultivation of dissociated adult DRG neurons.....	111
Isolation and cultivation of adult Schwann cells.....	112
Isolation and cultivation of adult fibroblasts .....	113
In vitro wound healing assay .....	113
Maintenance of embryonic stem (ES) cells .....	114
Electroporation of ES cells with targeting vector .....	114
Blastocyst injection of ES cells .....	115
ANIMALS .....	115
Generation and maintenance of MAP1S (conditional) knockout mice.....	115
ANTIBODIES .....	116

References.....	118
CURRICULUM VITAE.....	131

## List of figures and tables

Figure 1. Organisation of the cytoskeleton in polarised epithelial cells that line the small intestine (© Garland Science 2008, Alberts B., 2008).....	14
Figure 2. MAP1B HC co-immunoprecipitated with the MAP1A LC.....	36
Figure 3. MAP1A LC co-immunoprecipitated with the MAP1B HC.....	37
Figure 4. Schematic representation of MAP1 proteins.....	38
Figure 5. MAP1S LC forms a complex with the MH1 domain of MAP1B HC. ...	39
Figure 6. MAP1S LC interacts with the MH3 domain of MAP1B LC.....	40
Figure 7. Interaction of MAP1S LC with MAP1B LC.....	41
Figure 8. Sequence alignment of MAP1B, MAP1A and MAP1S LCs.....	42
Figure 9. Interaction of MAP1B LC and MAP1S LC with the PDZ domain of nNOS.....	43
Figure 10. MAP1S LC was not found to bind to nNOS in vivo. ....	44
Figure 11. Localisation of the LCs of MAP1B, MAP1A, and MAP1S on microtubules after treatment with the NO donor SNAP.....	45
Figure 12. Binding of MAP1B FL, MAP1S FL, and an uncleavable MAP1B FL mutant to microtubules after treatment with the NO donor SNAP.....	46
Figure 13. Binding to and bundling of microtubules by MAP1S after treatment with the NO donor SNAP. ....	47
Figure 14. An additional MAP1B LC isoform was detected in immunoblotting analysis of protein lysates of brain and neuroblastoma (N2a) cells under non-reducing conditions.....	48
Figure 15. Both cysteines of MAP1B LC and the activity of nNOS were necessary to form an additional MAP1B LC isoform. ....	49
Figure 16. Tissue specific cleavage pattern of MAP1S.....	51
Figure 17. MAP1 proteins including MAP1S are conserved around the presumptive cleavage site of the precursor protein.....	51
Figure 18. Cleavage pattern of MAP1S in different cell lines. ....	52
Figure 19. Cleavage pattern of endogenous MAP1S in N2a cells after treatment with the protein synthesis inhibitor cycloheximide.....	53
Figure 20. N- $\omega$ -propyl-L-arginine (NPA) did not influence the cleavage pattern of MAP1S.....	54
Figure 21. MAP1B LC was acetylated.....	55
Figure 22. A model for the formation of the faster migrating MAP1B LC isoform. ....	60
Figure 23. Schematic representation of the strategy to generate conditional MAP1S knockout mice.....	66
Figure 24. MAP1S expression in mouse tissues of strains C57BL/6J and 129.67	
Figure 25. Targeting the MAP1S locus. ....	68
Figure 26. Southern blot analysis using the neo probe revealed an additional band, which disappeared after back crossing. ....	70
Figure 27. PCR strategy to identify targeted MAP1S alleles.....	72

Figure 28. Immunoblot analysis of the expression of MAP1S in wild-type and MAP1S knockout mice. ....	74
Figure 29. Histological analysis of the brain did not show any differences between wild-type and MAP1S knockout mice. ....	75
Figure 30. Histological analysis of the testis did not reveal any differences between wild-type and MAP1S knockout mice. ....	76
Figure 31. Histological analysis of the liver showed disturbed organisation of small blood vessels or bile ducts in one MAP1S knockout mouse. ....	76
Figure 32. The expression pattern of the MAP1A light chain was not altered in the brain of MAP1S knockout mice. ....	77
Figure 33. The expression pattern of the MAP1B light chain was not altered in the brain of MAP1S knockout mice. ....	78
Figure 34. DRGNs from MAP1S knockout mice displayed a shift towards cells with more than one axon. ....	79
Figure 35. Schwann cells of MAP1S knockout mice did not differ in the number of protrusions. ....	80
Figure 36. Immunoblot analysis of the expression of MAP1S in fibroblasts of wild-type and MAP1S knockout mice. ....	81
Figure 37. The cell cycle distribution is altered in MAP1S knockout fibroblasts. ....	82
Figure 38. MAP1S knockout fibroblasts did not migrate significantly slower than wild-type fibroblasts in random migration assay. ....	83
Figure 39. MAP1S knockout fibroblasts closed the scratched wound slower than wild-type fibroblasts. ....	84
Figure 40. The appearance of the cytoskeleton was not altered in fibroblasts isolated from MAP1S knockout mice. ....	85
Figure 41. The number of focal adhesions and their size are not significantly altered in fibroblasts isolated from MAP1S knockout mice. ....	86
Figure 42. A model for MAP1S mediated effects in liver damage or disease. ..	90
Figure 43. A summary of potential functions of MAP1S in vivo. ....	97
Table 1. Breeding statistics of MAP1S knockout mice. ....	73
Table 2. Primers and PCR programs used to amplify the described PCR products. ....	102
Table 3. Plasmids and oligos used for cloning the MAP1S conditional knockout targeting vector. ....	104
Table 4. Tet-transactivator dependent expression constructs used for transfection of mammalian cell lines. ....	110
Table 5. List of primary antibodies. ....	116
Table 6. List of secondary antibodies. ....	117



## ABSTRACT

The microtubule associated protein 1 S (MAP1S) is the shortest member of the mammalian MAP1 family of proteins. In contrast to MAP1A and MAP1B, which are predominantly expressed in the nervous system, MAP1S is expressed in a wide range of tissues with the highest protein levels in brain and testis. All MAP1 proteins are synthesized as precursor proteins and then cleaved into a heavy and a light chain. MAP1S is partially cleaved in a tissue specific manner. As light chains of MAP1 proteins bind to both, microtubules and filamentous actin, MAP1S (as all the other members of the family) might act as crosslinker protein between microtubules and actin filaments. Other potential interaction partners of MAP1S (the testis-specific VCY2 protein, the fibroblast growth factor receptor associated protein LRPPRC, and the tumour suppressor protein RASSF1A) suggest functions of MAP1S in spermatogenesis, chromosome remodelling, cytokinesis, apoptosis, and tumourigenesis.

In the first part of my thesis I looked at interactions between MAP1 proteins and posttranslational modifications of MAP1S in comparison to MAP1B and MAP1A. I found that all members of the MAP1 family can take part in heterotypic complexes formed between heavy and light chains probably via domains conserved in all three MAP1 members. In contrast to MAP1B, the potential S-nitrosylation of MAP1S does not influence its microtubule binding ability. Moreover, MAP1S, unlike MAP1B, is not modified by N- $\epsilon$ -lysine acetylation.

In the second and major part of my thesis I investigated the role of MAP1S *in vivo* by generating MAP1S deficient mice. Since MAP1S is ubiquitously expressed and might play a role in mitosis, I decided to generate conditional knockout mice to avoid the potential embryonic lethality of a homozygous MAP1S deletion. Surprisingly, I found that homozygous MAP1S knockout mice are viable and fertile and show no overt phenotype. Histological analysis showed no obvious abnormalities in brain or other organs, except for a disturbed organisation of bile ducts in the liver in one MAP1S knockout mouse. Cultured MAP1S deficient primary neurons displayed a shift from one to two axons per cell body, indicating a role of MAP1S in neurotogenesis. Cultured

fibroblasts revealed a crucial role of MAP1S in cell cycle progression and migration.

# ZUSAMMENFASSUNG

Das Mikrotubuli assoziierte Protein 1 S (MAP1S) ist das kleinste Mitglied der MAP1 Proteinfamilie in Säugetieren. Im Gegensatz zu MAP1A und MAP1B, die vorwiegend im Nervensystem exprimiert werden, wird MAP1S in vielen verschiedenen Geweben exprimiert, mit dem höchsten Expressionslevel in Gehirn und Testes. Alle MAP1 Proteine werden als Precursor-Proteine translatiert und dann in eine schwere und eine leichte Kette gespalten. Die Spaltung von MAP1S ist gewebespezifisch. Da die leichte Kette der MAP1 Proteine sowohl an Mikrotubuli als auch an filamentöses Aktin binden, stellt MAP1S (sowie alle anderen MAP1 Proteinfamilienmitglieder) wahrscheinlich eine Verbindung zwischen Mikrotubuli und Aktinfilamenten her. Andere potentielle Interaktionspartner von MAP1S (das testisspezifische Protein VCY2, das Fibroblastenwachstumsfaktorrezeptor assoziierte Protein LRPPRC und das Tumorsuppressorprotein RASSF1A) lassen darauf schließen, dass MAP1S während der Spermatogenese, des Chromosomenremodelling, der Zytokinese, der Apoptose und der Tumorentstehung eine große Rolle spielt.

Im ersten Teil meiner Dissertation untersuchte ich Interaktionen zwischen MAP1 Proteinen und posttranslationale Veränderungen von MAP1S im Vergleich zu MAP1B und MAP1A. Ich entdeckte, dass alle Mitglieder der MAP1 Familie miteinander heterotypische Komplexe bilden. Die Proteine interagieren wahrscheinlich über konservierte Domänen miteinander. Im Gegensatz zu MAP1B verändert eine potentielle Nitrosylierung von MAP1S nicht die Fähigkeit von MAP1S an Mikrotubuli zu binden. Außerdem wird MAP1S im Gegensatz zu MAP1B nicht N- $\epsilon$ -Lysin-azetyliert.

Im zweiten und wichtigsten Teil meiner Dissertation habe ich die funktionelle Rolle von MAP1S in vivo untersucht, indem ich eine Mauslinie etabliert habe, welcher MAP1S fehlt. Da MAP1S ubiquitär exprimiert wird und in Verdacht steht eine Rolle während der Zellteilung zu spielen, entschied ich mich eine konditionelle Knockoutmaus herzustellen um das Risiko der embryonalen Lethalität einer homozygoten MAP1S Deletion zu umgehen. Überraschenderweise fand ich, dass homozygote MAP1S Knockoutmäuse überlebensfähig und fertil sind und keinen offensichtlichen Phenotyp zeigen.

Histologische Analysen zeigten keine Abnormalitäten im Gehirn oder in anderen Organen mit Ausnahme von veränderter Organisation der Gallengänge in der Leber in einer der drei untersuchten MAP1S Knockoutmäusen. Kultivierte primäre Neuronen von MAP1S Knockoutmäusen zeigten einen Wechsel von einem zu zwei Axonen pro Zellkörper. MAP1S scheint daher eine Rolle in der Neuritogenese zu spielen. Kultivierte primäre Fibroblasten zeigten, dass MAP1S während des Zellzyklus und der Zellmigration eine bedeutende Rolle spielt.

# INTRODUCTION

## THE CYTOSKELETON

The cytoskeleton is a remarkable system of filaments throughout the cytoplasm. On the one hand it forms stable structures and helps cells to establish their shape and to be physically robust, on the other hand the cytoskeleton is highly dynamic and adapts to changing circumstances. As stable structure, the cytoskeleton provides a scaffold to support the plasma membrane and to structure the cytoplasm. This scaffold provides the eukaryotic cell with mechanical stability and forms stable specialised cell surface protrusions like microvilli or cilia. The cytoskeleton is also responsible for large-scale cellular polarity and the maintenance of strong intercellular adhesive contacts. The dynamic of the cytoskeleton allows cells to change their shape and to rearrange their internal components as they grow, divide and adapt to changing circumstances. It separates chromosomes during mitosis and meiosis and guides the intracellular traffic of organelles. Additionally it enables cells, such as fibroblasts, to crawl across surfaces and others, such as sperms, to swim. Due to a functioning cytoskeleton, muscle cells are able to contract and nerve cells can extend axons and dendrites.

Most animal cells have three types of cytoskeletal filaments: intermediate filaments, actin filaments, and microtubules (figure 1). Additionally, hundreds of different cytoskeleton associated accessory proteins are essential for the regulation of the spatial distribution and the dynamic behaviour of the cytoskeletal filaments.

### **Intermediate filaments**

Intermediate filaments are expressed in some metazoans, including molluscs, nematodes, and vertebrates, but they are not present in every cell type. Intermediate filaments are mainly found in the cytoplasm of cells that are subject to mechanical stress.

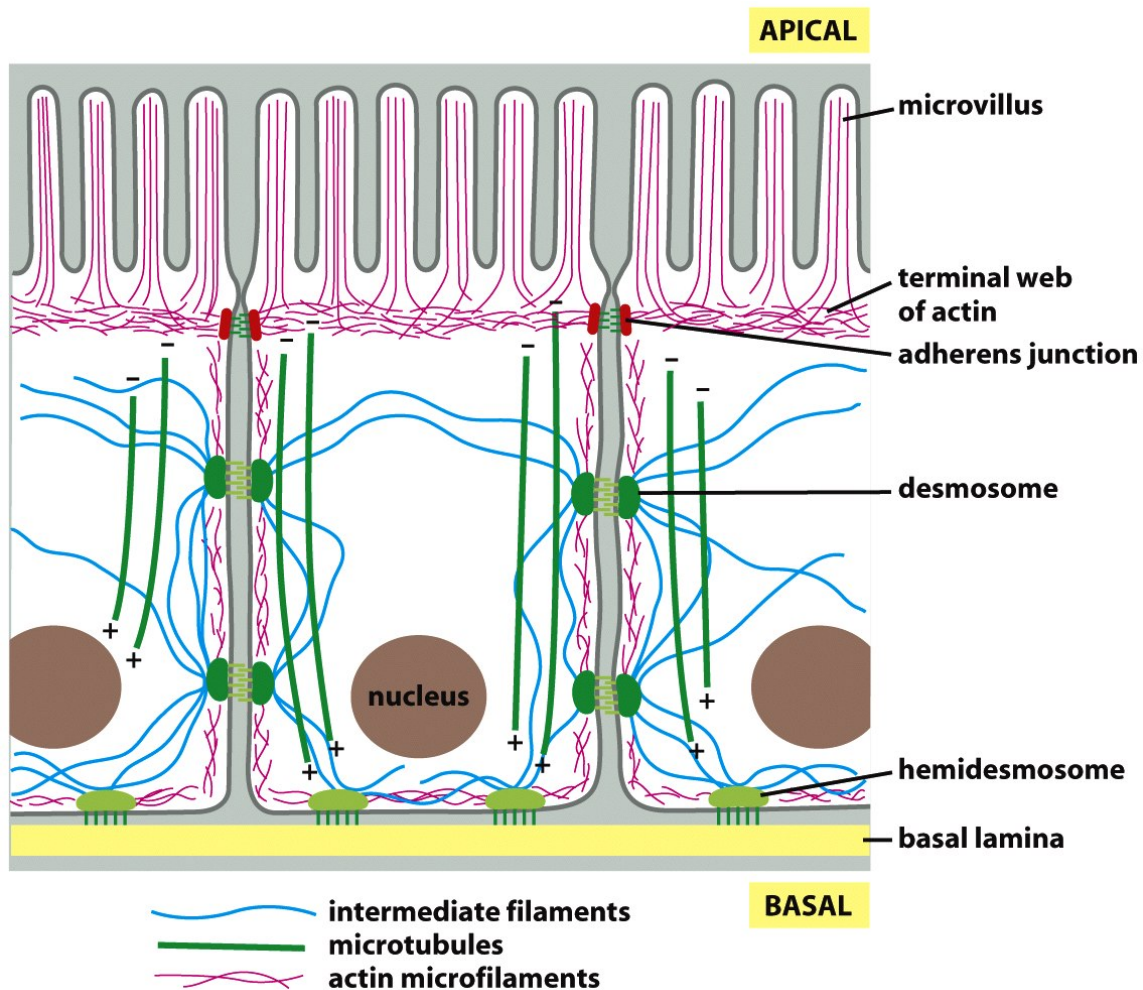


**Figure 1. Organisation of the cytoskeleton in polarised epithelial cells that line the small intestine (© Garland Science 2008, Alberts B., 2008).**

Regarding their structure, intermediate filaments are rope like fibres with a diameter of around 10nm. The individual polypeptides of intermediate filaments are molecules with an extended central  $\alpha$ -helical domain that form a parallel coiled coil with another monomer. Two of these dimers associate in an antiparallel fashion to form a tetramer. This tetramer forms the soluble subunit of intermediate filaments, which has, in contrast to the subunits of actin filaments and microtubules, no nucleoside triphosphate binding site. The subunits pack together laterally to build the filament, which includes eight parallel protofilaments made up of tetramers. Therefore, each individual intermediate filament consists of 32 individual  $\alpha$ -helical coils. Many intermediate filaments further bundle themselves by self-association, others are held together by accessory proteins such as filaggrin or plectin. Intermediate filaments are easy to bent, but hard to break.

In contrast to the conserved central  $\alpha$ -helical domain, the N- and C-terminal globular domain can vary to a great extent resulting in various types of intermediate filament proteins: nuclear, vimentin-like, epithelial and axonal types. Nuclear filaments like the lamins A, B, and C form the nuclear lamina, a meshwork beneath the inner nuclear membrane. Vimentin-like intermediate filaments consist of vimentin, desmin, glial fibrillary acidic protein, and peripherin. Whereas vimentin is found in many cells of mesenchymal origin, desmin is expressed only in muscles. Glial fibrillary acidic proteins are located in glia cells, peripherin is found in some neurons. Epithelial intermediate filaments, keratin type I and type II, are found in epithelial cells and their derivatives like hair and nails. They provide mechanical strength to epithelial tissues through adhesive structures like desmosomes and hemidesmosomes. Axonal types of intermediate filaments like neurofilaments are expressed predominantly along the axons of vertebrate neurons. The level of neurofilament gene expression controls the axonal diameter, which influences the speed of signal propagation in the axon.

## **Actin filaments**

In contrast to intermediate filaments, actin is strongly conserved in evolution and is found in all cells. Actin filaments, also known as microfilaments, are distributed throughout the whole cell with the highest concentration beneath the plasma membrane, called the cell cortex, to provide strength and shape to the cell and to form cell surface projections. Specialised actin structures enable for example fibroblasts to crawl across a surface. During mitosis those structures disassemble to round up the cell and actin and its associated motor protein myosin then form a belt around the middle of the cell, the contractile ring, which divides the cell in two.

Actin filaments are two-stranded helical polymers formed by globular actin monomers with a diameter of 5-9nm. In animal cells, actin filaments are organised into bundles or web-like (gel-like) networks. Nucleating proteins, like formins, induce the formation of actin bundles. The ARP complex catalyses the formation of web-like networks and is associated with structures at the leading

edge of migrating cells. External signals can regulate the nucleation of actin filaments in the cell cortex to change the cells shape and stiffness rapidly in response. Once nucleated, actin filaments generally elongate by the addition of soluble subunits. Straight, unbranched filaments can be cross-linked by other proteins to form parallel bundles.

The regular and parallel orientation of their subunits gives actin filaments a structural polarity. The two ends of the polymer show different dynamic behaviour, with the plus end exhibiting higher polymerisation and depolymerisation rates than the minus end. Each actin subunit has a binding site for the nucleotide ATP or ADP. On actin filaments, the ATP-binding cleft on the monomer points towards the minus end. If the ATP hydrolysis upon incorporation into the filament is not as fast as the addition of new subunits, an “ATP-cap” can be created on the plus end. On the minus end, ATP-bound actin subunits are added more slowly so that the ATP becomes hydrolysed to ADP before a new subunit is added. In this way an ATP-bound plus end and an ADP-bound minus end are generated. Individual filaments have a very short lifetime, because the cycle of actin polymerisation and disassembly in cells is extremely rapid. During the formation of cellular protrusions a phenomenon called treadmilling is very important: monomers are added at the plus end and removed at the minus end at the same speed, so the overall polymer length remains stable.

In most nonmuscle vertebrate cells the soluble monomer concentration of actin is rather high, but thymosin and other proteins bind to actin monomers and prevent them from associating to actin filaments and from hydrolysing or exchanging their bound nucleotide. Another monomer binding protein, profilin, can recruit actin to filaments. By binding to the actin monomer opposite the ATP-binding cleft, the side on the monomer that binds to the plus end, but not the side that binds to the minus end, is free. Profilin also binds to acidic membrane phospholipids at the cytosolic face of the plasma membrane and can be activated by extracellular signals to produce explosive local actin polymerisation and to build actin-rich motile structures, such as filopodia and lamellipodia. Actin-severing proteins are mostly members of the gelsolin superfamily, whose severing activity is activated by high levels of cytosolic  $\text{Ca}^{2+}$ , but requires no extra energy input.



As mentioned above, actin is extraordinarily well conserved. Actin sequences are about 90% identical among eukaryotes. However, there are small variations that can cause significant functional differences. There are three subtly different isoforms of actin in vertebrates, termed  $\alpha$ ,  $\beta$ , and  $\gamma$ -actin. Whereas  $\alpha$ -actin is expressed only in muscle cells,  $\beta$  and  $\gamma$ -actin are found together in almost all nonmuscle cells.

## **Microtubules**

Like actin filaments, microtubules are found in all cells. Microtubules are long, hollow cylinders that are often found emanating from the centre in a star-like cytoplasmic array in interphase cells. For cell division, the microtubule network is rearranged to form the bipolar mitotic spindle. Additionally, they build motile structures like cilia and flagella on the cell surface and are aligned to bundles in neuronal axons that serve as transport tracks. When epithelial cells form cell-cell junctions and become highly polarised, the microtubule minus ends move to a region near the apical plasma membrane and an array of nearly parallel microtubules forms along the long axis of the cell, with plus ends extending as far as the basal surface.

Structurally, microtubules are long, hollow cylinders with an outer diameter of 25nm formed from protein subunits of tubulin. Like actin, tubulin is a highly conserved protein. The tubulin subunit itself is a heterodimer made of two closely related globular proteins called  $\alpha$ -tubulin and  $\beta$ -tubulin, tightly bound together by noncovalent bonds. Each  $\alpha$  or  $\beta$  monomer has a binding site for one molecule of GTP. Whereas the GTP on  $\alpha$ -tubulin is physically trapped and never hydrolysed, the nucleotide on the  $\beta$ -tubulin is exchangeable. 13 parallel tubulin protofilaments form the hollow cylindrical structure of a microtubule. Due to strong longitudinal and comparatively weak lateral contacts among subunits, microtubules are more rigid than actin filaments, but they break easier than intermediate filaments when they are bent. Each protofilament in a microtubule points in the same direction giving microtubules structural polarity. Like in actin filaments, the end of the filament, where both growth and shrinkage are fast, is called the plus end, and the other end is called the minus end. On microtubules,

$\alpha$  subunits are exposed at the minus end, and  $\beta$  subunits are exposed at the plus end.

In mammals there are at least six forms of  $\alpha$ -tubulin and a similar number of forms of  $\beta$ -tubulin, each encoded by a different gene. Despite their similarity, they have distinct locations in a cell and perform slightly different functions. For example,  $\gamma$ -tubulin is involved in the nucleation of microtubule growth from the microtubule organising centre (MTOC). In most animal cells a single, well defined MTOC called the centrosome is located near the nucleus. The centrosome consists of a fibrous centrosome matrix containing over fifty copies of  $\gamma$ -tubulin ring complex ( $\gamma$ -TuRC) and a pair of cylindrical structures called centrioles, which organise the centrosome matrix and ensure its duplication at each cell cycle as the centrioles themselves duplicate. In animal cells, the astral configuration of microtubules is very robust, with dynamic plus ends pointing outward toward the cell periphery and stable minus ends collected near the nucleus.

The ends of microtubules are large and complex structures and therefore they provide many possibilities for accessory proteins. Some of them are simple capping proteins, others, like certain kinesin-related proteins are known as catastrophe factors, because they significantly increase the catastrophe rate, where microtubules change from a state of polymerisation to one of depolymerisation. The protein katanin is required for severing a microtubule. Katanin has to break thirteen longitudinal bonds and therefore requires ATP. It is made up of two subunits, the smaller subunit hydrolyzes ATP and performs the actual severing, and the larger one directs katanin to the centrosome. Katanin releases microtubules from their attachment on the MTOC and plays probably an important role in the rapid microtubule depolymerisation at the spindle poles during meiosis and mitosis. It may also be involved in microtubule release and depolymerisation in proliferating cells in interphase and in postmitotic cells such as neurons (Alberts B., 2008).

## MICROTUBULE ASSOCIATED PROTEINS

Proteins that bind along the sides of microtubules are collectively called microtubule associated proteins (MAPs). This diverse family of proteins plays an important role for the function of microtubules. Members of the MAP family were first classified according to their molecular weight, as revealed by SDS-PAGE, later according to their molecular structure and function (Schoenfeld and Obar, 1994; Wiche et al., 1991).

Due to their molecular structure and function, MAPs are grouped in three classes. The first class consists of proteins called structural MAPs, or simply MAPs. They bind to, stabilise and promote the assembly of microtubules and they copurify with tubulin during cycles of temperature-dependent microtubule assembly and disassembly. Members of this class are the MAP1 and MAP2 families and will be discussed later on in more detail. The second class includes proteins which are often found associated with microtubules, but they are normally not called MAPs at all. Examples are glycolytic enzymes (like GAPDH), kinases (like protein kinase A), proteins involved in biosynthesis (like elongation factor EF-1 $\alpha$ ), proteins linking microtubules to membrane receptors (like dynamin), and ribonucleoproteins containing mRNA. The third class of proteins is also known as motor proteins. These proteins generate movement along microtubules using chemical energy of ATP hydrolysis. Well known representatives of this class are kinesin and dynein. These proteins can bind tightly to microtubules, but they do not copurify through cycles of assembly and disassembly (Mandelkow and Mandelkow, 1995).

As mentioned above, proteins of the first class of MAPs, the structural MAPs, are divided into two families, namely the MAP2/Tau family and the MAP1 family. More specifically, the mammalian MAP2/Tau family members are MAP2, Tau, and MAP4. Whereas MAP2 and Tau are expressed predominantly in neurons, MAP4 is found in a wide range of tissues, but not in neurons. Possible functions of these proteins are stabilising microtubules, regulating microtubule networks in axons and dendrites of neurons, binding to filamentous (F) actin, recruitment of signalling proteins and regulation of microtubule-mediated transport. Tau is also implicated in dementias like Alzheimer's disease. Knockout experiments in

mice revealed that neither MAP2 nor Tau are essential for normal brain morphology, but the microtubule density was reduced in dendrites and in small-calibre axons in MAP2 and in Tau knockout mice, respectively. In addition, the dendrite length in cultured neurons from MAP2 knockout mice was reduced. The non-neuronal member of this family, MAP4, seems to play a role in the regulation of microtubule dynamics during metaphase, but as one component of a functionally redundant system (Dehmelt and Halpain, 2005).

## **MAP1 family proteins**

Most vertebrate genomes (including human, mouse and rat) contain three MAP1 family members: MAP1A, MAP1B and MAP1S. Two decades ago MAP1A and MAP1B were identified and characterised by their ability to bind and stabilise microtubules in vertebrate brain. Both high molecular mass proteins (~ 300kDa, 2500aa) are expressed predominantly in the nervous system and right from the start they were suspected to be involved in axon guidance and synaptic function (Drewes et al., 1998; Gonzalez-Billault et al., 2002; Matus, 1988; Schoenfeld and Obar, 1994; Takei et al., 2000; Wiche et al., 1991). The third member of the MAP1 family, MAP1S, was discovered and characterised only recently (Dallol et al., 2004; Liu et al., 2002; Orban-Nemeth et al., 2005; Song et al., 2005; Wong et al., 2004). In contrast, only one family member, Futsch, is found in *Drosophila*.

Futsch, the *Drosophila* homologue of the MAP1 family proteins, is about twice the size of MAP1B. Futsch and MAP1B show high homology in the N- and C-terminal domains. Futsch colocalises with microtubules and plays an important role in the organisation of the microtubule cytoskeleton during axonal growth and synaptogenesis (Gogel et al., 2006). It is involved in progressive neurodegeneration and *futsch*<sup>olk</sup> mutants exhibit several characteristics of human neurodegenerative diseases (Bettencourt da Cruz et al., 2005). Like MAP1B, Futsch appears to be regulated by phosphorylation of at least one conserved phosphorylation site mediated by glycogen synthase kinase 3 $\beta$  (GSK3 $\beta$ ). While Futsch was previously thought to be expressed as a single uncleavable protein (Gogel et al., 2006), a recent study showed that Futsch is

cleaved, like MAP1B, into a heavy (HC) and a light chain (LC), at a conserved cleavage site (Zou et al., 2008a).

## **MAP1A and MAP1B**

MAP1A and MAP1B are distantly related high molecular mass proteins. After their initial expression as polyprotein precursor, each is cleaved into a LC and a HC. By using MAP1B deletion mutants, a cleavage site of the precursor protein of MAP1B was predicted, that seems to be conserved in all MAP1 proteins (Tögel et al., 1999). The LCs of MAP1A and MAP1B are also called LC2 and LC1, respectively. Heavy and light chains assemble into complexes together with the separately encoded subunit LC3 (Halpain and Dehmelt, 2006). Not only homotypic complexes are formed, meaning that a MAP1A HC is associated with a MAP1A LC and a MAP1B HC is associated with a MAP1B LC, but also heterotypic complexes (Noiges et al., 2006).

LC3 is a subunit of MAP1A and MAP1B protein complexes that is encoded by a separate gene. Most LC3 molecules bind to microtubules via MAP1A or MAP1B. It is proposed that LC3 can regulate the microtubule binding activity of MAP1A and MAP1B (Mann and Hammarback, 1994). LC3 is implicated in autophagy in mammalian cells as a homologue of Apg8p, an essential protein for autophagy in yeast. In rats, LC3 is cleaved and posttranslationally modified to generate LC3-I and LC3-II in various cells. LC3-I is cytosolic, whereas LC3-II is membrane bound (Kabeya et al., 2000). In humans, three orthologs are found, named MAP1LC3A, MAP1LC3B, and MAP1LC3C, which also differ in their post-translational modifications (He et al., 2003).

MAP1A and MAP1B can bind to microtubules via a domain at the N terminus of their LCs (Mann and Hammarback, 1994; Noiges et al., 2002; Orban-Nemeth et al., 2005). Furthermore, their HCs both contain additional sequences that bind microtubules (Cravchik et al., 1994; Noble et al., 1989; Vaillant et al., 1998; Zauner et al., 1992). Interestingly, amino acids within these microtubule-binding domains are not conserved.

MAP1B LC induces formation of stable but flexible microtubule bundles that are resistant against the effects of taxol and nocodazole. This MAP1B LC activity can be inhibited by the MAP1B HC. Therefore the MAP1B HC might act as a

regulatory subunit of the MAP1B complex to control LC activity (Tögel et al., 1998).

MAP1B and MAP1A can also interact with actin filaments. For binding to actin filaments, an F-actin binding domain at the C terminus was identified (Noiges et al., 2002). In addition, LCs can dimerise or oligomerise. Domains for the interactions between LCs and between LC and HC are homologous between MAP1A and MAP1B (Tögel et al., 1998).

As already mentioned, MAP1A and MAP1B are expressed predominantly in the nervous system. The expression is developmentally regulated. In murine brain, the expression level of MAP1A is low at birth and then increases over the next three weeks, whereas MAP1B expression is already high at birth, increases slightly over the next few days and then drops to lower levels. These findings suggest that MAP1B regulates the cytoskeleton during neurogenesis, and MAP1A functions in the cytoskeleton in mature neurons (Garner et al., 1990; Schoenfeld et al., 1989; Schoenfeld and Obar, 1994). Also in the neurons derived from rat retina, MAP1A was not detected until 7 days postnatal (Bates et al., 1993; Okabe et al., 1989; Tucker and Matus, 1988). However, studies in human foetal brains reveal a different expression pattern. MAP1A is found in human foetal brain in the telencephalic proliferative zone and within the internal capsule. While MAP1A is expressed between 18 and 22 weeks of gestation, MAP1B is found only from the 26th week to the 33 week in the internal capsule. Nevertheless, MAP1B is already expressed in early embryonic human spinal cord (Riederer, 2007).

In the nervous system, both proteins, MAP1A and MAP1B, are modified by phosphorylation (Avila et al., 1994a). So far, many phosphorylation sites on MAP1B have been identified in proteomic studies, but only little is known about the function of all these phosphorylation sites (Riederer, 2007). At least two modes of MAP1B phosphorylation could be distinguished by the use of different antibodies to phosphorylation-sensitive epitopes so far. The first one, termed mode I phosphorylation, is carried out by proline-dependent kinases (PDKs) and is found in outgrowing axons and is diminished during brain development. The second one, termed mode II phosphorylation, is carried out by the Casein Kinase II (CKII) and is found in axons and dendrites and remains into adulthood

(Avila et al., 1994b; Diaz-Nido et al., 1988; Gonzalez-Billault et al., 2004; Riederer, 2007; Ulloa et al., 1993).

MAP1B is phosphorylated via signalling kinases, including the glycogen synthase kinase-3  $\beta$  (GSK3 $\beta$ ), cdk5, and Jun N-terminal kinase 1 (JNK1) (Chang et al., 2003; Del Rio et al., 2004; Goold and Gordon-Weeks, 2003; Goold et al., 1999). GSK3 $\beta$  phosphorylates mouse MAP1B at two residues, Ser1260 and Thr1265, and is restricted to growing axons with highest levels in the distal part. Phosphorylated MAP1B regulates microtubule dynamics by maintaining microtubules in growth cones in a dynamically unstable state, which is required during path finding (Goold et al., 1999; Johnstone et al., 1997; Trivedi et al., 2005). Moreover, the axon guidance cue Netrin 1 controls the mode I phosphorylation of MAP1B via GSK3 $\beta$  and CDK5 (Del Rio et al., 2004). Another pathway upstream of the activation of GSK3 $\beta$  is the MAPK pathway. Partly through the MAPK pathway and the further phosphorylation of MAP1B, nerve growth factor (NGF) increases neurite growth rates (Goold and Gordon-Weeks, 2005). Another kinase that phosphorylates MAP1B is the Jun N-terminal kinase 1 (JNK1). In JNK1 knockout mice, MAP1B is found to be hypophosphorylated, resulting in a compromised ability to bind to microtubules and to promote their assembly (Chang et al., 2003). Additionally, contact with myelin-associated glycoprotein (MAG) appears to trigger an increase the amount of phosphorylated MAP1B in dorsal root ganglia neurons (DRGNs) (Franzen et al., 2001). It was shown that, depending on its phosphorylation state, MAP1B is transported in the axons of sciatic nerves of adult rats at two different rates. The relatively fast transport of phosphorylated MAP1B may be responsible for its high concentration in the distal end of growing axons. The difference in transport velocity of phosphorylated versus non phosphorylated MAP1B is possibly due to the association with different proteins (Ma et al., 2000).

Less is known about the regulation of MAP1A. A recent study identified MAP1A LC as a substrate for CK1 $\delta$ , a member of the casein kinase 1 family of serine/threonine-specific kinases. Thus, CK1 $\delta$  may modulate microtubule dynamics by changing the phosphorylation status of the MAP1A LC (Wolff et al., 2005).

## MAP1B Gene Targeting studies

To define the role of MAP1B *in vivo*, MAP1B deficient mice have been generated. Four independent research groups have generated mice with disrupted MAP1B genes till now. In every mouse line, brain development is disturbed, although the severity of the phenotypic effects is quite different in these four mouse lines (Edelmann et al., 1996; Gonzalez-Billault et al., 2000; Meixner et al., 2000; Takei et al., 1997). Homozygous MAP1B deficient mice from Edelmann et al. and González-Billault et al. die during embryogenesis or shortly after birth, respectively (Edelmann et al., 1996; Gonzalez-Billault et al., 2000). Edelmann et al. generated mice which carry an insertion, a neo cassette in reverse transcriptional orientation, in exon 5 of the MAP1B gene leading to a depletion of the MAP1B protein. Homozygotes die during embryogenesis, heterozygotes grow slower, they lack the visual acuity in one or both eyes, and they suffer from motor system abnormalities (Edelmann et al., 1996). González-Billault et al. analysed MAP1B mutant mice generated by a gene trapping approach. In these mice, an IRES $\beta$ gal/neo sequence inserted between exon 2 and 3 of the MAP1B gene leads to the expression of the  $\beta$ -galactosidase marker and the premature termination of MAP1B translation (Chowdhury et al., 1997; Gonzalez-Billault et al., 2000). Homozygotes die shortly after birth. In their brain, lateral ventricles are enlarged, the corpus callosum appears interrupted, in the cerebellum the wide band of Purkinje cells is absent and the normal laminar organisation in the hippocampus and in the cerebellum is disturbed (González-Billault et al., 2000). In contrast, homozygotes from Takei et al. and Meixner et al. are viable (Meixner et al., 2000; Takei et al., 1997). Homozygotes from Takei et al., in which a neo cassette replaces exon 1 of MAP1B still express low levels of a presumably truncated form of MAP1B from an alternative promoter, exhibit a slightly decreased brain weight and a delay in the development of the nervous system. Cultured neurons obtained from these mice show delayed axon outgrowth, a reduced rate of elongations, aberrant growth cone formation, and increased actin-based protrusive activity (Takei et al., 1997). Homozygotes from Meixner et al., in which exon 3 to 5 of MAP1B are deleted, are missing the corpus callosum. The cerebral white matter ends medially in a thick bundle of myelinated fibers, resembling the Probst bundle



present in agenesis of the corpus callosum. In the peripheral nervous system, axonal and myelination defects resulting in reduced motor nerve conduction velocity are observed (Meixner et al., 2000).

Reasons for these great phenotypic differences in these four MAP1B deficient mouse lines are probably their different genetic backgrounds and differently designed knockout strategies. First, the genetic background may have an influence on the effect of the loss of MAP1B. For example, mice from Edelmann et al. are derived from 129OP2/Ola, a strain that displays axonal guidance problems and defects in brain development already in wild-type mice (Wahlsten, 1982). Therefore, the additional reduction or ablation of MAP1B expression may lead to more severe developmental problems (Meixner et al., 2000). Interestingly, Takei et al. could show the influence of the genetic background on the phenotype of their MAP1B mice: MAP1B knockout mice with a genetic background of predominantly C57BL/6J (>93%), instead of a mixed background, have a partial postnatal lethality (Takei et al., 2000). Second, different knockout strategies may cause these different phenotypes. Takei et al. argue that the severely abnormal phenotype in MAP1B deficient mice, generated from Edelmann et al., might be caused by expression of a 571 amino N-terminal fragment of MAP1B, acting in a dominant-negative fashion rather than a loss of function (Meixner et al., 2000; Takei et al., 1997). Mice from Takei et al. and González-Billault et al. still contain approximately 5% of the amount of MAP1B protein present in their wild-type littermates, therefore these mice are deficient in MAP1B gene expression, but they are not null mutant mice. The reason for residual MAP1B expression is the use of alternative promoters inside the MAP1B gene that drive expression of five prime truncated alternatively spliced MAP1B transcripts. Alternative spliced isoforms are expressed containing uncoding exon 3A or 3U at their five prime joined to exon 3 of the regular transcript. They are expressed at about 1 to 10% of the level of regular transcripts (Kutschera et al., 1998; Lien et al., 1994). In the mutants generated by Takei et al. and González-Billault et al. have been demonstrated to give rise to alternatively spliced isoforms albeit at low level (Gonzalez-Billault et al., 2000; Kutschera et al., 1998; Takei et al., 1997). Interestingly, alternative isoforms of MAP1B were found in affected brain regions of heterozygous mice from Gonzalez-Billault et al. The expression level of this isoforms was low, but higher

in the mutants than in the wild-types (Gonzalez-Billault et al., 2000). Meixner et al. could show that their targeting strategy prevented the expression of regular as well as alternative transcripts of MAP1B, resulting in a complete loss of MAP1B (Meixner et al., 2000).

To elucidate the role of MAP1B in more detail, MAP1B knockout mice from Meixner et al. were analysed in several studies. Most of them concentrated on dorsal root ganglia neurons (DRGNs), primary sensory neurons which transmit somatic and sensory information from peripheral tissues to the spinal cord. DRGNs consist only of a cell body and one or more axons, but no dendrites or afferent synapses. In contrast to wild-type DRGNs, MAP1B knockout DRGNs show enhanced neurite branching and impaired axonal turning behaviour. Furthermore, the amount of acetylated microtubules within growth cones was reduced, whereas the distribution of tyrosinated and detyrosinated microtubules was normal in MAP1B knockout DRGNs (Bouquet et al., 2004). When treated with lysophosphatidic acid (LPA), an extracellular signalling phospholipid triggering changes in actin distribution and cell morphology, growth cones from wild-type DRGNs collapse and retract, whereas axons from MAP1B knockout DRGNs do not retract although the growth cones collapse. LPA induces actin contraction, but further effects on the microtubules that lead to axon retraction appeared to be MAP1B dependent. MAP1B is coupling actin and microtubule movements probably via its binding to actin and tubulin (Bouquet et al., 2007). Another study revealed that MAP1B is an important component in the S-nitrosylation dependent signal-transduction pathway that is involved in the regulation of the axonal cytoskeleton. Whereas wild-type DRGNs show enhanced growth cone retraction after nitric oxide treatment, MAP1B knockout DRGNs show no reaction. Cys 2457 in the C terminus of MAP1B is a substrate for S-nitrosylation in vivo. The nitrosylation of MAP1B leads to enhanced interaction with microtubules. It is proposed that MAP1B acts by inhibiting a microtubule- and dynein-based mechanism that normally prevents axon retraction (Stroissnigg et al., 2007). Additionally, Schwann cells (SCs) have been investigated. In cell migration assays, SCs from MAP1B knockout mice migrate slower. The speed of migration was less than half of that of wild-type controls. It was shown, that the LPA dependent retraction of SC processes is MAP1B dependent (Bouquet et al., 2007).

MAP1B knockout mice also show a distinct behavioural phenotype. They lack exploring activity in the cage (Meixner et al., 2000) and perform poorly in the Morris water maze test. The multiple T-maze tests revealed that MAP1B knockout mice are extremely sensitive to starvation. Detailed results of these tests indicate that the locomotor activity in MAP1B knockout mice is reduced. On the other hand, there are no significant differences in cognitive function and memory retention (Pangratz-Fuehrer et al., 2005).

Double knockout mice with disrupted MAP1B and additionally disrupted Tau or MAP2 have been generated (Takei et al., 2000; Teng et al., 2001). For these double knockout studies the MAP1B deficient mouse line from Takei et al. was used. While this MAP1B knockout mouse line and the Tau knockout mouse line are viable and display only minor abnormalities in the nervous system (Harada et al., 1994; Takei et al., 1997), double knockout mice show a markedly more severe phenotype. These mice are suffering from severe brain defects. Primary cultures of hippocampal and cerebellar neurons exhibit inhibited axonal elongation, delayed neuronal migration, and suppressed neurite elongation.

These results indicate that MAP1B and Tau act in a synergistic fashion, especially as regulators of microtubule organisation in axonal elongation and neuronal migration (Takei et al., 2000). Furthermore, MAP2 and MAP1B seem to act in a synergistic way as well. While MAP2 deficient mice are viable and display no apparent abnormalities, double knockout mice died perinatal. Their cerebral cortex is disorganised, showing an “inside-out” pattern in their cortical layer. A dispersed arrangement of cell layers is also found in the hippocampus. The olfactory bulb and the cerebellum exhibit disrupted laminar structures (Teng et al., 2001).

### **The role of MAP1B in human diseases**

MAP1B plays a role in several human neurodegenerative diseases like Alzheimer’s disease, Parkinson’s disease, giant axonal neuropathy, fragile X syndrome and spinocerebellar ataxia type 1.

Alzheimer’s disease, an age-related neurodegenerative disorder, is characterised by plaques of aggregated  $\beta$ -amyloid peptides, neurofibrillary

tangles, and neuronal loss in affected brains. It was shown that  $\beta$ -amyloid peptide can bind to the HC of MAP1B (Gevorkian et al., 2008).

Contradicting results exist how accumulative  $\beta$ -amyloid peptides alter MAP1B expression. One study shows that  $\beta$ -amyloid peptides induce MAP1B mRNA transcription, especially the alternative transcript containing exon 3U. The resulting overexpression of MAP1B might act as an effector of cell death (Uchida, 2003). Another study finds that  $\beta$ -amyloid peptides lead to a time-dependent degradation of MAP1B resulting from the  $\beta$ -amyloid-mediated activation of caspase-3 and calpain (Fifre et al., 2006). Supporting this study, MAP1B is found downregulated in affected brain regions compared to unaffected regions in samples taken post-mortem from patients (Yokota et al., 2006).

Parkinson's disease, another neurodegenerative disorder, is characterised by Lewy bodies, intraneuronal inclusions comprising  $\alpha$ -synuclein-containing filaments. MAP1B was found in around 80% of cortical Lewy bodies. MAP1B binds to  $\alpha$ -synuclein and may therefore play a general role in the pathogenesis of Lewy bodies (Jensen et al., 2000).

Giant axonal neuropathy (GAN) is an autosomal recessive disorder caused by mutations in the GAN gene, which encodes the ubiquitously expressed protein gigaxonin. Gigaxonin is necessary for the function and survival of neurons by controlling protein degradation. Cytopathologically, GAN is characterised by cytoskeletal abnormalities. Gigaxonin can bind directly to the LC of MAP1B. Mutations in the GAN gene disrupt this interaction of gigaxonin and MAP1B (Ding et al., 2002). Therefore, the cross talk between microtubules and intermediate filaments is disturbed (Bomont and Koenig, 2003). Ablation of gigaxonin results in a substantial accumulation of MAP1B LC in neurons leading to the characteristic cell death in GAN disorder. Reducing MAP1B levels significantly improves the survival rate of those neurons (Allen et al., 2005).

The fragile X syndrome is one of the leading causes of inherited mental retardation and is caused by the absence of the fragile X mental retardation (FMRP) protein. The lack of FMRP causes misregulation of MAP1B translation and a delayed decline of MAP1B expression in the brain of FMRP knockout mice. The overexpression of MAP1B leads to increased microtubule instability

and seems to be an important underlying factor for the pathogenesis of fragile X mental retardation (Lu et al., 2004).

Spinocerebellar ataxia type 1 belongs to a group of autosomal dominant neurodegenerative disorders, in which patients suffer from degeneration of the cerebellum, leading to uncoordinated movements. It is caused by trinucleotide CAG repeat expansions in the ataxin 1 gene coding for polyglutamine. One candidate mediator of ataxin 1 toxicity is the leucin-rich acidic nuclear protein, which interacts with MAP1B and modulates the effects of MAP1B on neurite extension (Opal et al., 2003).

## **MAP1S**

The microtubule associated protein 1 short, MAP1S, was characterised recently as a novel member of the MAP1 family. As its name indicates, MAP1S is rather short (~120kDa, 973aa) compared to the high molecular mass proteins MAP1A and MAP1B (~300kDa, 2500aa). Like MAP1A and MAP1B, MAP1S is encoded by seven exons, but no alternative splicing forms have been found. The difference in size is mainly due to differences in the length of exon 5, the other exons show hardly any differences concerning length. Like all MAPs, MAP1S copurifies with microtubules from murine brain through repeated cycles of temperature-induced polymerisation and depolymerisation.

In contrast to MAP1A and MAP1B, which are expressed mainly in the nervous system, MAP1S is widely expressed in mouse tissues, with the highest protein levels in brain and testis. Like MAP1A and MAP1B, MAP1S is synthesised as a precursor protein that is cleaved into a HC and a LC. In case of MAP1S, the cleavage appears to be regulated in a tissue specific manner. In brain the majority of the protein is cleaved. In testis, kidney, and liver the cleaved and uncleaved forms were found at approximately equal levels. In heart, lung, and spleen MAP1S is found mainly in the uncleaved form. The expression level of MAP1S in brain is already high at birth and increases slightly over the first three weeks after birth.

Similar to MAP1A and MAP1B, the HC and LC of MAP1S interact with each other. The MAP1S LC can bind to actin filaments through its C terminus. With its N-terminal domain it can bind, bundle and stabilise microtubules. The

possibility of binding to both, microtubules and actin, suggests that also the LC of MAP1S can act as a crosslinker between microtubules and actin filaments. The LC alone can bundle microtubules. When the complete MAP1S is expressed, microtubule binding is still observed, but microtubule bundling and stabilisation are absent, suggesting a regulatory function of the MAP1S HC (Orban-Nemeth et al., 2005).

Between mice and human, 63% of the amino acids of MAP1S are conserved. The murine protein contains 86 amino acids less, the majority is located in exon 5 (Orban-Nemeth et al., 2005). The human homologue of MAP1S is located on chromosome 19 and has previously been named C19ORF5. In yeast two-hybrid screens C19ORF5 is identified as possible interaction partner of LRPPRC, VCY2 and RASSF1A (Dallol et al., 2004; Liu et al., 2002; Liu and McKeehan, 2002; Wong et al., 2004).

### **Putative functions of MAP1S**

Interaction partners of MAP1S provide indications of putative functions of MAP1S. One possible interaction partner of MAP1S is the leucine rich PPR-motif containing protein, LRPPRC, also called LRP130, a leucine rich protein that copurifies with the fibroblast growth factor receptor (Liu et al., 2002; Liu and McKeehan, 2002). LRPPRC associates with nuclear and mitochondrial mRNAs and is therefore a potential candidate for coordinating nuclear and mitochondrial gene expression (Mili and Pinol-Roma, 2003). Two mutations in LRPPRC are identified to cause Leigh syndrome, French-Canadian type (LSFC), a human cytochrome c oxidase deficiency (Mootha et al., 2003). MAP1S may link LRPPRC to microtubules and mitochondria. Liu et al. show that overexpressed MAP1S colocalises not only with microtubules, but also with mitochondria and may induce perinuclear aggregates of mitochondria. This mitochondrial aggregation can result in degradation of DNA, a cell-death related process named mitochondrial aggregation and genome destruction (MAGD) (Liu et al., 2005a; Liu et al., 2005b). MAP1S may therefore have MAGD activity and play a role in apoptosis.

Due to its interaction with VCY2, MAP1S is also named VCY2 interacting protein 1 (VCY2IP-1) (Wong et al., 2004). The exact function of VCY2, which is

located in the frequently deleted azoospermia factor c region on the Y chromosome, is still unknown, but its impaired expression in infertile men suggests an involvement in the pathogenesis of male infertility (Tse et al., 2003). It has been proposed that VCY2 acts via MAP1S on the microtubule network suggesting that both proteins might play an important role in spermatogenesis (Wong et al., 2004).

So far, most information about the potential functions of MAP1S was gained in studies on RASSF1A. RASSF1A is an important tumour suppressor protein and plays a role in mitosis. As a tumour suppressor protein, RASSF1A is inactivated in many types of human cancers by promoter-specific CpG island hypermethylation. Overexpression of RASSF1A in several cancer cell lines causes drastic reduction of tumourigenicity (Dallol et al., 2004; Dammann et al., 2003; Rong et al., 2004). RASSF1A knockout mice are significantly tumour-prone, both for spontaneous tumour formation at an advanced age (18-20 months) and for chemically induced tumours. Homozygotes and heterozygotes show increased tumour multiplicity and tumour size relative to control animals (Tommasi et al., 2005). Through interaction with the tumour suppressor protein RASSF1A, MAP1S may be involved in tumorigenesis (Dallol et al., 2004). Because of its interaction with RASSF1A, MAP1S is also called RABP1 (RASSF1A binding protein 1) (Song et al., 2005).

During mitosis, RASSF1A is found on the centrosome and the mitotic spindle (Liu et al., 2003; Rong et al., 2004; Song et al., 2004). Overexpression of RASSF1A increases mitotic events with aberrant monopolar spindles, where RASSF1A colocalises with these monopolar spindles (Liu et al., 2003). Its binding to microtubule is essential for RASSF1A to mediate its growth inhibitory effects. After deletion of the microtubule binding sites of RASSF1A, the protein was not able to induce growth inhibition and cell death any more (Vos et al., 2004). Two naturally occurring tumour-associated missense mutants of RASSF1A disturb the association of RASSF1A with microtubules. In addition, wild-type RASSF1A, but not the two mutants, is able to block DNA synthesis (Dallol et al., 2004). Overexpression studies showed that RASSF1A induces mitotic arrest at prometaphase, and this arrest is accompanied by the accumulation of cyclin A and B. RASSF1A interacts with Cdc20, an activator of the anaphase promoting complex (APC), resulting in inhibition of APC

activation. Depletion of RASSF1A by using small interfering RNA leads to faster degradation of cyclin A and B and mitotic progression as a result of premature APC activation. Depletion of RASSF1A also causes cell division defects characterised by centrosome abnormalities and multipolar spindles (Song et al., 2004).

Through its interaction with RASSF1A, MAP1S is suspected to play a crucial role in mitosis and tumorigenesis. Song et al. showed that the overexpression of MAP1S increases the abundance of cyclin A and B and leads to an arrest in prometaphase in a RASSF1A-dependent manner. MAP1S depletion by siRNA accelerates the cell cycle. MAP1S itself is located on the centrosome and it is supposed to be required for recruitment of RASSF1A to the spindle poles and for its inhibition of APC/Cdc20 activity. In MAP1S-siRNA depleted cells, RASSF1A fails to localise to the centrosome during mitosis and no interaction between RASSF1A and Cdc20 is found. Although MAP1S is not interacting with Cdc20, the recruitment of RASSF1A to spindle poles by MAP1S seems to be required for the interaction of RASSF1A with Cdc20 during mitosis. Therefore, MAP1S depletion accelerates mitotic progression, but increases the number of abnormal mitosis (Song et al., 2005). Contradictory results were obtained by Dallol et al.. After MAP1S depletion by siRNA, the level of cyclin B increased modestly, cells were able to go through metaphase, but they were not able to form a stable metaphase plate with all the chromosomes aligned to it. Furthermore, MAP1S depletion caused premature sister chromatid separation and multipolar spindles. MAP1S was shown to localise to microtubule-organising centers (MTOCs). Knockdown of MAP1S resulted in disrupted MTOCs and microtubule nucleation from several sites (Dallol et al., 2007).

A close relative to RASSF1A is NOREA1. MAP1S as well as MAP1B interact with NORE1A (Moshnikova et al., 2008). NORE1A is a growth and tumour suppressor protein, which is inactivated in a variety of cancers. NORE1A is localised to microtubules and centrosomes and this association of NORE1A with cytoskeletal elements is suggested to be essential for NORE1A-induced growth suppression. Furthermore, the ERK pathway is a target for NORE1A growth-suppressive activities (Moshnikova et al., 2006). Moshinova et al. ruled out that this localisation is MAP1S dependent (Moshnikova et al., 2008).



MAP1S itself was identified as a potential tumour suppressor gene by using a modified version of GINI (gene identification by nonsense-mediated decay inhibition). With this method, colon cancer cells lines have been screened for bi-allelic inactivating mutations. Amongst others, MAP1S was identified as a candidate tumour suppressor gene (Ivanov et al., 2007). This data supports the idea that MAP1S may play a role in tumourigenesis.

In addition to its potential role in cell cycle progression, MAP1S may regulate axonal transport in neurons. Mice deficient in gigaxonin serve as a model for the human disorder giant axonal neuropathy (GAN) and show an impaired retrograde axonal transport. MAP1S levels are found to be increased in gigaxonin null mice. Accumulated MAP1S in cultured wild-type cells alters the microtubule network and traps dynein. Finally, this accumulation leads to neuronal death in cultured wild-type neurons, replicating the process occurring in GAN null mutants (Ding et al., 2006a).

Another interaction partner of MAP1S is NR3A. The interaction was confirmed in vitro and in vivo and binding of MAP1S was localised to the membrane-proximal part of the NR3A C-terminus. NR3A is a subunit of the N-methyl-D-aspartate receptor (NMDAR). NMDARs are glutamate-gated ion channels that are widely expressed in the nervous system and play a role in excitatory synaptic transmission. Most NMDARs consist of two NR1 and two NR2 subunits. Receptors containing NR3A show specific permeation properties and seem to play a role in the brain disorder white matter injury (Paoletti and Neyton, 2007). NR3A is widely expressed in perisynaptic and extrasynaptic sites and appears to be weakly associated with the postsynaptic density. NR3A and MAP1S are both found in neurite shafts and occasionally in filopodia-like processes. MAP1S may link NR3A to the cytoskeleton and regulate the localisation of NR3A-containing receptors at the synapse and regulate their movement between synaptic and extrasynaptic sites (Eriksson et al., 2007).

Recently, human MAP1S was identified as a novel interacting protein of the cytokine-induced suppressor of cytokine signalling protein 3 (SOCS3). SOCS3 is thought to be important for the down regulation of interleukin-6 (IL-6) signalling. IL-6 is a proinflammatory cytokine and strongly induces activation of STAT1 and STAT3. The phosphorylation of STATs can be inhibited by lipopolysaccharide (LPS) induced SOCS3. After MAP1S depletion by siRNA,

the inhibition of SOCS3 on STAT3 phosphorylation is partially hindered in the presence of IL-6 and LPS, suggesting that the interaction between MAP1S and SOCS3 and the integrity of the microtubule cytoskeleton play an important role in the negative regulation of SOCS3 on IL-6 signalling (Zou et al., 2008b).

## **AIMS OF THE THESIS**

Since MAP1S was described as a member of the MAP1 family proteins in our laboratory, we were interested in the further characterisation of MAP1S by biochemical and genetic approaches. Therefore, I set out to analyse posttranslational modifications of MAP1S in comparison to MAP1A and MAP1B. As the S-nitrosylation of MAP1B leads to enhanced interaction with microtubules and leads to axon retraction (Stroissnigg et al., 2007), I wanted to investigate the potential S-nitrosylation of MAP1S and its impact on microtubule binding. Additionally, I was interested in the potential formation of heterotypic complexes formed from all three MAP1 protein subunits. However, the main aim of this project was to generate MAP1S deficient mice. By analysing these mice, I expected to gain more insight into the *in vivo* function of MAP1S. MAP1S is known to be expressed in all tissues and at all development stages. Therefore, I intended to generate conditional knockout mice and to look especially into the development of MAP1S knockout mice.

**PART I –  
POSTTRANSLATIONAL MODIFICATIONS  
OF MAP1S  
IN COMPARISON TO MAP1A AND MAP1B**

# RESULTS

## Homotypic and heterotypic complexes of MAP1 proteins

All three MAP1 proteins are synthesised as precursor proteins and cleaved posttranslationally into a HC and a LC. Co-immunoprecipitation and co-purification analyses revealed that the HC and the LC of each protein can form a homotypic protein complex (Orban-Nemeth et al., 2005; Schoenfeld et al., 1989). Additionally, a heterotypic complex consisting of the MAP1B LC and the MAP1A HC was found (Kuznetsov et al., 1986; Schoenfeld et al., 1989). Furthermore, LCs themselves can oligomerise. It was shown that the MAP1B LC can interact with itself and with the LC of MAP1A (Noiges et al., 2006; Tögel et al., 1998). To investigate the formation of a heterotypic complex consisting of the MAP1B HC and the MAP1A LC, I performed co-immunoprecipitation analysis of murine brain. Therefore, brain lysates were immunoprecipitated with an antibody against MAP1A LC and analysed by immunoblotting. MAP1A HC, as well as MAP1B HC were found in the precipitates (figure 2). Furthermore, the reciprocal co-immunoprecipitation was performed (figure 3) to confirm this interaction (Noiges et al., 2006).

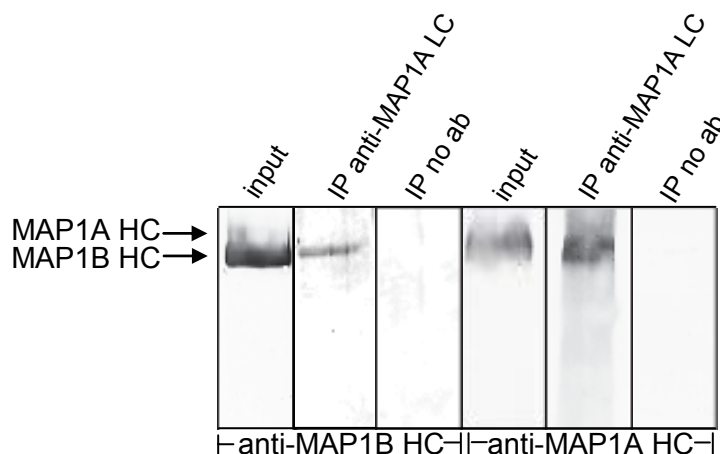


**Figure 2. MAP1B HC co-immunoprecipitated with the MAP1A LC.** Whole brain protein lysates of 13-day-old mice (input) were immunoprecipitated (IP) with an antibody against the MAP1A LC (anti-MAP1A LC) or without antibody (no ab) as negative control. Precipitates were analysed by SDS-PAGE and immunoblotting with antibodies against the MAP1B HC (anti-MAP1B HC) or

MAP1A HC (anti-MAP1A HC). The position of the respective heavy chain on the blot is indicated. A fraction of MAP1B HC present in the lysate was co-immunoprecipitated with anti-MAP1A LC.

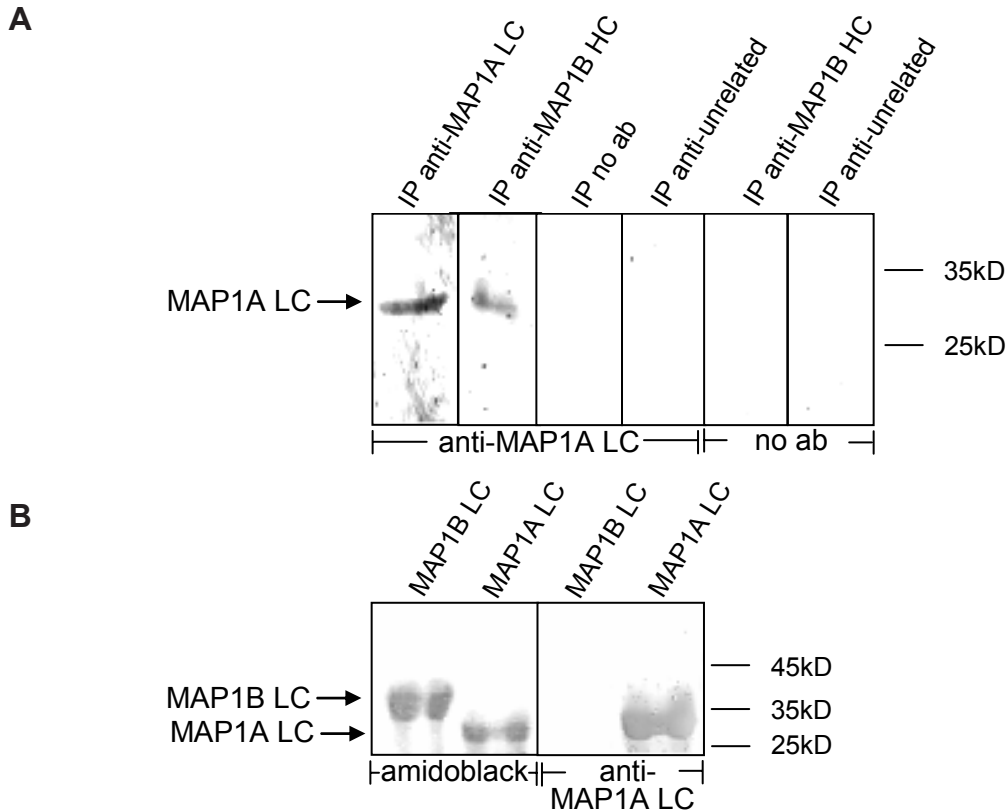


**Figure 3. MAP1A LC co-immunoprecipitated with the MAP1B HC.** (A) Whole brain protein lysates of 21-day-old mice (input) were immunoprecipitated (IP) with an antibody against the MAP1B HC (anti-MAP1B HC), without antibody (no ab) or with an antibody against an unrelated protein (chFIP-2; anti-unrelated). Precipitates were analysed by SDS-PAGE and immunoblotting with an antibody against the MAP1A LC (anti-MAP1A LC) or with the secondary antibody only (no ab). The position of the MAP1A LC is indicated. The MAP1A LC was precipitated from brain lysates with the antibody against MAP1A LC (anti-MAP1A LC) and co-immunoprecipitated with the antibody against MAP1B HC (anti-MAP1B HC). Controls with secondary antibody only (no ab) were done to rule out that the MAP1A LC signal after precipitation with MAP1B HC was merely due to reaction of the second antibody with the light chain of the antibody used in immunoprecipitation which is similar in size to MAP1A LC. (B) Approximately 1µg of recombinant MAP1B LC or MAP1A LC were fractionated on SDS-PAGE, blotted and probed with amido black to reveal the presence of the two proteins on the blot or with anti-MAP1A LC (anti-MAP1A LC). The antibody reacted exclusively with MAP1A LC.

To identify binding domains, co-transfections and blot overlay analysis using recombinant protein domains were performed. Two MAP1 homology (MH) domains, namely MH1 and MH3, of MAP1B HC were found to interact with the LCs of MAP1B and MAP1A (Noiges et al., 2006; Tögel et al., 1998). The interactions between the N terminus of the MAP1B HC and the MH3 domain of the MAP1A LC and the MH3 domain of the MAP1B LC were shown recently in a yeast 2-hybrid  $\beta$ -galactosidase assay. The interactions of the MAP1A LC with the MH3 and the MH1 domains of MAP1B were demonstrated in blot overlay assay. Consequently, it was assumed that heterotypic complexes are formed due to the binding of the MH1 domain to the MH3 domain (Noiges et al., 2006). MH domains are shared by all MAP1 proteins (Langkopf et al., 1992; Noiges et al., 2006; Orban-Nemeth et al., 2005). Figure 4 shows the schematic representation of MAP1A, MAP1B and MAP1S indicating MH1, 2, and 3.

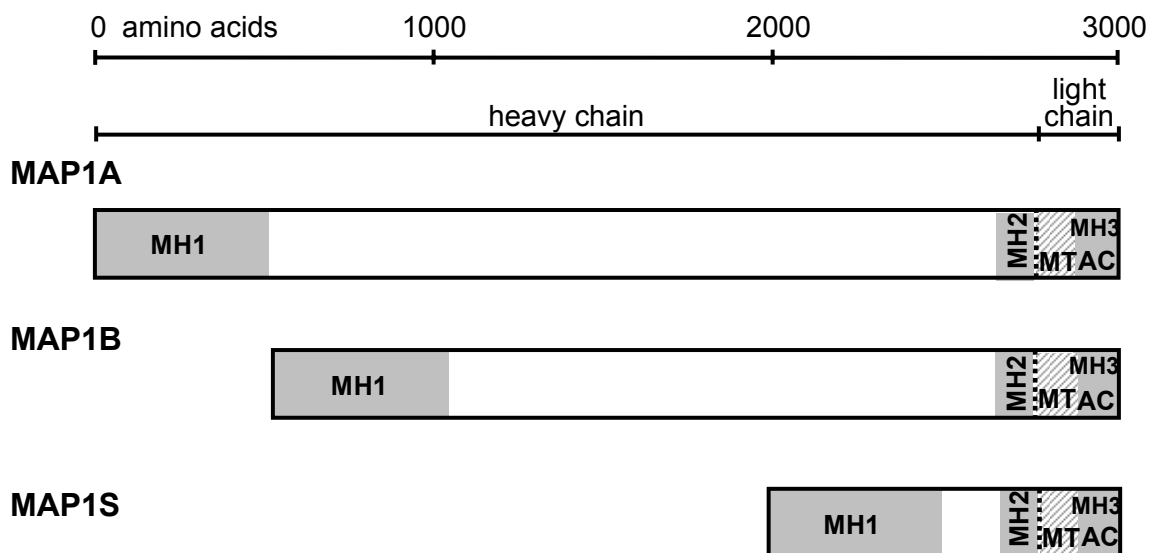


**Figure 4. Schematic representation of MAP1 proteins.** Grey boxes indicate conserved homologous domains (MH1, MH2, and MH3) of MAP1A, MAP1B, and MAP1S. Binding sites of the LCs to microtubules (MT) and actin (AC) are indicated. The microtubule binding domains are not conserved in sequence.

MAP1S shares these sequence homology domains. Thus, I wanted to investigate potential heterotypic interactions including MAP1S. First, potential complex formation between MAP1S LC and MAP1B HC were analysed in cultured cells. MAP1S LC alone localised on microtubules, the MH1 domain of MAP1B alone was distributed diffusely in the cytoplasm. In the presence of

MAP1S light chain, the MH1 domain of MAP1B was found to co-localise with MAP1S LC on microtubules (figure 5), indicating that the MH1 domain of MAP1B could interact with MAP1S LC.

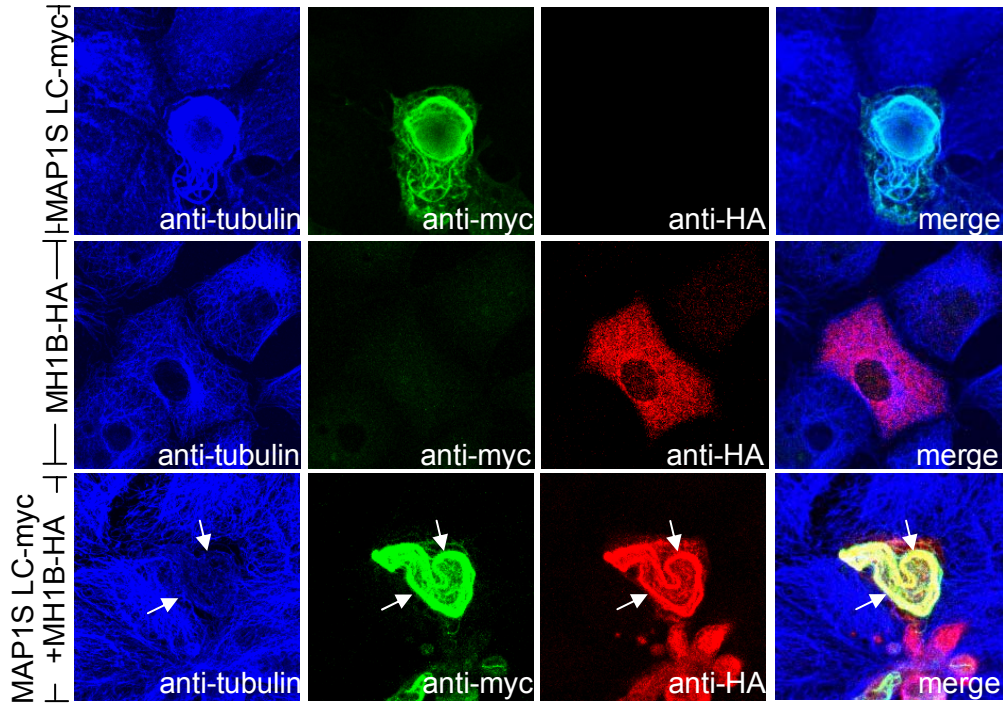


**Figure 5. MAP1S LC forms a complex with the MH1 domain of MAP1B HC.** PtK2 cells were transfected with constructs encoding myc-tagged MAP1S LC (MAP1S LC-myc), HA-tagged MH1 domain of MAP1B HC (MH1B-HA) or co-transfected with both constructs. After incubation for 48 hours to allow for protein expression, cells were fixed and analysed by triple immunofluorescence microscopy using antibodies against tubulin (anti-tubulin), the myc-tag (anti-myc) and the HA-tag (anti-HA). MAP1S LC was localised on microtubules, MH1B was diffusely distributed throughout the cytoplasm. In the presence of MAP1S LC, MH1B was found to co-localise with MAP1S LC on microtubules (arrows).

Next, the potential heterodimer formation of MAP1S LC and MAP1B LC was analysed. PtK2 cells were co-transfected with MAP1S LC and the MH3 domain of MAP1B. MAP1S LC alone localised on microtubules, the MH3 domain of MAP1B alone was distributed in the nucleus and in the cytoplasm. In the presence of MAP1S LC, the MH3 domain of MAP1B was found to co-localise with MAP1S LC on microtubules, indicating that the MH3 domain of MAP1B

could bind to MAP1S LC and the two LCs could possibly form heterodimers (figure 6).

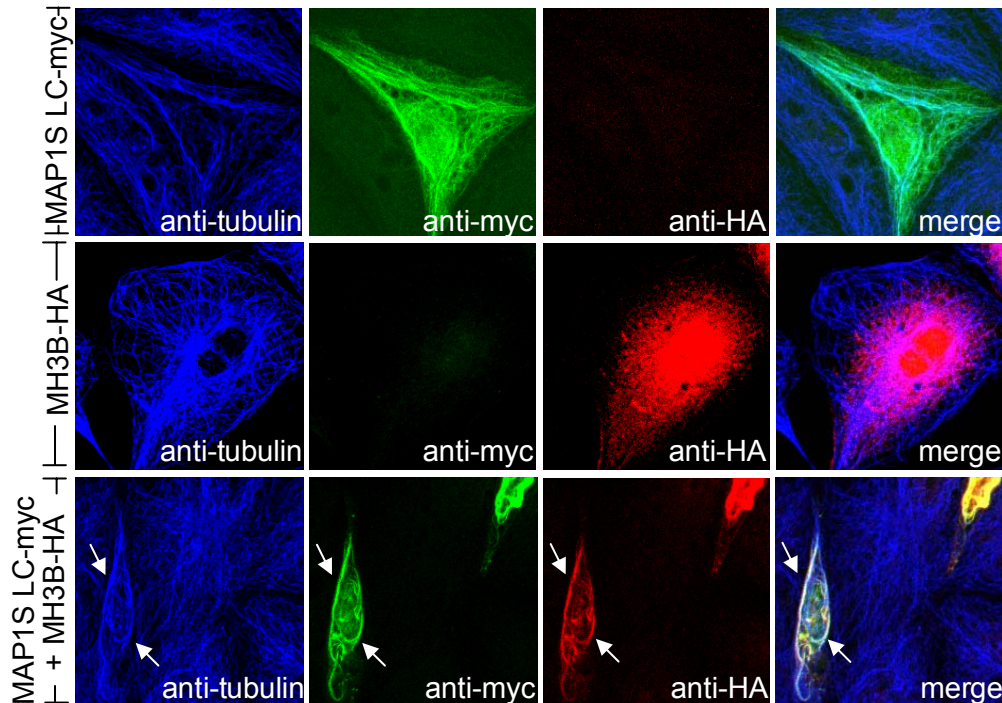


**Figure 6. MAP1S LC interacts with the MH3 domain of MAP1B LC.** PtK2 cells were transfected with constructs encoding myc-tagged MAP1S LC (MAP1S LC-myc), HA-tagged MH3 domain of MAP1B LC (MH3B-HA) or co-transfected with both constructs. After incubation for 48 hours to allow for protein expression, cells were fixed and analysed by triple immunofluorescence microscopy using antibodies against tubulin (anti-tubulin), the myc-tag (anti-myc) and the HA-tag (anti-HA). MAP1S LC was localised on microtubules, MH3B was diffusely distributed in the nucleus and in the cytoplasm. Nuclear localisation of MH3B was observed previously (Tögel, 1998) and is probably due to passive diffusion of this protein domain into the nucleus due to its small size. In the presence of MAP1S LC, MH3B was found to co-localise with MAP1S LC on microtubules (arrows).

Blot overlay analysis using recombinant proteins was performed to confirm the interaction between MAP1S LC and MAP1B LC (figure 7). Immunoblotting with antibodies against MAP1B LC showed that recombinant MAP1B LC could interact with recombinant MAP1S LC fractionated on SDS-PAGE.



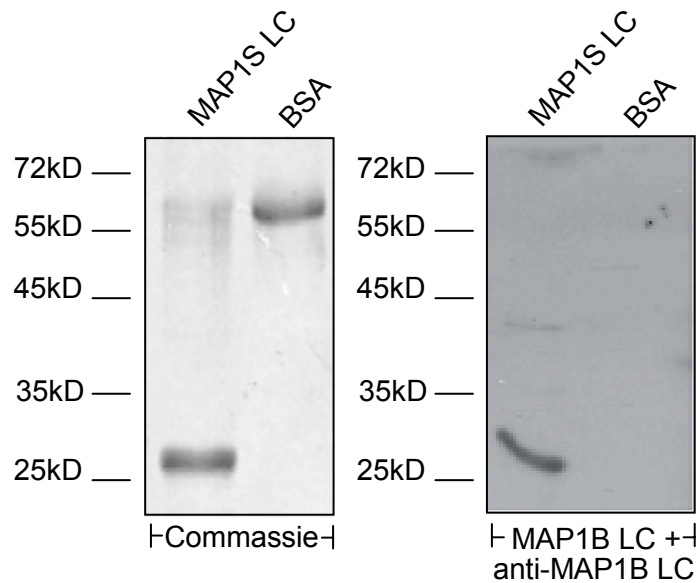


**Figure 7. Interaction of MAP1S LC with MAP1B LC.** 3-6 $\mu$ g (depending on the protein size to achieve equal molarity) of purified His-tagged recombinant MAP1S LC and BSA (negative control) were fractionated by SDS-PAGE. The gel was stained with Commassie to verify the protein content. Replica gels were blotted, probed with purified recombinant His-tagged MAP1B LC and immunodecorated with antibodies against MAP1B LC (anti-MAP1B LC). MAP1S LC, but not BSA, interacted with MAP1B LC.

### **The potential S-nitrosylation of MAP1S and its influence on microtubule binding compared to other MAP1 proteins**

It was shown that MAP1B LC is S-nitrosylated on cys 2457 (Stroissnigg et al., 2007). Sequence alignment of MAP1A LC, MAP1B LC and MAP1S LC revealed that all three LCs contain two cysteins and that the nitrosylated cystein of the MAP1B LC is conserved in all three LCs (figure 8).

```

MAP1A LC madpeglsseesgrverlre--kgrpgrrapg-rakpasparrl
MAP1B LC mvdpealaieqnlgkalkkdlkekaktkkggtktsksspvkkg
MAP1S LC mvdpealpprarqplnttn--psr-srkapa-rpsasatpra

MAP1A LC dirgk---rsptpg--kgpvdrtsr-----t
MAP1B LC dgkskpsaaspkpgalkessdkvsrvaspkkesvekamkttt
MAP1S LC atvaa---kktgpa---gdrnrpls-----a

MAP1A LC vprprstpsqvtsaeekdghspmsk-glvnglkag----stal
MAP1B LC tpevkatrggeekdetknaanasas-ksvktatagpgttktak
MAP1S LC rsepadrpgrvpltrkpsvpktvpkmasatrlssg----psgr

MAP1A LC gskggsppvyvdlayipnhcsgktadqdffrrvrasyyvvs
MAP1B LC sstvpplpvyldlcyipnhsnsknvdveffkrvrssyyvvs
MAP1S LC paplaagspvylldaylpgggagh-ldqnfflrvalcyvisg

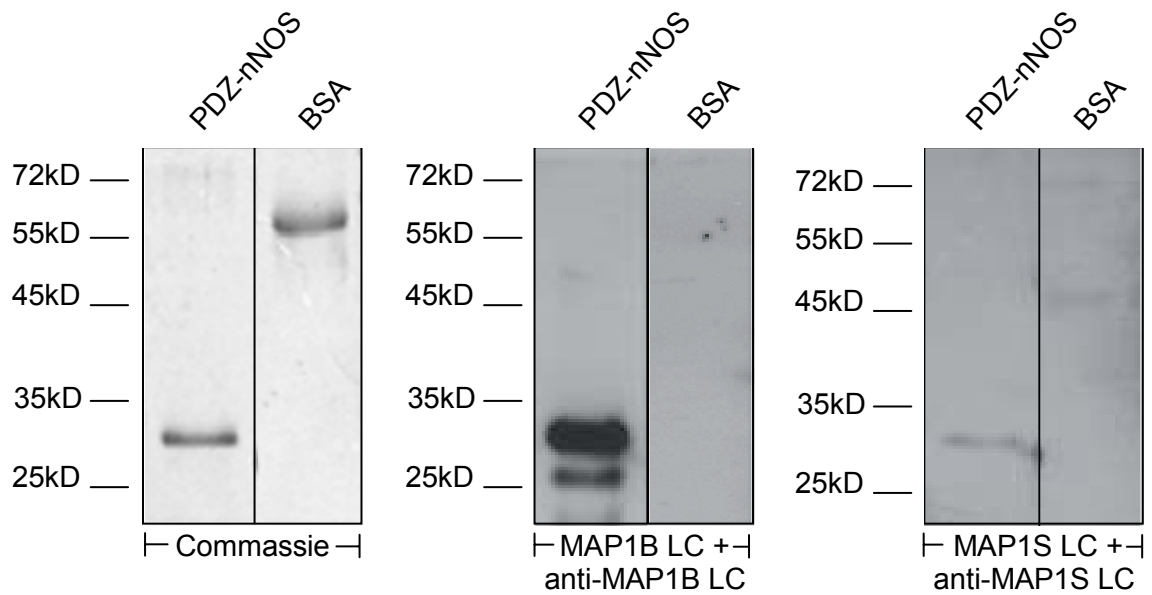
MAP1A LC ndpangepsravldallegkaqwenlqvthdtevtrew
MAP1B LC ndpaaeepsravldallegkaqwsnmqvthdsevmrew
MAP1S LC qgqrqeeqlravldallagkrqwdldlqvthdtevtrew

MAP1A LC yqqtheqqqqlnvlvlassstvvmqdesfpackief
MAP1B LC yqethekqqdlnimvlassstvvmqdesfpackiel
MAP1S LC yeethaqhgalgirvlgsgslvsmqdeafpackvef

```

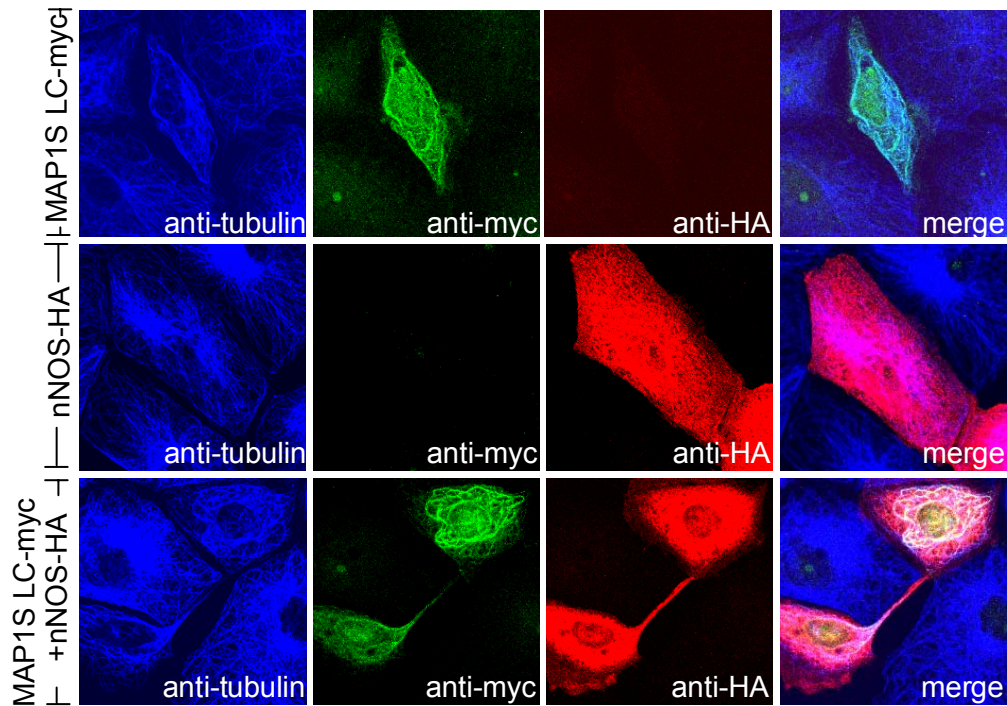
**Figure 8. Sequence alignment of MAP1B, MAP1A and MAP1S LCs.** Sequences of murine MAP1A LC, MAP1B LC and MAP1S LC were compared. Blue letters indicate amino acids conserved in all three proteins, orange letters amino acids conserved in MAP1A and MAP1B, green letters amino acids conserved in MAP1A and MAP1S and red letters amino acids conserved in MAP1B and MAP1S. All three MAP1 LC sequences contain two cysteines (in squares). The cysteine at the C terminus (cys 2457 in MAP1B, which can be nitrosylated) is conserved in its position and flanking sequences in all three LCs.

One requirement for the S-nitrosylation is the close proximity of the nitric oxide producing enzyme nNOS and its target protein (Stamler et al., 1997). Evidence for the interaction of MAP1B LC with the PDZ domain of nNOS was obtained by yeast 2-hybrid  $\beta$ -galactosidase assay (Stroissnigg et al., 2007). To analyse the interaction between MAP1S LC and nNOS, blot overlay analysis with recombinant proteins was performed (figure 9). The interaction between MAP1B and the PDZ domain of nNOS could be confirmed and a weak interaction between MAP1S and nNOS was also found.



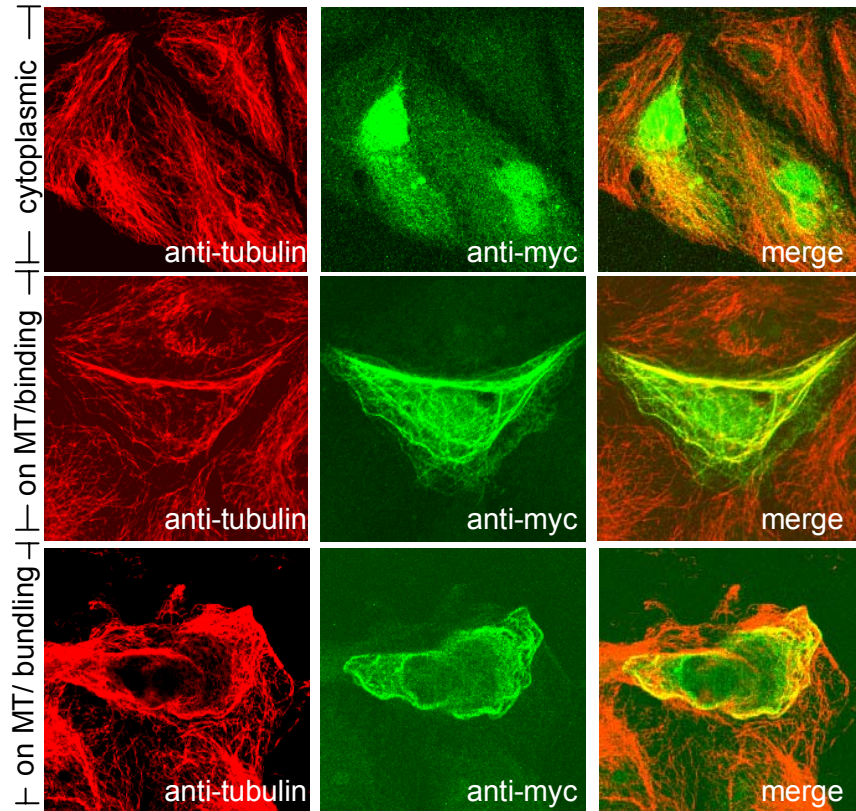
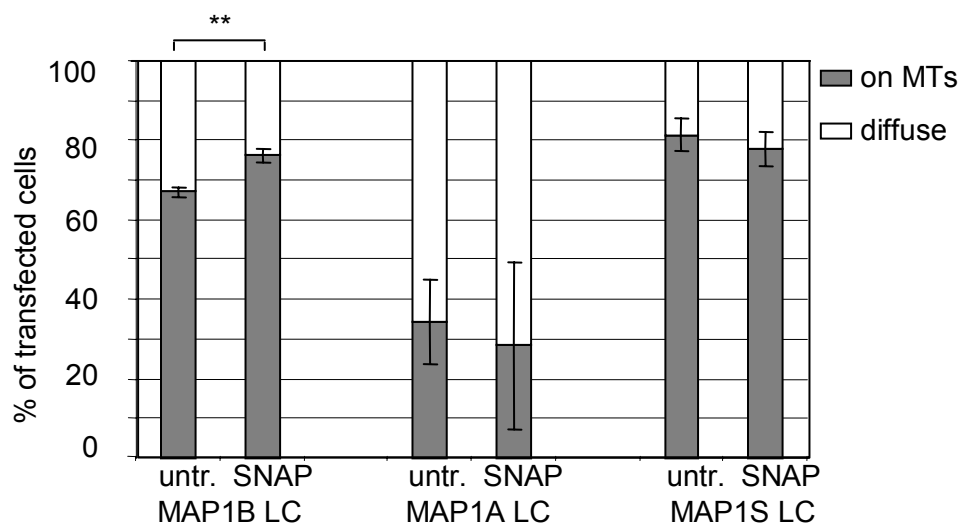
**Figure 9. Interaction of MAP1B LC and MAP1S LC with the PDZ domain of nNOS.** 3-6 $\mu$ g (depending on the protein size to achieve equal molarity) protein purified His-tagged recombinant PDZ-domain of nNOS (PDZ-nNOS) and BSA (as negative control) were fractionated by SDS-PAGE. The gel was stained with Coomassie to verify the protein content. Replica gels were blotted, probed with recombinant His-tagged MAP1B LC or with recombinant MAP1S LC and immunodecorated with antibodies against MAP1B LC (anti-MAP1B LC) or MAP1S LC (anti-MAP1S LC), respectively. MAP1B LC interacted with the PDZ domain of nNOS (the upper band reflects the band detected with Coomassie, the lower band shows the binding of MAP1B LC to a minor protein species perhaps representing a degradation product of PDZ-nNOS isolated from E.coli) and MAP1S LC interacted weakly with the PDZ domain of nNOS.

Moreover, interaction and close proximity of MAP1B LC and nNOS was shown in co-transfected PtK2 cells. Whereas nNOS was found to be diffuse in cytoplasm when transiently transfected in PtK2 cells, it was found on microtubules co-localising when co-transfected with MAP1B LC. Likewise, the interaction between MAP1S LC and nNOS was analysed by co-transfecting PtK2 cells. PtK2 cells were co-transfected with MAP1S LC and the full length nNOS protein. In contrast to the results obtained with MAP1B LC, nNOS was still found diffusely distributed throughout the cytoplasm despite the presence of MAP1S LC on microtubules suggesting that nNOS and MAP1S do not interact in vivo (figure 10).



**Figure 10. MAP1S LC was not found to bind to nNOS in vivo.** PtK2 cells were transiently transfected with myc-tagged MAP1S light chain (MAP1S LC-myc), HA-tagged nNOS (nNOS-HA) or co-transfected with both constructs. After incubation for 48 hours to allow for protein expression, cells were fixed and analysed by triple immunofluorescence microscopy using antibodies against tubulin (anti-tubulin), the myc-tag (anti-myc) and the HA-tag (anti-HA). MAP1S LC was localised on microtubules, nNOS was diffusely distributed throughout the cytoplasm in the absence or presence of MAP1S LC.

S-nitrosylation of MAP1B by treatment with the NO donor SNAP increased its microtubule binding activity (Stroissnigg et al., 2007). To analyse if the potential nitrosylation of MAP1A and MAP1S influences their microtubule binding activity, PtK2 cells were transiently transfected with MAP1A LC, MAP1B LC, or MAP1S LC and treated with SNAP or left untreated. While the binding of MAP1B LC to microtubules was significantly increased after SNAP treatment, no changes were observed in MAP1A or MAP1S expressing cells after SNAP treatment. In general, MAP1S LC was found more often on microtubules than MAP1B LC and MAP1A LC (figure 11).

**A****B**

**Figure 11. Localisation of the LCs of MAP1B, MAP1A, and MAP1S on microtubules after treatment with the NO donor SNAP.** PtK2 cells were transiently transfected with the myc-tagged LCs of MAP1B, MAP1A, or MAP1S. After incubation for 48 hours to allow for protein expression, cells were treated with 100µM SNAP for 4 hours or left untreated and subsequently were fixed and analysed by double immunofluorescence microscopy using antibodies against tubulin (anti-tubulin) and the myc-tag (anti-myc). Cells were scored for localisation of the ectopically expressed protein in the cytoplasm or on microtubules. **(A)** Representative immunofluorescence

pictures were taken from transfected cells showing the expressed construct distributed diffusely in the cytoplasm (cytoplasmic) or binding (on MT/binding) to or binding to and bundling to microtubules (on MT/bundling). (B) Results from three independent experiments are presented as mean values, error bars representing standard deviations. Whereas the binding of MAP1B LC to microtubules was significantly increased after SNAP treatment ( $p=0.004$ , t-test), no changes were observed in MAP1A LC or MAP1S LC expressing cells.

Next, PtK2 cells were transfected with constructs encoding full length proteins of MAP1B, MAP1S and a mutated, uncleavable form of MAP1B. The binding of MAP1B to microtubules was increased after SNAP treatment, confirming previous results (Stroissnigg, 2007). Binding of MAP1S or the uncleavable mutant of MAP1B to microtubules was not increased after SNAP treatment (figure 12).

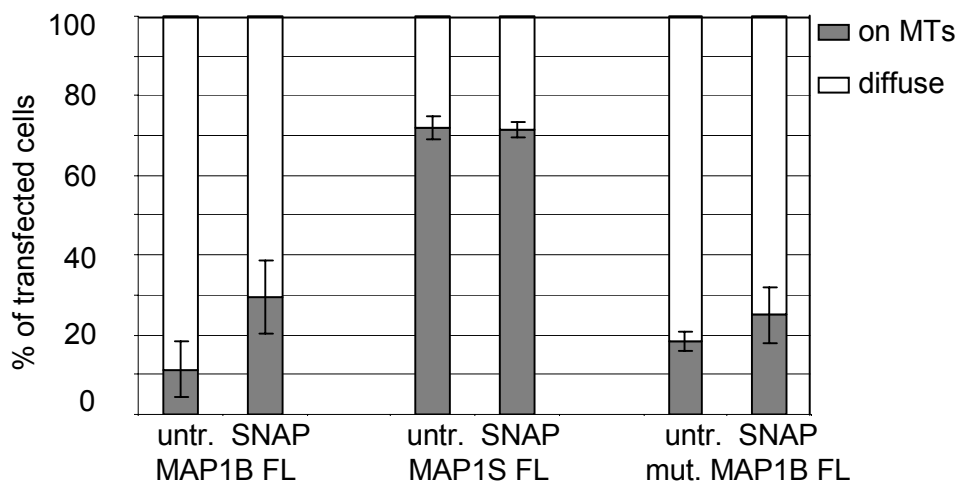


**Figure 12. Binding of MAP1B FL, MAP1S FL, and an uncleavable MAP1B FL mutant to microtubules after treatment with the NO donor SNAP.** PtK2 cells were transiently transfected with myc-tagged MAP1B FL, MAP1S FL or an uncleavable MAP1B FL mutant (lacking aa 2191-2221). After incubation for 48 hours to allow for protein expression, cells were treated with 100 $\mu$ M SNAP for 4 hours or left untreated, fixed, and analysed by double immunofluorescence microscopy using antibodies against tubulin and the myc-tag. Cells were scored for localisation of the ectopically expressed protein in the cytoplasm or on microtubules. Results from three independent experiments are presented as mean values, error bars representing standard deviations. A tendency of increased binding of MAP1B FL to microtubules was observed after SNAP treatment confirming previous results (Stroissnigg, 2007).

Binding of MAP1S FL or the uncleavable mutant of MAP1B FL to microtubules was not increased after SNAP treatment.

When transiently overexpressed in PtK2 cells, MAP1S FL and MAP1S LC were found predominantly on microtubules (in 70-80%) of the cells. The appearances of microtubules decorated with MAP1S can either remain unchanged compared to non-transfected cells or changed to microtubule bundles (figure 11A). We were interested, whether SNAP can alter the ratio between MAP1S binding and bundling of microtubules. However, no differences were found after SNAP treatment. MAP1S LC was found more often to bundle microtubules compared to the MAP1S FL, independent of SNAP (figure 13).

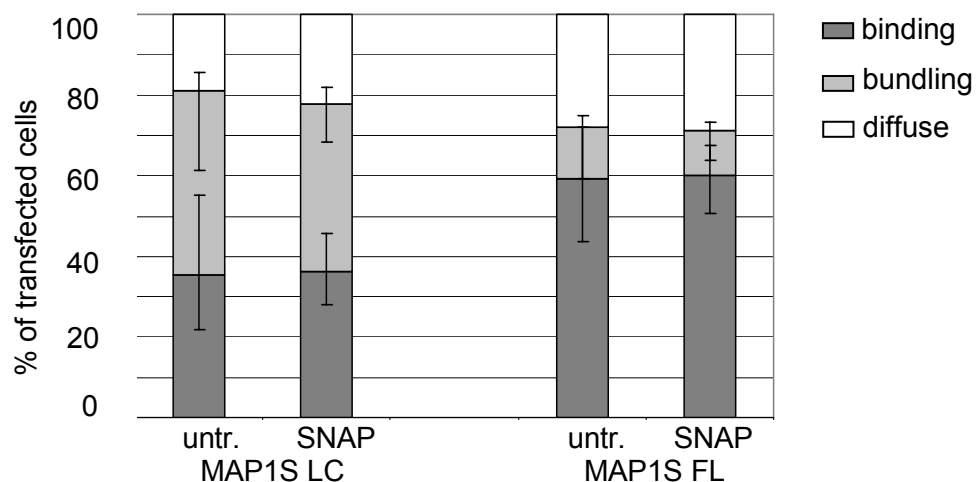


**Figure 13. Binding to and bundling of microtubules by MAP1S after treatment with the NO donor SNAP.** PtK2 cells were transiently transfected with myc-tagged MAP1S LC or MAP1S FL. After incubation for 48 hours to allow for protein expression, cells were treated with 100 $\mu$ M SNAP for 4 hours or left untreated, fixed and analysed by double immunofluorescence microscopy using antibodies against tubulin and the myc-tag. Cells were scored for localisation of the ectopically expressed protein in the cytoplasm, binding to, and bundling of microtubules. Results from three independent experiments are presented as mean values, error bars representing standard deviations. No effects of SNAP on microtubule binding and bundling of MAP1S LC or MAP1S FL were observed.

## The influence of S-nitrosylation on the formation of an additional LC isoform

In our laboratory, an additional MAP1B LC isoform was detected with an antibody against MAP1B LC as an additional band in immunoblotting analysis of protein lysates of brain under non-reducing conditions (unpublished data, Daniel Lackner). We were interested to investigate if LCs of MAP1A and MAP1S also form additional isoforms and if the formation of MAP1B isoforms is connected to its nitrosylation. I confirmed the detection of the additional MAP1B LC isoform in brain lysates and also detected it in lysates of neuroblastoma (N2a) cells. Results concerning MAP1A isoforms were not clear. Concerning MAP1S LC, only one band was found (figure 14).

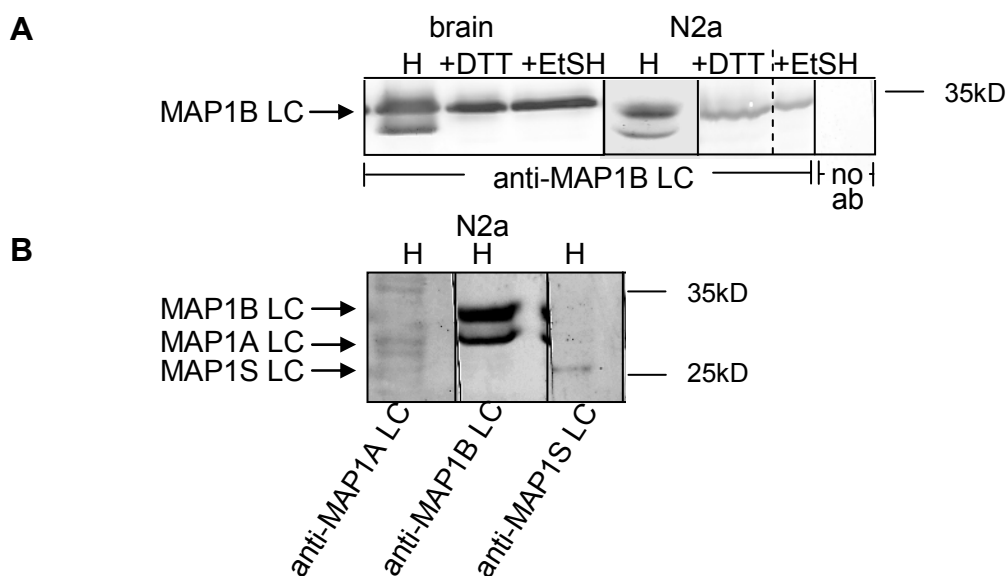


**Figure 14. An additional MAP1B LC isoform was detected in immunoblotting analysis of protein lysates of brain and neuroblastoma (N2a) cells under non-reducing conditions.** (A) Whole mouse brain (adult) and N2a cells were homogenised in a non-reducing buffer (H). Aliquots of the lysates were treated with DTT (+DTT) or EtSH (+EtSH). 120µg of protein from these samples were analysed by SDS-PAGE and immunoblotting with an antibody against MAP1B LC (anti-MAP1B LC) or with secondary antibody only (no ab). The position of the MAP1B LC is indicated. Two bands were seen on blots of brain and N2a cell lysates under non-reducing condition. The lower band was not detected after adding DTT or EtSH. (B) 120µg of protein (total lysate) from N2a cells, homogenised in a non-reducing buffer (H), were analysed by



SDS-PAGE and immunoblotting with antibodies against MAP1A LC (anti-MAP1A LC), MAP1B LC (anti-MAP1B LC) or MAP1S LC (anti-MAP1S LC). Results obtained with anti-MAP1A LC are not clear, as more, probably unspecific, bands were detectable. Two bands were detected with anti-MAP1B LC, but only one with anti-MAP1S LC.

To analyse the role of nitrosylation of MAP1B LC in the formation of the additional band, N2a cells were transfected with constructs encoding myc-tagged MAP1B LC or mutated MAP1B LCs, in which one of two cysteine residues was replaced with serine. Both cysteins were necessary for the appearance of the additional MAP1B LC band (figure 15A). In addition, after treatment with NPA, an nNOS inhibitor, only one band appeared (figure 15B). This suggests that the nitrosylation of MAP1B LC and the presence of the two cysteins were important for the formation of the additional MAP1B LC isoform. To test if this formation occurs in vivo, I treated N2a cells with NEM, which reacts with and blocks free S-H groups in the cells in vivo. Only one band appeared after treatment with NEM, indicating that the additional band of MAP1B LC is formed not in vivo, but during the homogenisation process (figure 15C).

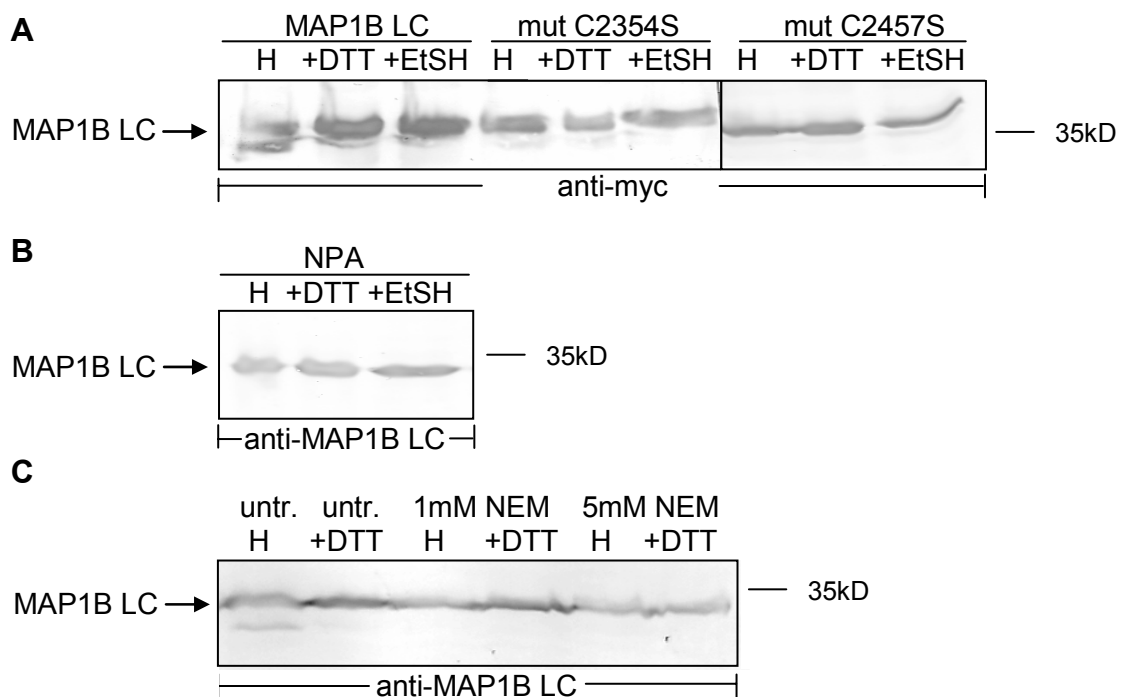


**Figure 15. Both cysteins of MAP1B LC and the activity of nNOS were necessary to form an additional MAP1B LC isoform. (A)** N2a cells were transfected with

constructs encoding myc-tagged MAP1B LC, myc-tagged C2354S mutant or the myc-tagged C2457S mutant. In these mutants the cysteine on position 2354 or 2457 is replaced with serine. 120µg of protein (total lysate) were analysed by SDS-PAGE and immunoblotting with an antibody against myc (anti-myc). The position of the MAP1B LC is indicated. Two bands were observed on blots of lysates of cells transfected with constructs encoding MAP1B LC, only one after transfection with mutated MAP1B LCs. Both cysteines were necessary for the formation of the additional MAP1B LC band. **(B)** N2a cells were treated with 1mM of the nNOS inhibitor NPA for 1 hour and homogenised in a non-reducing buffer (H). Aliquots of the lysates were treated with DTT (+DTT) or EtSH (+EtSH). 120µg of protein from these samples were analysed by SDS-PAGE and immunoblotting with an antibody against MAP1B LC (anti-MAP1B LC). Only one band of MAP1B LC appeared after NPA treatment. The activity of nNOS was necessary for the formation of the additional MAP1B LC. **(C)** N2a cells were left untreated (untr.) or treated with 1mM or 5mM NEM (binds to S-H groups in the cells in vivo) for 15 minutes and homogenised in a non-reducing buffer (H). Aliquots of the lysates were treated with DTT (+DTT). 120µg of protein (total lysate) were analysed by SDS-PAGE and immunoblotting with an antibody against MAP1B LC (anti-MAP1B LC). Two bands were detected in untreated cell lysates. Only one band was visible after treatment with NEM, indicating that the additional band of MAP1B LC is formed not in vivo, but during the homogenisation process.

## **Posttranslational cleavage of MAP1S**

All members of the MAP1 family are synthesised as precursor proteins and posttranslationally cleaved into HC and LC. Whereas MAP1A and MAP1B precursor proteins are hardly detected in protein extracts, MAP1S appears to be cleaved in a tissue specific pattern (Orban-Nemeth et al., 2005). I confirmed the cleavage pattern of MAP1S. Whereas MAP1S was completely cleaved in brain and testis cells, it was only partially cleaved in lung and nearly completely uncleaved in spleen (figure 16). Sequence alignment of murine MAP1A, MAP1B and MAP1S revealed that the cleavage site is highly conserved (figure 17).

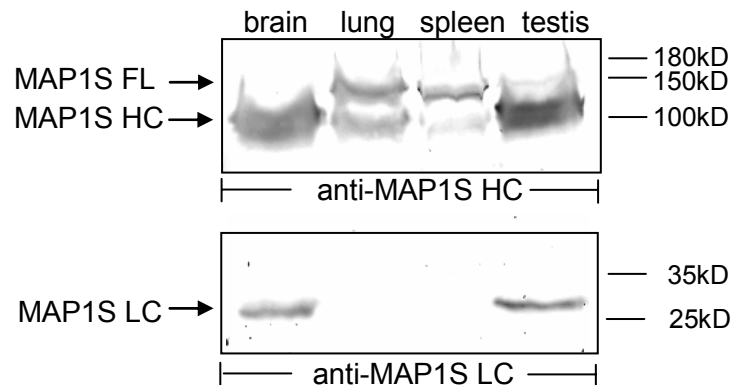


**Figure 16. Tissue specific cleavage pattern of MAP1S.** 120µg of protein (total lysate) from the indicated mouse tissues (adult) were analysed by SDS-PAGE and immunoblotting with affinity-purified antibodies against MAP1S HC (anti-MAP1S HC) or LC (anti-MAP1S LC). Protein bands of 120kD correspond to the uncleaved MAP1S FL polyprotein precursor (MAP1S FL). Protein bands of 100kD and 26kD correspond to the HC and the LC of MAP1S, respectively. The MAP1S precursor was not detectable in brain and testis indicating that most or all of it was cleaved into a HC and a LC. In contrast, the FL precursor was only partially cleaved in lung and spleen. In lung and spleen, a band corresponding to the LC was not detected with anti-MAP1S LC, probably due to the comparatively lower level of expression of MAP1S in these tissues and the lack of complete cleavage of the FL MAP1S polyprotein precursor.

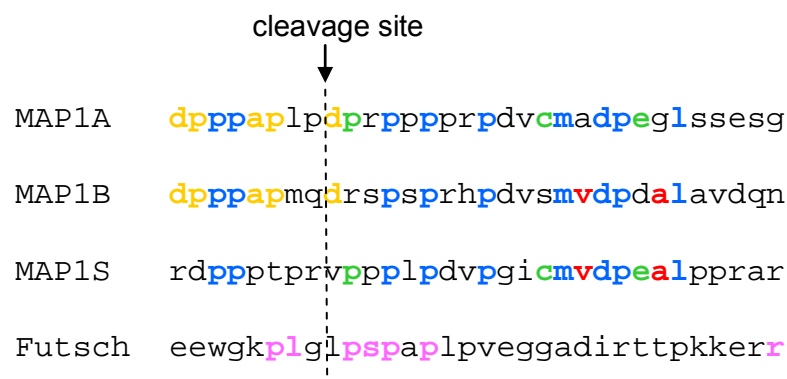


**Figure 17. MAP1 proteins including MAP1S are conserved around the presumptive cleavage site of the precursor protein.** Alignment of murine MAP1A, MAP1B, MAP1S, and drosophila Futsch showed a highly conserved sequence at the presumptive cleavage site (Zou et al., 2008a). Blue letters indicate amino acids conserved in all three proteins, orange letters amino acids conserved in MAP1A and MAP1B, green letters amino acids conserved in MAP1A and MAP1S, and red letters

amino acids conserved in MAP1B and MAP1S. Pink letters indicate amino acids conserved in Futsch and any of the murine MAP1 protein.

To investigate the cleavage of MAP1S, an appropriate cell culture system had to be found. Therefore, different cell lines were analysed by immunoblotting. N2a cells and NIH3T3 cells expressed partially cleaved MAP1S. In PtK2 cells no MAP1S was detected (figure 18).

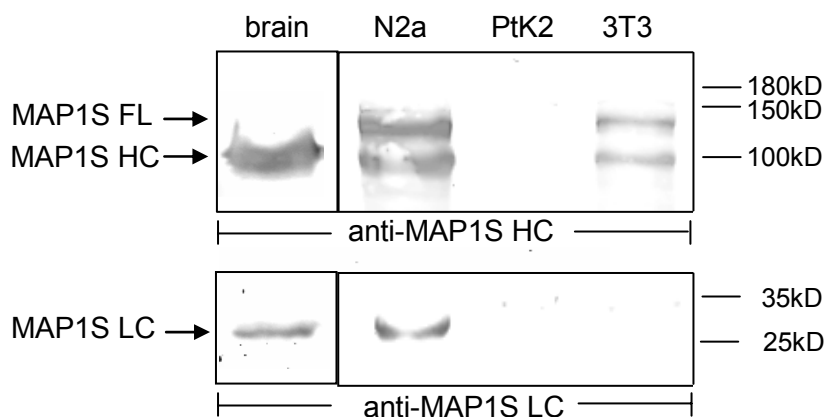


**Figure 18. Cleavage pattern of MAP1S in different cell lines.** 120µg of protein (total lysate) from adult mouse brain and the indicated cell lines were analysed by SDS-PAGE and immunoblotting with antibodies against MAP1S HC (anti-MAP1S HC) or LC (anti-MAP1S LC). Protein bands of 120kD correspond to the MAP1S FL. Protein bands of 100kD and 26kD correspond to the HC and the LC of MAP1S, respectively. MAP1S was expressed and partially cleaved in neuroblastoma N2a cells and NIH3T3 fibroblasts. MAP1S was not detected in PtK2 cells, perhaps due to the lack of crossreactivity of the anti-mouse MAP1S antibodies used here with potoroo MAP1S (PtK2 cells).

N2a cells, derived from murine neuroblastoma, were chosen to examine the length of time between the synthesis of MAP1S, its cleavage and its degradation. One method to measure the protein metabolism is to label proteins with <sup>35</sup>S methionine/cysteine as described under materials and methods. Due to difficulties with the immunoprecipitation of radioactively labelled cells, the small amount of protein and inconsistent results, a faster and easier method was used to examine cleavage time and time for degradation. N2a cells were treated with the protein translation suppressor cycloheximide for one to six hours and MAP1S proteins were analysed by immunoblotting. No differences in the

cleavage pattern were found, indicating that the MAP1S precursor as well as the HC were stable proteins with comparatively slow turnover (figure 19).

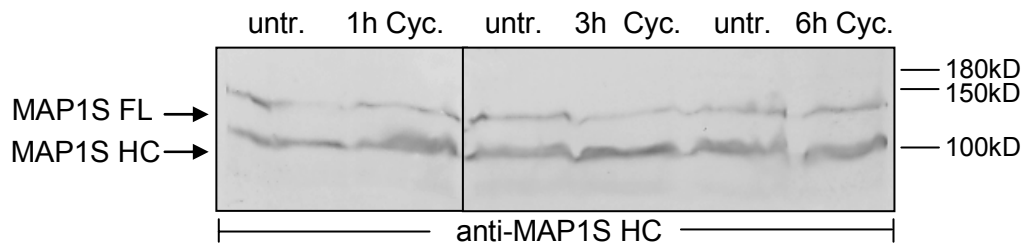


**Figure 19. Cleavage pattern of endogenous MAP1S in N2a cells after treatment with the protein synthesis inhibitor cycloheximide.** 120µg of protein (total lysate) from N2a cells treated with 100µg/ml cycloheximide (Cyc.) for 1, 3 or 6 hours or left untreated (untr.) were analysed by SDS-PAGE and immunoblotting with an antibody against MAP1S HC (anti-MAP1S HC). The positions of the MAP1S FL and the MAP1S HC are indicated. The protein level of MAP1S stayed constant over the tested period. No difference in the cleavage pattern was found, indicating that the MAP1S precursor as well as the HC were stable proteins with comparatively slow turnover.

### **The influence of S-nitrosylation on the posttranslational cleavage of MAP1S**

To analyse the potential influence of S-nitrosylation of MAP1S on the cleavage pattern of MAP1S, N2a cells were treated with the nNOS inhibitor NPA. Cell lysates were analysed by immunoblotting. Treatment with NPA had no influence on the cleavage pattern of endogenous or ectopically expressed MAP1S (figure 20).

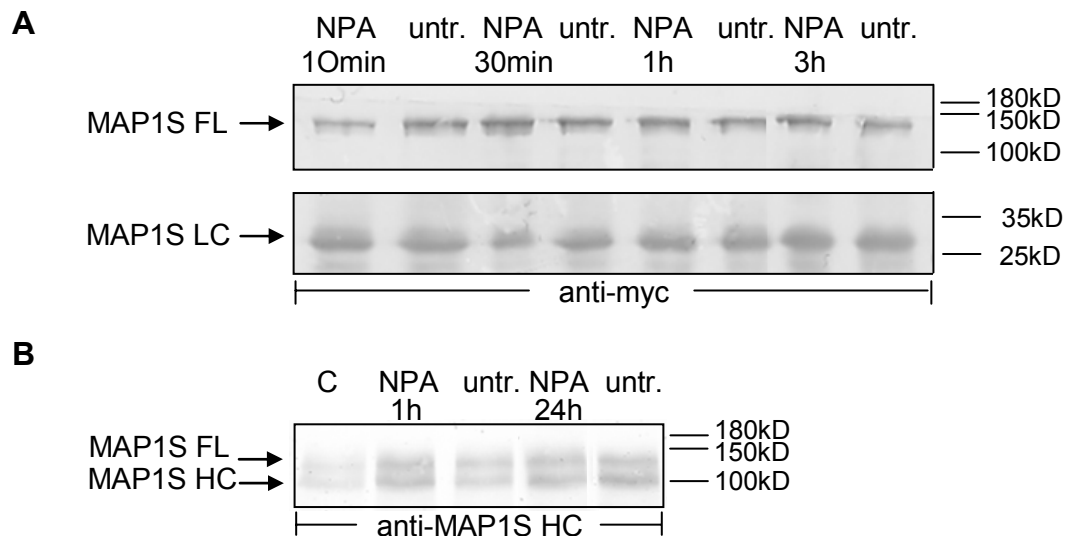


**Figure 20. N- $\omega$ -propyl-L-arginine (NPA) did not influence the cleavage pattern of MAP1S.** (A) N2a cells were transiently transfected with COOH-terminally myc-tagged MAP1S FL and treated with 1mM NPA in serumfree medium for 10 minutes, 30 minutes, 1 hour or 3 hours or left untreated (untr.). 120 $\mu$ g of protein (total lysate) from these cells were analysed by SDS-PAGE and immunoblotting with an antibody against myc (anti-myc). The positions of the myc-tagged MAP1S uncleaved precursor protein (MAP1S FL) and the MAP1S LC are indicated. (B) 120 $\mu$ g of protein (total lysate) from untransfected N2a cells grown in growth medium containing serum (C) or treated with 1mM NPA or without NPA (untr.) in serumfree medium for 1 or 24 hours were analysed by SDS-PAGE and immunoblotting with antibodies against MAP1S HC (anti-MAP1S HC). The positions of the MAP1S FL and the MAP1S HC were indicated. Treatment with NPA for 10 minutes showed decreased level of MAP1S FL, but this effect was not consistently observed in a repeated experiment (data not shown). Therefore we conclude that NPA had no influence on the cleavage pattern of the ectopically and endogenously expressed MAP1S.

## N- $\epsilon$ -acetylation of MAP1 proteins

To analyse the potential N- $\epsilon$ -acetylation of MAP1 proteins on lysine residues, microtubule proteins were purified from wild-type and MAP1B knockout mouse brains and analysed by immunoblotting. The antibody against N- $\epsilon$ -acetylated lysine showed that MAP1B LC was acetylated. MAP1S was not detected and therefore appeared to be not acetylated (figure21).

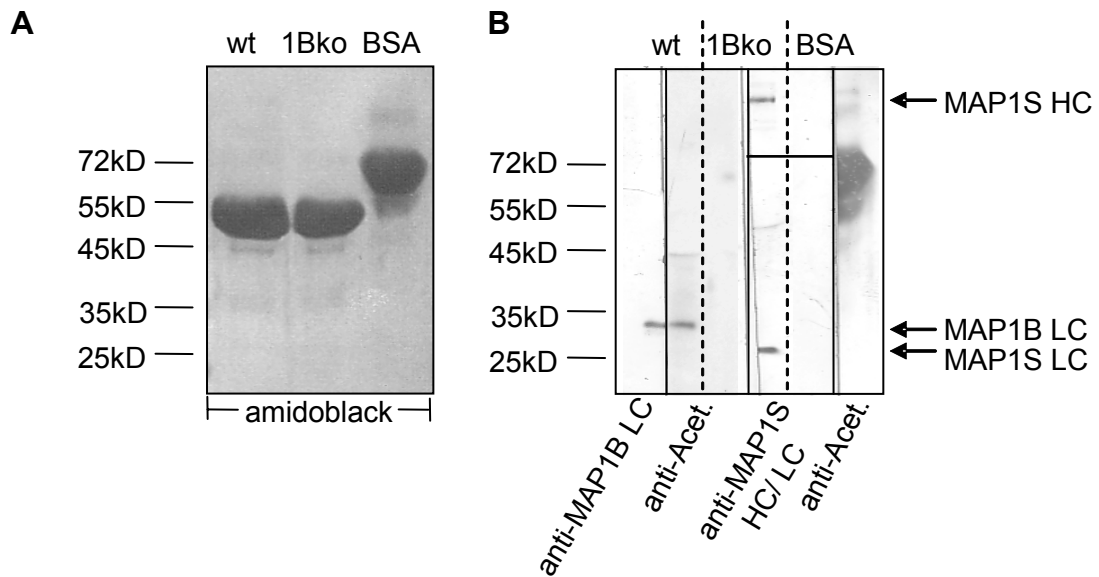


**Figure 21. MAP1B LC was acetylated.** Purified microtubule proteins from brains from one to four day old C57BL/6J (wt) or MAP1B knockout (1Bko) mice were analysed by SDS-PAGE and immunoblotting. Acetylated BSA was used as a positive control. **(A)** Blots were stained with amidoblack to verify protein content on the blot. **(B)** The same blots were then immunodecorated with antibodies against MAP1B LC (anti-MAP1B LC), N- $\epsilon$ -acetylated lysine (anti-Acet.), MAP1S HC (anti-MAP1S HC) and MAP1S LC (anti-MAP1S LC). Positions of MAP1S HC, MAP1S LC and MAP1B LC are indicated. Dashed lines indicate original protein lanes, solid lines show where the blot was cut for the incubation with indicated antibodies. The antibody against N- $\epsilon$ -acetylated lysine showed that MAP1B LC was acetylated. It remains unclear why the antibody against N- $\epsilon$ -acetylated lysine did not detect tubulin, which was expected to be acetylated.

# DISCUSSION

## Homotypic and heterotypic complexes of MAP1 proteins

Homotypic complexes, consisting of MAP1B HC-MAP1B LC, MAP1A HC-MAP1A LC, or MAP1S HC-LC, and the heterotypic complex consisting of MAP1A HC-MAP1B LC were found in co-immunoprecipitation analysis (Kuznetsov et al., 1986; Langkopf et al., 1992; Noiges et al., 2006; Orban-Nemeth et al., 2005; Schoenfeld et al., 1989). I found the heterotypic complex MAP1B HC-MAP1A LC in mouse brain at certain times in development, when both proteins are co-expressed. These heterotypic complexes may play an important role in the function of MAP1A and MAP1B, especially during brain development. The capacity to form homotypic as well as heterotypic complexes may provide neurons the opportunity to subtly regulate the formation of microtubules and actin filaments during the critical transition period, when neurons shift from axon extension to axon stabilisation and synaptogenesis (Noiges et al., 2002; Tögel et al., 1998). Due to results from blot overlay and yeast 2-hybrid  $\beta$ -galactosidase assays, we assumed that the homotypic as well as heterotypic complexes are formed through direct interaction between the MH1 domain of HCs and the MH3 domain of LCs (Noiges et al., 2006). As these domains are conserved between all three MAP1 proteins, MAP1S might also form heterotypic complexes. I could show in co-transfection experiments that the MAP1S LC can also form heterotypic complexes via MH1 and MH3 domains of MAP1B. Furthermore the interaction between MAP1S LC and MAP1B LC was shown in overlay blot assay with recombinant proteins.

Previous studies identified MAP1A as well as MAP1B complexes consisting of one HC and two LCs (Mei et al., 2000; Schoenfeld et al., 1989). To form such complexes, two LCs form probably homo- or heterodimers and bind as such to a single site in the HC (Noiges et al., 2006). Our results indicate that the MAP1S LC can integrate in these complex formations. On the one hand MAP1S LC could bind directly to the MAP1B HC, on the other hand MAP1S LC could bind indirectly to the MAP1B HC via forming a heterodimer with the MAP1B LC. Due to the conserved domains in MAP1A, MAP1S may also take part in the



formation of MAP1A complexes in the same way. While MAP1A is expressed at low levels at birth and then increases over the next three weeks and MAP1B is expressed at high levels at birth and then decreases, MAP1S is expressed at a high level at birth and remains at high levels in adulthood (Orban-Nemeth et al., 2005; Schoenfeld and Obar, 1994). Thus MAP1S is co-expressed with MAP1A or MAP1B at all times in brain development and putative heterotypic complexes may have specific individual properties, which are essential for the proper development and function of the murine brain.

### **The potential S-nitrosylation of MAP1S and its influence on microtubule binding compared to other MAP1 proteins**

The S-nitrosylation of the MAP1B LC was demonstrated in vivo, in cultured cells and in vitro. This nitrosylation of MAP1B LC leads to enhanced binding to microtubules and causes neurite retraction (Stroissnigg et al., 2007). We were interested to see whether the MAP1S LC is also S-nitrosylated. Sequence alignment illustrates that the nitrosylated cysteine of the MAP1B LC (cysteine 2457) is conserved in the MAP1A LC and MAP1S LC. As S-nitrosylation is a covalent modification of cysteine residues achieved through a non-catalysed chemical modification, it is not enzyme driven as for example phosphorylation. Therefore the reaction specificity does not rely on the recognition of a target structure by an enzyme (Martinez-Ruiz and Lamas, 2004). Nevertheless, due to the strong reactivity of the NO $\cdot$  radical the close proximity of the oxidising enzyme nNOS and its target protein is one of the requirements for S-nitrosylation (Martinez-Ruiz and Lamas, 2004; Stamler et al., 1997). In blot overlay assays, an interaction of the PDZ domain of nNOS and the MAP1S LC was seen, but this interaction was relatively weak compared to the interaction with MAP1B LC. In co-transfected PtK2 cells, no interaction between MAP1S LC and nNOS was found. Immunofluorescence analysis had revealed that the MAP1B LC interacts not only with the PDZ domain of nNOS, but there exist probably additional interaction sites, because the MAP1B LC was also co-localising with an nNOS mutant lacking the PDZ domain (Trančiková, 2007; Trančiková, PhD thesis 2007). These data suggest that, although the MAP1S

LC binds to the PDZ domain of nNOS *in vitro*, this binding is not efficient for the interaction of the MAP1S LC with the nNOS protein *in vivo*. MAP1S LC probably misses additional interaction sites, which might be necessary for the binding to nNOS *in vivo*. To clarify whether MAP1S LC is nitrosylated or not, more experiments would have to be done. Several methods are known to detect individual S-nitrosylated proteins. So far, the “biotin switch” method, in which the cysteine-bound NO is replaced by a biotin label, in combination with immunoblot to confirm modification of individual proteins would be the most adequate method to verify the S-nitrosylation of MAP1S LC (Jaffrey and Snyder, 2001; Martinez-Ruiz and Lamas, 2004).

The S-nitrosylation of MAP1B LC does not alter its interaction with actin (Stroissnigg, PhD thesis 2005), but leads to increased microtubule binding (Stroissnigg et al., 2007). When Ptk2 were transfected to transiently overexpress MAP1B FL or LC, treatment with the NO donor SNAP increased the microtubule binding activity of MAP1B (Stroissnigg et al., 2007; Trančíková, PhD thesis 2007). To compare the effect of the NO donor SNAP on the microtubule binding of MAP1A, MAP1B, and MAP1S, Ptk2 cells were transfected with constructs encoding MAP1A LC, MAP1B LC, MAP1S LC, MAP1B FL, MAP1S FL and an uncleavable mutant of MAP1B FL. Besides confirming the increase of the microtubule binding activity of MAP1B FL and LC, no other alterations were found after SNAP treatment. As both, MAP1S FL and MAP1S LC, were found predominantly on microtubules (70-80%), I speculated that the effect of the SNAP treatment might be masked and looked for changes in the ratio between MAP1S binding and bundling of microtubules. I could find no alteration after SNAP treatment in the ratio between MAP1S binding and bundling of microtubules. According to our results one might speculate that MAP1S and MAP1A are not modified by S-nitrosylation, but we cannot exclude it. If MAP1S and MAP1A LCs were to be nitrosylated, their nitrosylation would not affect their microtubule binding activity. Definitely, one can conclude that the regulation of the microtubule binding activity by S-nitrosylation is a unique and specific attribute of MAP1B LC among the members of the MAP1 family. Two recent reports indicated that MAP1B and MAP1S interfere with dynein motor activity and can block dynein-dependent retrograde transport (Ding et al., 2006a; Jimenez-Mateos et al., 2006). Stroissnigg et al. propose that the

increased binding of the MAP1B HC-LC complex to microtubules, due to S-nitrosylation of the MAP1B LC, might inhibit dynein action and lead to a reduction of the extension force, resulting in axon retraction (Stroissnigg et al., 2007). My findings suggest that MAP1S does not act via the same mechanism. Interestingly, the ability of the different LCs to bind to microtubules varies (34% of MAP1A LC, 67% of MAP1B LC, 81% of MAP1S LC expressing cells) in untreated cells. In contrast to MAP1B FL, ectopically expressed MAP1S FL binds very well to microtubules (Orban-Nemeth et al., 2005). Ding et al. showed that overexpressing MAP1S impaired the retrograde axonal transport in DRGs lacking GAN (Ding et al., 2006a). One can speculate that the binding of the unmodified MAP1S LC to microtubules is sufficient enough to impair this retrograde axonal transport.

Previous studies in our laboratory suggest that both, the proteolytic processing of MAP1B and the presence of the MH1 domain are essential for its microtubule binding, whereas the MH2 domain has an inhibitory effect. Several constructs were used to obtain these results, but a mutant lacking only the cleavage site was never tested (Trančíková, PhD thesis 2007). Here I analysed the binding ability of a mutant MAP1B FL lacking only 31 amino acid residues (in rat MAP1B 2193-2223) including and flanking the cleavage site presumably at amino acid 2204 of MAP1B (Tögel et al., 1999; Zou et al., 2008a). Surprisingly, comparing the results of MAP1B FL (11% of cells showed microtubule binding) to the mutant MAP1B FL (18% of cells showed microtubule binding), no significant difference in the microtubule binding ability was found. According to these results, we could clarify that the proteolytic processing of MAP1B is not essential for its microtubule binding. Concerning the previous studies in our laboratory by Trančíková (Trančíková, PhD thesis 2007), the influence of MH1 and MH2 seems to be crucial for the microtubule binding ability of MAP1B.

### **The influence of S-nitrosylation on the formation of an additional LC isoform**

Previous results from our laboratory showed an additional MAP1B LC band detected with an antibody against MAP1B LC in immunoblot analysis of protein

lysates of brain under non-reducing conditions (unpublished data, Daniel Lackner). I could show that this additional MAP1B LC isoform was present in protein lysates of brain and neuroblastoma (N2a) cells under non-reducing conditions. Concerning MAP1S, only one isoform was detectable. According to these results, the nitrosylation of MAP1B LC and the presence of the two cysteins are important for the formation of the second MAP1B LC isoform. To test if this isoforms occur in living cells before homogenisation or are perhaps a product of MAP1B LC oxidation during cell lysis, cells were treated with NEM, which binds to free S-H groups in the cells in vivo. Only one isoforms was detectable after treatment with NEM prior to cell lysis, indicating that the additional isoform of MAP1B LC is not present in live cells, but is generated during the homogenisation process. According to these data, I propose a model for the formation of the additional MAP1B LC isoform. The additional band might represent a more compact isoform of the MAP1B LC, which is formed via a disulfide bridge between the two cysteins (C-S-S-C) during the homogenisation process and migrates faster on the gel (figure 22).

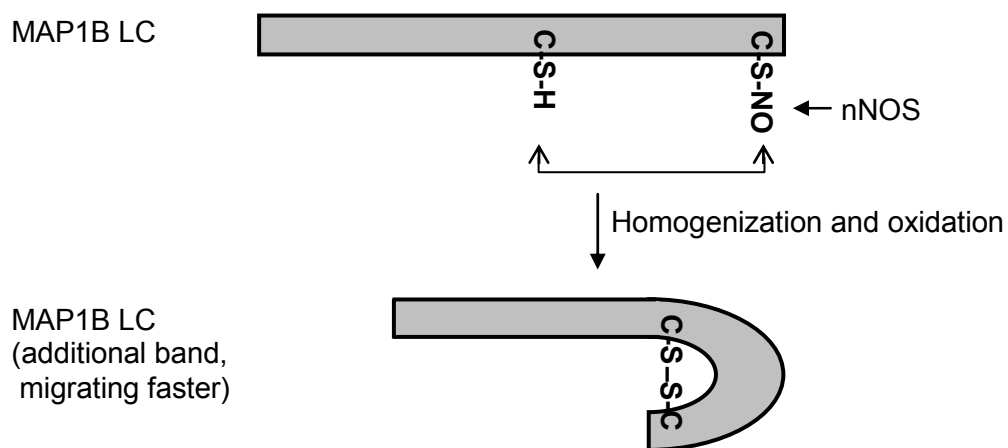


**Figure 22. A model for the formation of the faster migrating MAP1B LC isoform.**

The additional MAP1B LC band detected on blots of polyacrylamid gels run under non-reducing conditions probably represents a more compact isoform of MAP1B LC formed via a disulfide bridge between the two cysteins (C-S-S-C). This putative isoform of the MAP1B LC was only observed with the wild-type MAP1B LC where both cysteins are present, and when nNOS was active. If only one cystein was present, like in the MAP1B LC mutants, no bridge would be formed. After NPA treatment of the cells the additional isoform was not detectable. Thus, it is conceivable that oxidation of the

nitrosylated form of MAP1B LC by oxygen during homogenisation leads to formation of a disulphide bridge and a more compact isoform of MAP1B LC. NEM treatment of cells prior to homogenisation prevented the formation of this compact isoform, indicating that it was formed during the homogenisation process. NEM covalently modifies free S-H groups, preventing the subsequent oxidation and formation of disulfide bridges. If the compact isoform of MAP1B LC would already exist *in vivo*, NEM treatment just before homogenisation would not affect the existing disulfide bridges (C-S-S-C) and the faster migrating isoform should still be detectable after NEM treatment.

## **The influence of nNOS activity on posttranslational cleavage of MAP1S**

All members of the MAP1 family are synthesised as precursor proteins that are posttranslationally cleaved into HCs and LCs. Generally, protein precursors are seen as inactive proteins and their proteolytic cleavage represents an irreversible activation or maturation into an active form. It is conceivable that protein precursors act as a reservoir of inactive isoforms that can be activated on short notice and/or in large quantities. Sequence alignment revealed that the cleavage site is highly conserved in all members of the MAP1 family. The exact cleavage site was determined and the strong sequence conservation suggests a conserved cleavage mechanism (Zou et al., 2008a). However, no candidate mechanism or protease has been identified up to now. Whereas MAP1A and MAP1B precursor proteins are hardly detected in protein extracts, MAP1S is only partially cleaved in a tissue specific pattern (Orban-Nemeth et al., 2005). Interestingly, in brain, where MAP1B and MAP1A are predominantly expressed, MAP1S is found to be cleaved completely. One possibility is that all three MAP1 proteins are cleaved by the same cleavage mechanism and that this mechanism is differentially active in certain tissues. The limitation of the cleavage mechanism might be due to distinct availability of the protease.

It was proposed that the MAP1B HC acts as a regulatory subunit to control the activity of the MAP1B LC (Tögel et al., 1998). Also the MAP1S HC seems to regulate the activity of MAP1S LC, because when the MAP1S LC is expressed together with the HC, microtubule bundling and stabilisation are absent (Orban-Nemeth et al., 2005). Treatment with the protein translation suppressor

cycloheximide revealed that the MAP1S FL as well as the MAP1S HC are stable over 6 hours. Moreover, Ding et al. reported that even eight hours after cycloheximide addition, the majority of the MAP1S LC still remains (Ding et al., 2006a). These results indicate that the precursor protein as well as the cleaved MAP1S are relatively stable proteins with comparatively slow turnover and that the precursor MAP1S may act as long time storage. Nevertheless, the question remains, why the amount of cleaved versus uncleaved MAP1S varies in a tissue specific manner. On the one hand the active, cleaved MAP1S may be potentially harmful in some tissues, but under specific conditions active MAP1S is needed. On the other hand the precursor protein itself may perform a biological function.

So far, the mechanism of regulation of the cleavage of MAP1S has not been investigated. We found no influence of NPA on the cleavage of MAP1S, indicating that the inhibition of nNOS and therefore the inhibition of the potential S-nitrosylation of MAP1S does not influence the cleavage pattern of MAP1S.

## **N- $\epsilon$ -acetylation of MAP1 proteins**

Acetylation occurs as a co-translational and posttranslational modification of proteins, for example, histones, p53, and tubulins. Beside N- $\alpha$ -terminal acetylation, posttranslational  $\epsilon$ -amino lysine acetylation is emerging as a significant posttranslational regulatory mechanism of cytoskeletal proteins (Glozak et al., 2005). We purified MAPs from murine brain and analysed these proteins for their potential N- $\epsilon$ -acetylated lysine residues by using specific antibodies (Iwabata et al., 2005). We found only the MAP1B LC to be N- $\epsilon$ -acetylated. MAP1S LC and HC did not react with the antibody against N- $\epsilon$ -acetylated lysine indicating that they are not N-acetylated. Concerning MAP1A this question was not resolved as MAP1A is not expressed at high level in brain of mice of young age.

Lysine residues are targets for both acetylation and ubiquitination. It is proposed, that acetylation status regulates protein stability, because one of these modifications seems to prevent the other (Glozak et al., 2005). Therefore, the acetylation of MAP1B LC might enhance its stability. Furthermore, the

acetylation of a protein can potentially modify its activity and might crosstalk with other posttranslational modifications (Yang and Seto, 2008). Interestingly, microtubules in cells transfected with MAP1B were observed to be more stable and were found to be enriched in acetylated tubulin (Takemura et al., 1992). Our finding of the acetylation of MAP1B LC provides an opportunity to investigate the mechanism of acetylation and stabilisation of tubulin by MAP1B LC.

**PART II –  
GENERATION AND FIRST ANALYSIS OF  
MAP1S KNOCKOUT MICE**



# RESULTS

The second and main part of this thesis deals with the generation and first analysis of a MAP1S deficient mouse line to gain insight into the function of MAP1S. After giving an overview of the knockout strategy and the generation of this new mouse line, the first analysis of its phenotype will be described.

## The conditional knockout strategy

MAP1S is expressed in many mouse tissues and development stages (Orban-Nemeth et al., 2005) and seems to play a role in mitosis (Dallol et al., 2007; Song et al., 2005). To circumvent the potential early lethality of MAP1S deletion, we decided to generate a conditional knockout mouse instead of a conventional knockout mouse.

Strategies for conditional gene targeting in mice are based on the cre/loxP or flp/frt recombination system. In principle, the target gene is modified by homologous recombination in embryonic stem (ES) cells so that it is flanked by loxP sites orientated in the same direction. Mice carrying this mutation are then crossed with mice expressing cre in the desired target cell type to delete the gene only in these cells. The flp/frt recombination system operates the same way with an frt-site specific flp recombinase (Dymecki, 1996; Lewandoski, 2001; Sauer, 1998). An outline of the MAP1S conditional targeting strategy is given in figure 23. First, a targeting vector containing two loxP sites and an frt-flanked neomycin resistance gene was constructed (figure 25). Then ES cells were electroporated with the targeting vector to modify the MAP1S gene (wild-type) by homologous recombination. Successfully targeted ES cell clones were then used to generate mice with a targeted MAP1S gene also designated as being floxed. Next, the neomycin-resistance gene can be removed by the flp recombinase. This can be done by crossing mice with transgenic mice ubiquitously expressing flp recombinase (flp deleter mice). The gene expression of the floxed MAP1S gene should not be affected, since the first loxP site is integrated in an intron sequence and the second loxP site is integrated downstream of the exons of MAP1S. To cause gene ablation, this mouse line

can be crossed with another mouse line containing a cre transgene, expression of which is controlled by a defined promoter. In their offspring, recombination between the loxP sites will take place resulting in the deletion of the region flanked by the loxP sites.

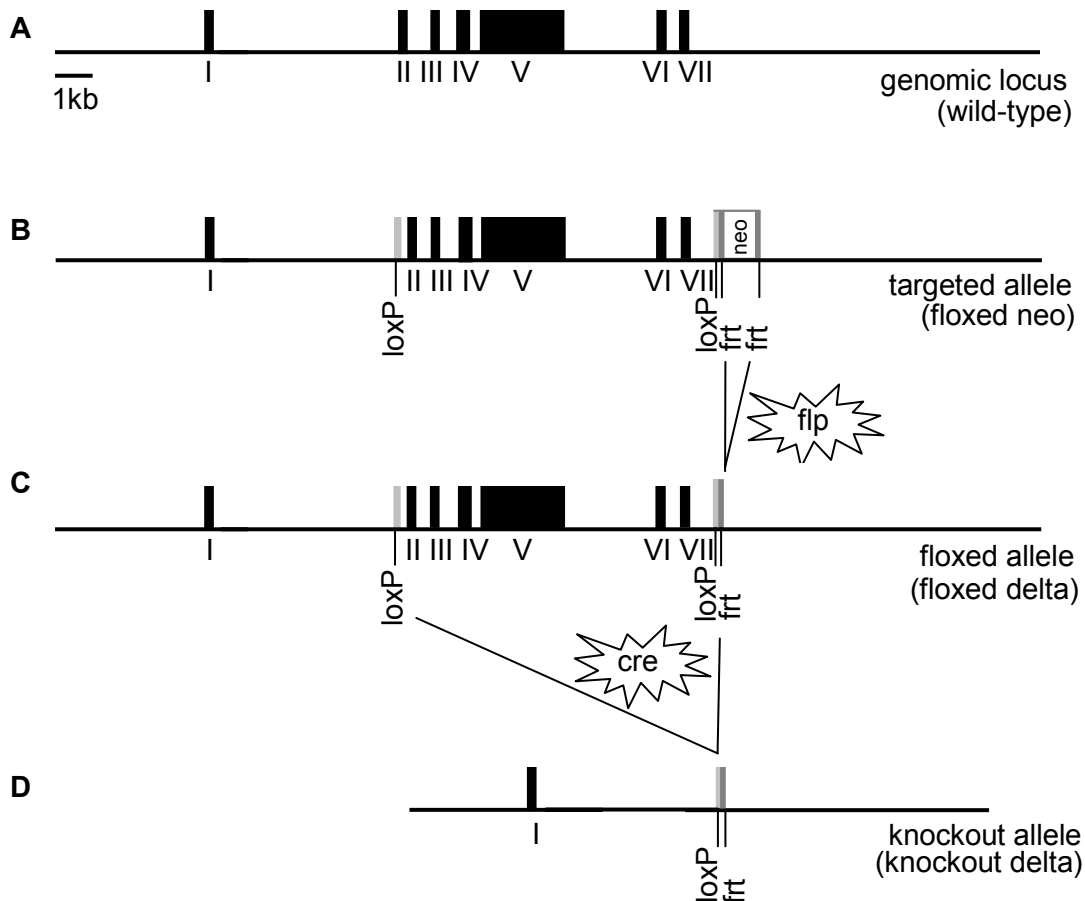


**Figure 23. Schematic representation of the strategy to generate conditional MAP1S knockout mice.** (A) The genomic locus of MAP1S in wild-type mice consists of 7 exons (I-VII) on chromosome 8. (B) After targeting this locus with the targeting construct (figure 25) in ES cells, the MAP1S locus will contain two loxP sites (light grey rectangle) flanking exon II to VII and a neomycin-resistance (neo) gene flanked by frt sites (dark grey rectangle). The neomycin-resistance is needed for the selection of the ES clones. (C) First, mice with the targeted allele will be crossed to an flp expressing mouse strain to remove the neomycin-resistance gene and to generate a MAP1S allele that should function in a way indistinguishable from the wild-type allele except that it is susceptible to deletion of exon II to VII upon expression of cre recombinase. (D) To ablate exon II to VII, the cre recombinase will mediate the recombination between the two loxP sites.

The conditional knockout mice will have a mixed background, as the targeting vector will consist of DNA from the C57BL/6 strain, and ES cells will contain DNA from the 129 strain additionally. To elucidate differences in the MAP1S expression levels in the C57BL/6 and 129 mice, immunoblot analysis was performed (figure 24). MAP1S was found to be expressed in the same pattern and intensity in both mouse strains.

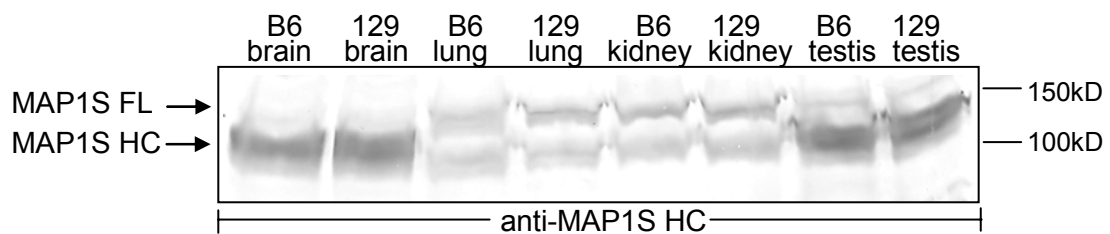


**Figure 24. MAP1S expression in mouse tissues of strains C57BL/6J and 129.** 100µg of protein (total lysate) from the indicated mouse tissues (adult) from C57BL/6 (B6) or 129 were analysed by SDS-PAGE and immunoblotting with antibodies against the MAP1S heavy chain (anti-MAP1S HC). Protein bands of 120kD correspond to the uncleaved MAP1S FL. Protein bands of 100kD correspond to the heavy chain (HC). MAP1S was expressed in both mouse strains in the same pattern and intensity.

## Generation of conditional MAP1S knockout mice

For the generation of the conditional MAP1S knockout mouse line several steps were necessary. First, a targeting vector was constructed. This vector contains exon II to exon VII of the MAP1S gene, flanked by two loxP sites, and a neomycin resistance gene, flanked by two frt sites (figure 25A). The cloning strategy is described in detail in Materials and Methods.

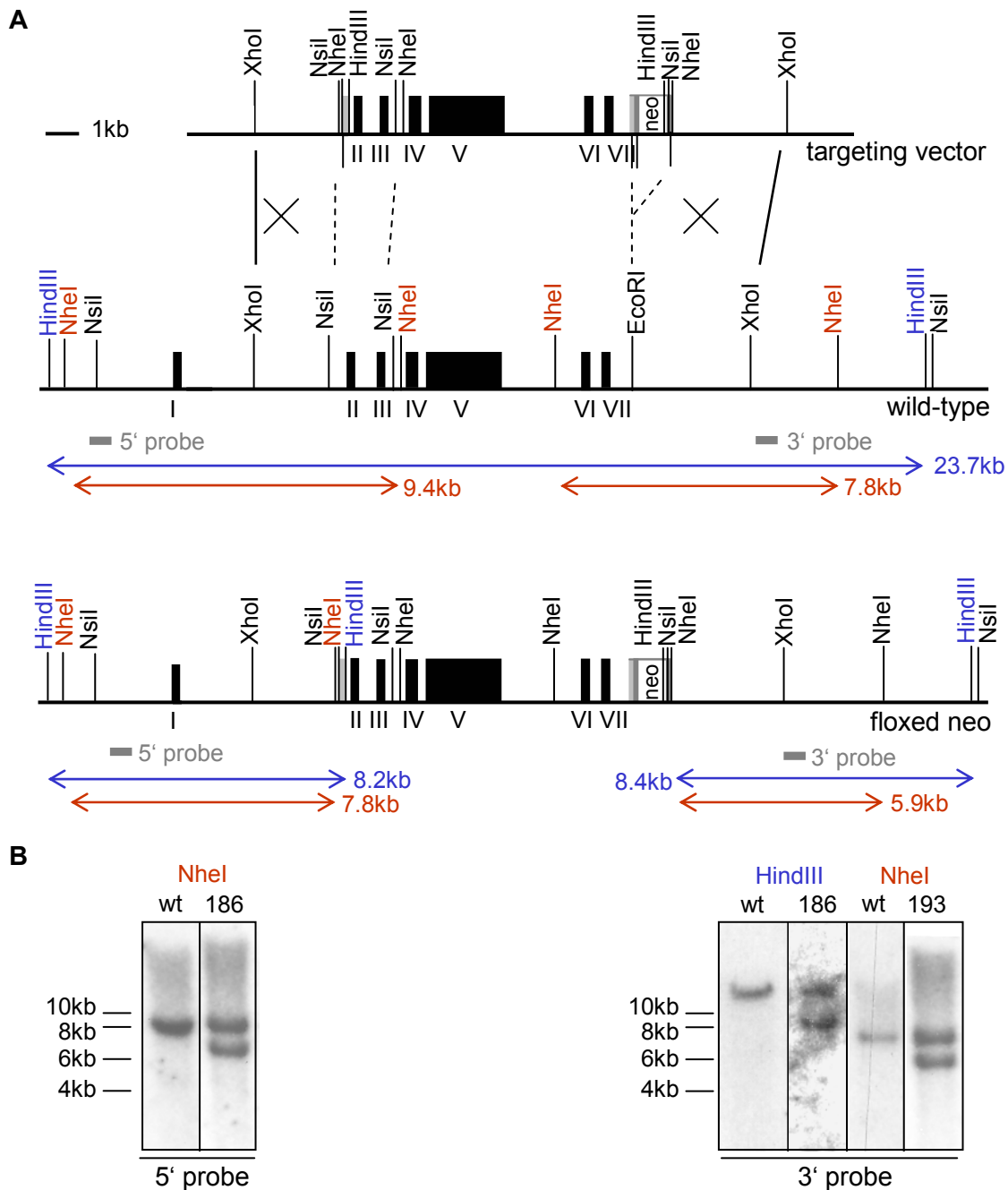


**Figure 25. Targeting the MAP1S locus.** (A) Schematic representation of the targeting construct (targeting vector), the MAP1S genomic locus (wild-type), and targeted allele (floxed neo) after homologous recombination (crosses). Exons (black boxes), restriction sites, and positions of external probes (grey boxes) are indicated. The targeting construct comprised a 13221bp XhoI fragment of genomic mouse DNA (strain C57BL/6, obtained from BAC RPCI-23\_374C22) containing exon II to VII of the MAP1S gene plus flanking sequences. This fragment was modified through insertion (dashed lines) of an NsiI fragment, which was synthesised by PCR and contained exon II, exon III and one loxP site upstream of exon II. Additionally, a second loxP site and a neomycin-resistance gene flanked by frt sites were inserted (dashed lines) at an EcoRI

site downstream of exon VII. Through homologous recombination, the targeted construct was inserted in the genomic locus. To analyse the 5' side of the targeted locus, genomic DNA was digested with HindIII or NheI to detect with the 5' probe a 23.7kb or 9.4kb fragment from wild-type, respectively and an 8.2kb or 7.8kb fragment from the floxed neo allele. To analyse the 3' side of the targeted locus, genomic DNA was digested with HindIII or NheI to detect with the 3' probe a 23.7kb or 7.8kb fragment from wild-type, respectively and an 8.4kb or 5.9kb from the mutated allele. **(B)** Southern blot analysis (autoradiography) was performed of genomic DNA prepared from an ES cell clone with an unaltered MAP1S locus (wt) and from successfully targeted clones (186 and 193) using 5' probe or 3' probe.

Prior to electroporation into A9 ES cells (kindly provided by A. Meixner, IMP), the targeting vector was linearised. A9 ES cells are C57BL/6 and 129 hybrids and have an X/Y genotype. These ES cells were transfected by electroporation, neomycin (G418) resistant clones were picked, and genomic DNA was prepared and analysed for the type of recombination event by Southern blot analysis (figure 25). The Southern blot strategy had been tested before on DNA from C57BL/6 and 129 mice (data not shown). DNA from both mouse strains gave the same fragments (wild-type). To demonstrate the correct insertion of the targeting construct, two probes (5' and 3') external to the targeting construct were used for hybridisation. From 276 analysed clones, three obtained the desired targeted MAP1S allele. Cells from one positive ES cell clone, number 186, were then injected into blastocysts of C57BL/6 mice and blastocysts were transferred into foster mice (kindly done by C. Theussl and J. Wojciechowski). From three foster mice, seven male chimeras were obtained. Chimeric mice were then breed with C57BL/6 mice for back crossing. Some chimeric mice were crossed directly with cre deleter mice, transgenic mice ubiquitously expressing cre recombinase to generate mice carrying the ko neo allele in the germline. All chimera were fertile and transfered the targeted MAP1S allele to their offspring. Around 50% (41 out of 88) of the pups inherited the targeted allele. Southern blot analysis using external probes confirmed their genotype. Additionally, southern blot analysis using an internal probe, that hybridises with the neomycin resistance gene (neo probe), was performed (figure 26). This southern blot analysis, performed on DNA from offspring from chimeras mated

with either C57BL/6 or cre deleter mice, showed the predicted 7.5kb or 6.0kb Bgl II-fragment in diagnostic for the floxed neo and ko neo alleles, respectively. Surprisingly, a second band was detected with the neo probe.

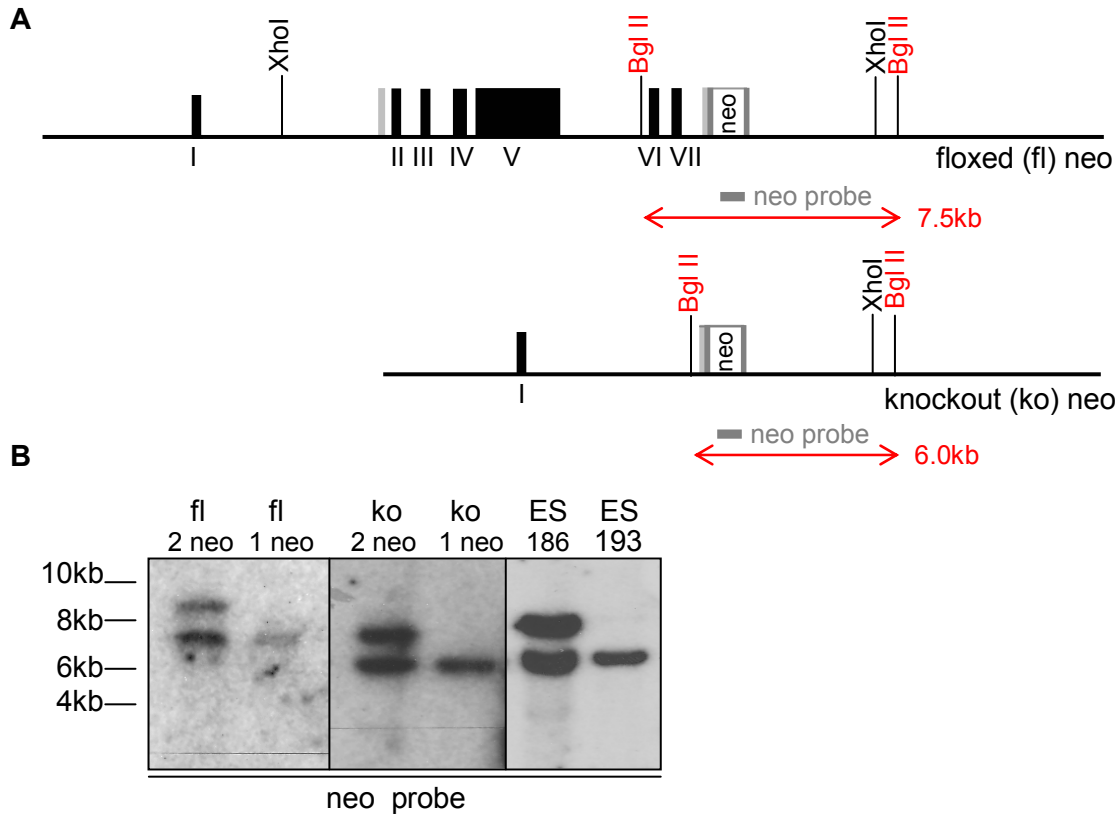


**Figure 26. Southern blot analysis using the neo probe revealed an additional band, which disappeared after back crossing. (A)** Schematic representation of the floxed neo allele and the knockout allele. Exons (black boxes), restriction sites, and the position of the internal neo probe (grey box) are indicated. To analyse the integration of the targeting vector, the genomic DNA was digested with Bgl II to detect with the neo probe a 7.5kb or a 6.0kb fragment from the floxed neo or the knockout neo allele, respectively. **(B)** Southern blot analysis (autoradiography) was performed of genomic DNA prepared from heterozygous floxed (fl) neo, from heterozygous knockout (ko) neo mice derived from 186 ES cell clone, and from 186 and 193 ES cell clones using the neo probe. In addition to the expected 7.5kb and 6.0kb Bgl II-fragments diagnostic for floxed neo and ko neo mice, respectively, a second band appeared (2 neo). This additional band disappeared after back crossing (1 neo) in both genotypes. ES clone (ES) number 186 showed two neo bands, ES clone 193 showed one neo band.

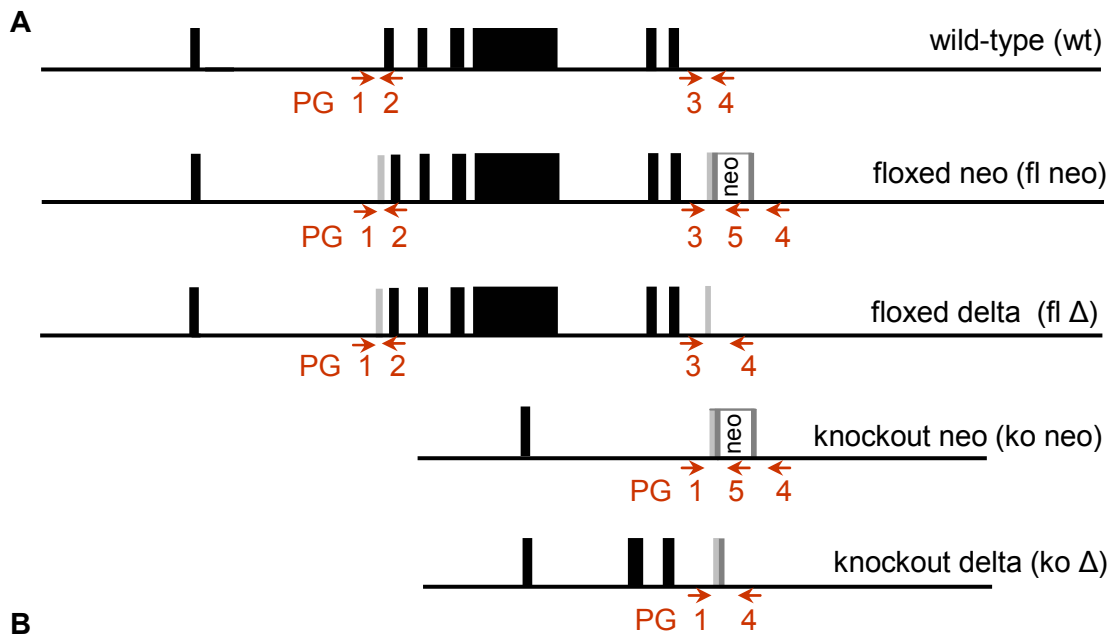
The neomycin resistance does not exist in the wild-type genome (no band detected, data not shown), but in the targeting vector. Therefore we suspected

that the targeting vector, or at least a fragment containing the neomycin resistance gene, integrated not only in the MAP1S genomic locus, but also by non-homologous recombination at a second site. If this second integration took place on another chromosome or at sufficient distance from the MAP1S locus on chromosome 8, it would be possible to obtain mice with only one integrated vector through backcrossing. Indeed, after three generations of backcrossing, mice showing just the expected band in southern blot analysis with the neo probe were obtained.

Additionally, southern blot analysis of DNA from ES clones was performed. The ES clone number 186 showed two bands after hybridisation with the neo probe. Another positive ES cell clone, which contained the desired targeted MAP1S allele, showed only one band. This clone, number 193, was then injected into blastocysts of C57BL/6 mice and blastocysts were transferred into foster mice (kindly done by C. Theussl and J. Wojciechowski). From two foster mice, one female and five male chimeras were obtained. All of them were fertile and transferred the targeted MAP1S locus to their offspring.

To facilitate and accelerate genotyping of mice, a PCR strategy was designed and established (figure 27). PCR analysis was performed on murine genomic DNA, isolated from tail tips. Five different primers were designed, named PG (Primer for Genotyping) 1 to 5. Three different PCRs were used to distinguish five different alleles. As all primers bind inside the region of the targeting vector, genotyping by PCR was only used once the correct targeting of the MAP1S locus was established by southern blotting.

Mice heterozygous for the ko neo allele (obtained by breeding chimeras with cre deleter transgenics) were not distinguishable from their wild-type littermates. Heterozygous animals were then intercrossed to obtain mice homozygous for the ko neo allele.



	PCR products obtained from the indicated genotype				
primers	wt	fl neo	fl $\Delta$	ko neo	ko $\Delta$
PG3,PG4, PG5	324bp (PG 3+4)	445bp (PG 3+5) 1573bp (PG 3+4)	452bp (PG 3+4)		
PG1,PG2, PG5	261bp (PG 1+2)	311bp (PG 1+2)	311bp (PG 1+2)	525bp (PG 1+5)	
PG1,PG3, PG4	324bp (PG 3+4)	1573bp (PG 3+4)	452bp (PG 3+4)	1653bp (PG 1+4)	532bp (PG 1+4)

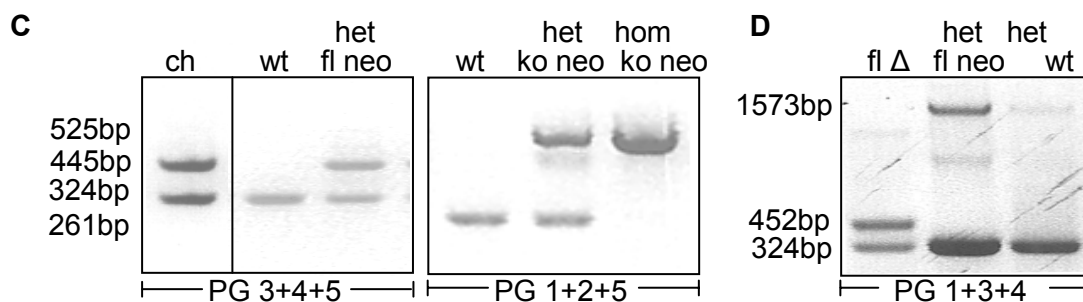


**Figure 27. PCR strategy to identify targeted MAP1S alleles.** (A) Schematic representation of the wild-type genomic locus (wt), the floxed neo (fl neo), the floxed delta (fl  $\Delta$ ), the knockout neo (ko neo) and the knockout delta (ko  $\Delta$ ) allele. (B) Table of PCR products amplified with the appropriate primers to identify the indicated genotype. (C) PCR products obtained from DNA of a chimera (ch, line 186), a wt mouse, a heterozygous (het) fl neo, and a het ko neo were analysed on 1.8% agarose gels. Primers used to perform the PCR are indicated. (D) PCR products were analysed on a 0.8% agarose gel.



## General examination of homozygous knockout mice

Intercrossing of heterozygous knockout neo mice revealed that homozygous knockout mice were viable. They were obtained at approximately Mendelian ratio (Table 1). Their litter size with an average of  $6.89 \pm 2.6$  pups was equal to the litter size of C57BL/6 mice (6-8 pups). Homozygous knockout neo mice showed no apparent phenotype compared to their wild-type littermates. They were viable and fertile.

	Number of progeny					
	wild-type		het knockout neo		hom knockout neo	
	n	%	n	%	n	%
Total born	28	34	38	46	16	20
Adult male	9		19		8	
Adult female	19		19		8	
Postnatal lethality	0	0	0	0	0	0

**Table 1. Breeding statistics of MAP1S knockout mice.** Heterozygous MAP1S knockout neo mice were paired and their offspring were genotyped at the age of three weeks. From 82 offspring, 34% (28) were wild-type, 46% (38) heterozygous (het) knockout neo, and 20% (16) homozygous (hom) knockout neo mice. No postnatal lethality after weaning was found.

All of the following analyses were carried out using mice derived from ES clone 186 and homozygous for the MAP1S ko neo allele and their wild-type littermates as controls. Hence, mice homozygous for the ko neo allele will be referred to as MAP1S knockout or MAP1S deficient mice. To confirm that the knockout neo allele is a null allele no longer encoding MAP1S, immunoblot analysis was performed of brain, lung, testis, spleen and liver from MAP1S knockout mice and their wild-type littermates (figure 28). No MAP1S expression could be detected in tissues from MAP1S knockout mice. As the antibody against the MAP1S heavy chain binds to the C terminus of the heavy chain, the expression of an N-terminal MAP1S fragment potentially encoded by exon I, which remain intact in the targeted allele, could not be analysed. The potentially encoded N-terminal MAP1S fragment would be 41 amino acids long.

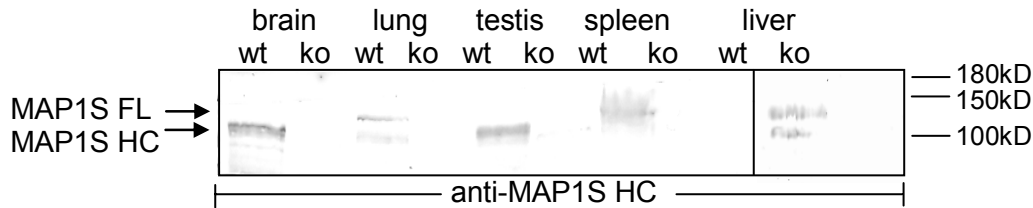


**Figure 28. Immunoblot analysis of the expression of MAP1S in wild-type and MAP1S knockout mice.** 80  $\mu$ g of protein (total lysate) extracted from the indicated mouse tissues (adult) from wild-type (wt) and MAP1S knockout (ko) mice were analysed by SDS-PAGE and immunoblotting with antibodies against MAP1S heavy chain (anti-MAP1S HC). Protein bands of 120kD correspond to the uncleaved full-length MAP1S polyprotein precursor (MAP1S FL). Protein bands of 100kD correspond to the heavy chain (HC). MAP1S was expressed in wild-type, but not in MAP1S knockout mice.

## Histological analysis

For histological analysis, we sent three adult MAP1S knockout mice and their wild-type littermates, perfused by I. Fischer, to H. Lassmann. The mice were four months (male), six months (female), and 13 months (male) old. All organs were screened for histological differences.

In brain and testis, where MAP1S is expressed at highest levels (Orban-Nemeth et al., 2005), no histological disparities were found (figure 29 and 30).

The liver of the four month old male knockout mouse showed disturbed organisation of bile ducts. The number of bile ducts seemed increased. In addition to bile ducts found in portale triads next to the hepatic portal vein in wild-type liver, bile ducts were found widespread in the portal lobule in MAP1S knockout liver (figure 31). In the liver of the two other MAP1S knockout mice, the organisation of bile ducts appeared normal.

In all other organs examined, no abnormalities were found in MAP1S knockout mice (data not shown).

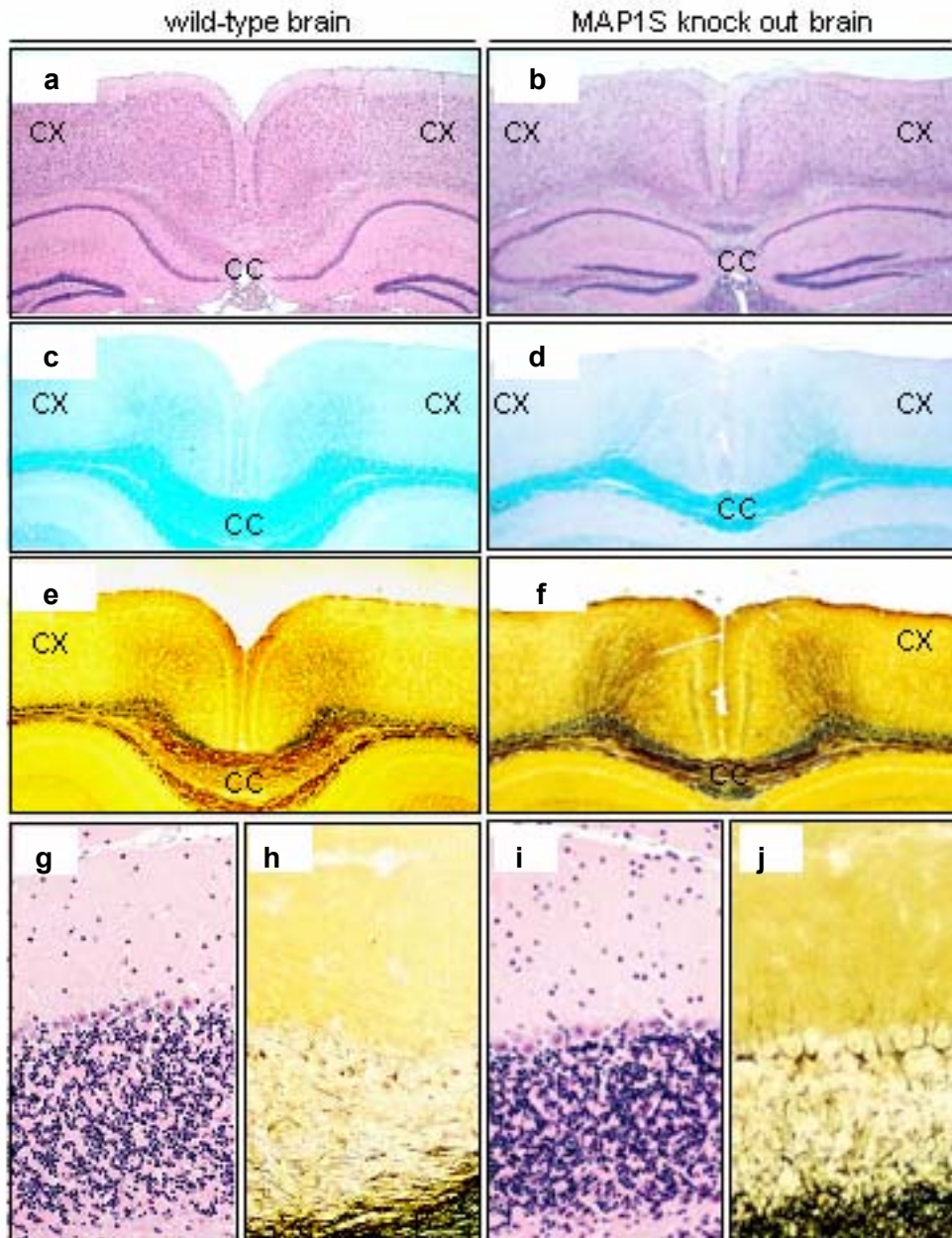


**Figure 29. Histological analysis of the brain did not show any differences between wild-type and MAP1S knockout mice.** Frontal sections through the cerebral white matter and corpus callosum were stained with hematoxylin and eosin (a,b), luxol fast blue myelin staining (c,d) or Bielschowsky silver impregnation for axons (e,f). The cerebral cortex (CX), the corpus callosum (CC) and the hippocampus of a normal wild-type mouse brain (a,c,e) and a MAP1S knockout mouse (b,d,f) showed normal architecture of myelinated fiber tracts including the corpus callosum (a-f) and axons (e,f, dark brown). The corpus callosum in wild-type brain appeared thicker due to an oblique section. Sections through the cerebellar cortex were stained with hematoxylin and eosin (g,i) and Bielschowsky silver impregnation (h,j). No differences between wild-type and MAP1S knockout mice were found.

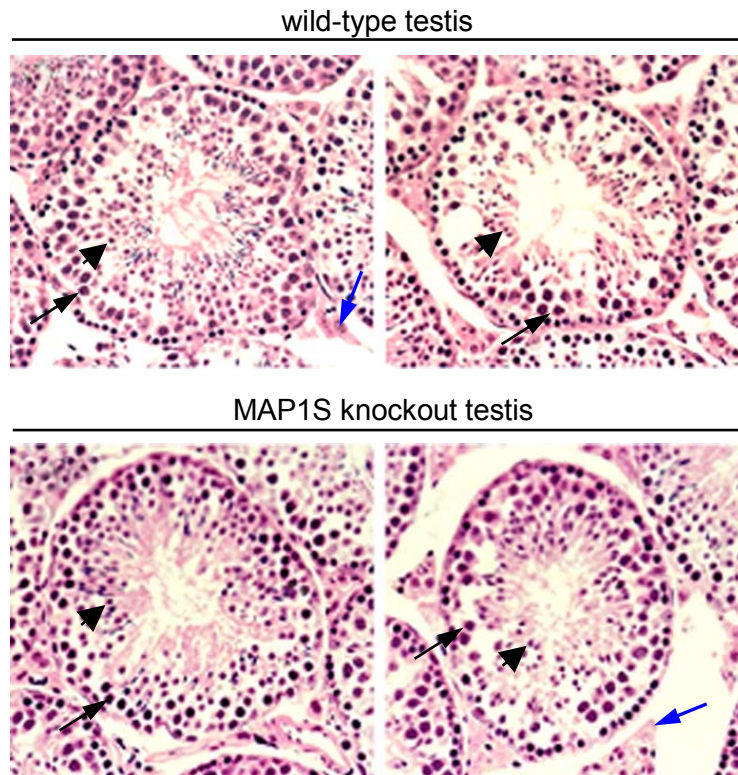


**Figure 30. Histological analysis of the testis did not reveal any differences between wild-type and MAP1S knockout mice.** Sections through testis were stained with hematoxylin and eosin. Leydig cells (blue arrow), spermatocytes (black arrow), and spermatids (black arrowhead) were organised normally. No abnormalities were found in MAP1S knockout mice.

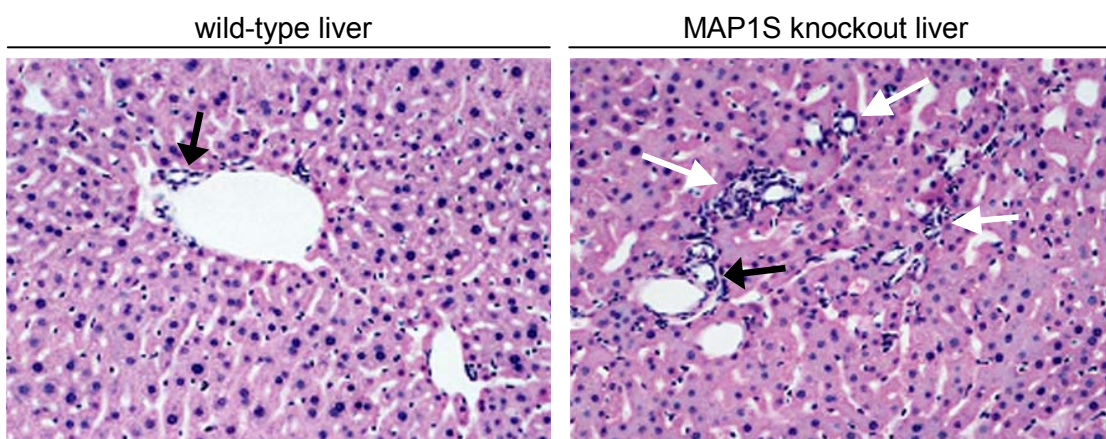


**Figure 31. Histological analysis of the liver showed disturbed organisation of small blood vessels or bile ducts in one MAP1S knockout mouse.** Sections through the liver were stained with hematoxylin and eosin. Wild-type liver sinusoids and bile ducts (black arrow) were organised normally. In the liver from one homozygous knockout neo mouse, bile ducts were found not only in portales triads next to the hepatic

portal vein as in wild-type liver (black arrow), but additionally widespread in the portal lobule (white arrows).

## The expression pattern of MAP1A and MAP1B in the brain of MAP1S knockout mice

As no abnormalities were found in the brain of MAP1S knockout mice, MAP1S seemed to be dispensable for brain development. To analyse if the loss of MAP1S might be compensated for by other proteins of the MAP1 family, immunoblot analysis was performed. Total protein lysates from whole brain, pieces of the cortex and the cerebellum were extracted. In immunoblot analysis the expression pattern of the MAP1A light chain was not altered in the brain of homozygous knockout mice (figure 32).

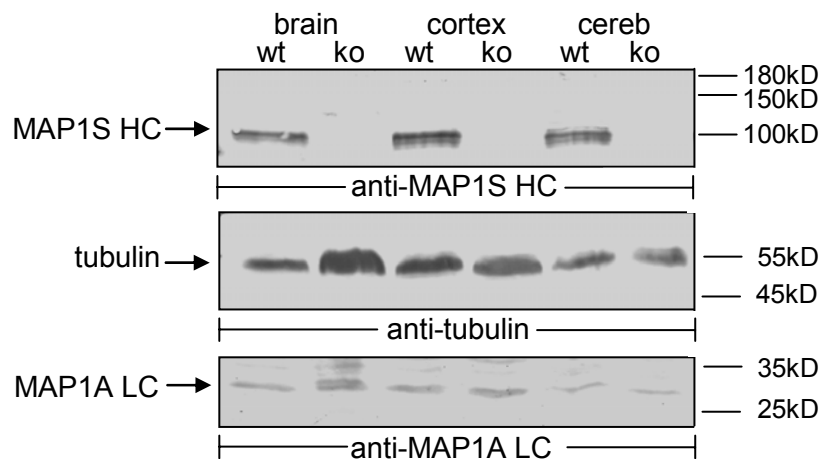


**Figure 32. The expression pattern of the MAP1A light chain was not altered in the brain of MAP1S knockout mice.** 80µg of protein (total lysate) extracted from the brains of adult wild-type (wt) and MAP1S knockout (ko) mice were analysed by SDS-PAGE and immunoblotting with antibodies against MAP1S heavy chain (anti-MAP1S HC), tubulin (anti-tubulin) and MAP1A light chain (anti-MAP1A LC). The positions of the respective proteins are indicated. MAP1S was expressed in the whole brain (brain), in the cerebral cortex (cortex) and in the cerebellum (cereb) in wild-type, but not in MAP1S knockout mice. Tubulin staining served as internal control. The expression level of the MAP1A light chain showed no differences between wild-type and MAP1S knockout mice.

Additionally, immunoblot analysis to detect the expression of the MAP1B light chain was performed. The expression pattern of the MAP1B light chain was not altered in the brain of homozygous knockout mice (figure 33).

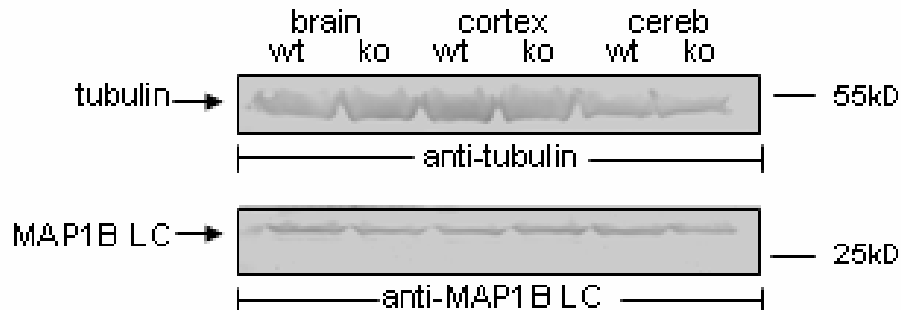


**Figure 33. The expression pattern of the MAP1B light chain was not altered in the brain of MAP1S knockout mice.** 80µg of protein (total lysate) extracted from the brains of adult wild-type (wt) and MAP1S knockout (ko) mice were analysed by SDS-PAGE and immunoblotting with affinity-purified antibodies against tubulin (anti-tubulin) and against MAP1B light chain (anti-MAP1B LC). The positions of the respective proteins are indicated. Tubulin staining served as internal control. The expression level of the MAP1B light chain showed no differences in wild-type and MAP1S knockout mice.

## MAP1S knockout DRGNs

As previously mentioned, MAP1B is expressed in DRGs and cultured DRGNs lacking MAP1B are able to regenerate their axons, but show enhanced neurite branching and impaired axonal turning behaviour (Bouquet et al., 2004). MAP1S too was shown to be expressed in DRGs (Ding et al., 2006b). To analyse the influence of MAP1S on axon regeneration, DRGNs from MAP1S knockout mice and their wild-type littermates were isolated, cultured, fixed, stained for tubulin and analysed by confocal microscopy. All protrusions longer than one diameter of the associated cell body were counted as axons. DRGNs from MAP1S knockout mice displayed a shift towards cells with more than one axon. Whereas 42% of the wild-type DRGNs elaborate a single branched axon, significantly less (29%,  $p=0.03$ , t-test) of the DRGNs isolated from MAP1S

knockout mice display just one axon, while cells with two or more axons emanating from the cell body appear to be more frequent (figure 34).

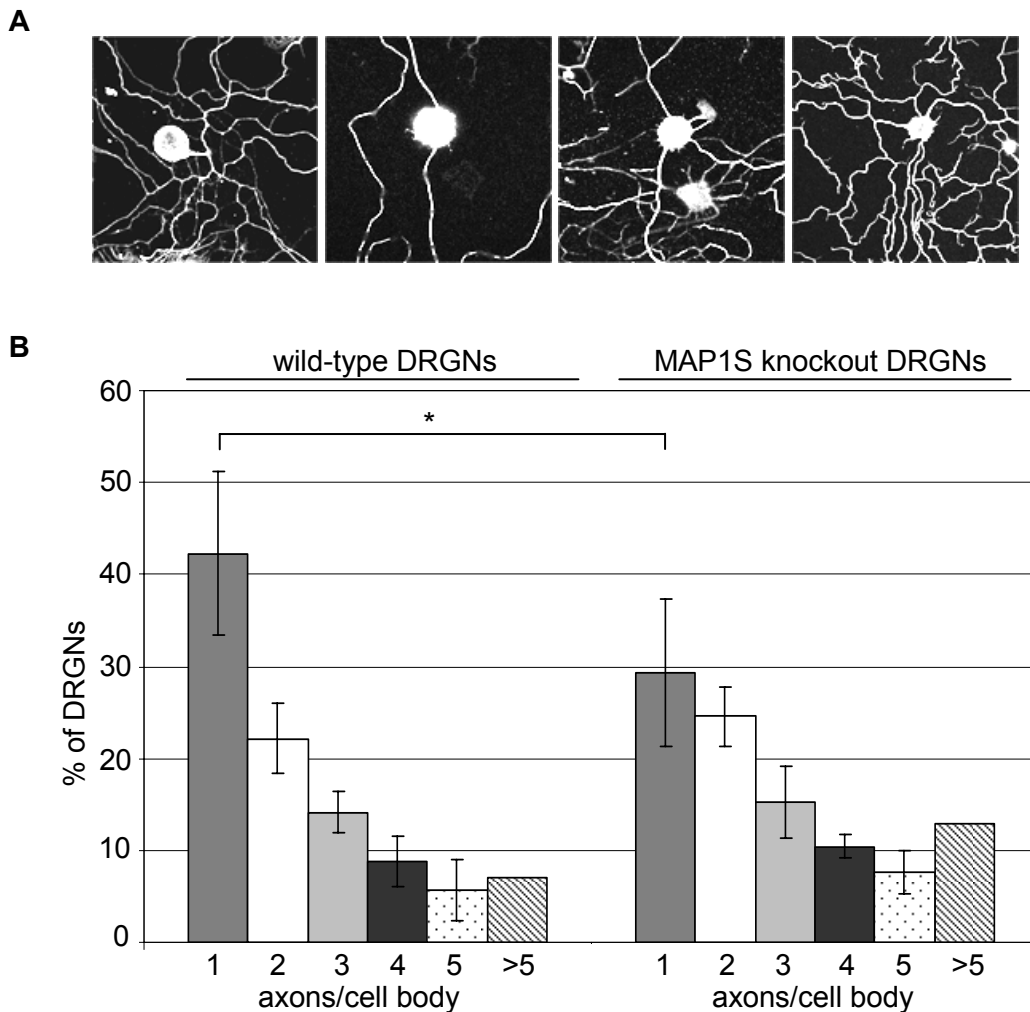
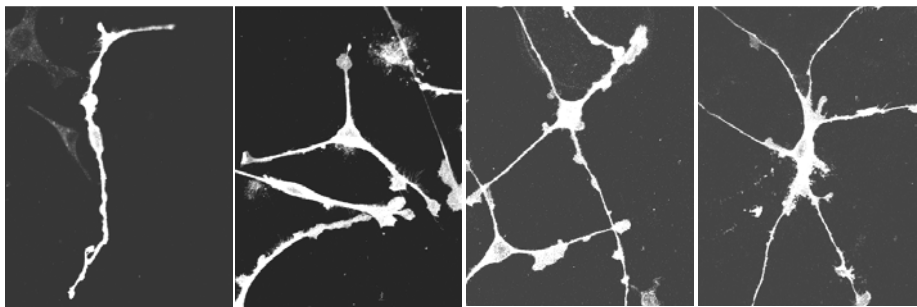


**Figure 34. DRGNs from MAP1S knockout mice displayed a shift towards cells with more than one axon.** DRGNs of adult wild-type and homozygous knockout mice were cultured for 24 to 48 hours, fixed, and stained for tubulin and analysed by confocal fluorescence microscopy. **(A)** Representative immuno-fluorescence pictures were taken from DRGNs showing cell bodies with 1, 2, 3 or 4 axons per cell body. All extensions which were longer than one diameter of the associated cell body were counted as axons. **(B)** From each genotype at least 100 cells were counted in three independent experiments and presented as mean values with error bars representing standard deviations. 42% of the DRGNs of wild-type mice elaborate a single axon, DRGNs of MAP1S knockout mice show significantly less DRGNs with one axon (29%,  $p=0.03$ , t-test).

## MAP1S knockout Schwann cells

Schwann cells provide myelin insulation to axons in the peripheral nervous system. MAP1B is expressed in adult Schwann cells and its expression increases when they de-differentiate and proliferate after a peripheral lesion and migrate into the lesion site. It was shown that MAP1B is required for provoked motility of Schwann cells in migration assays (Bouquet et al., 2007; Ma et al., 1999).

**A**



**B**

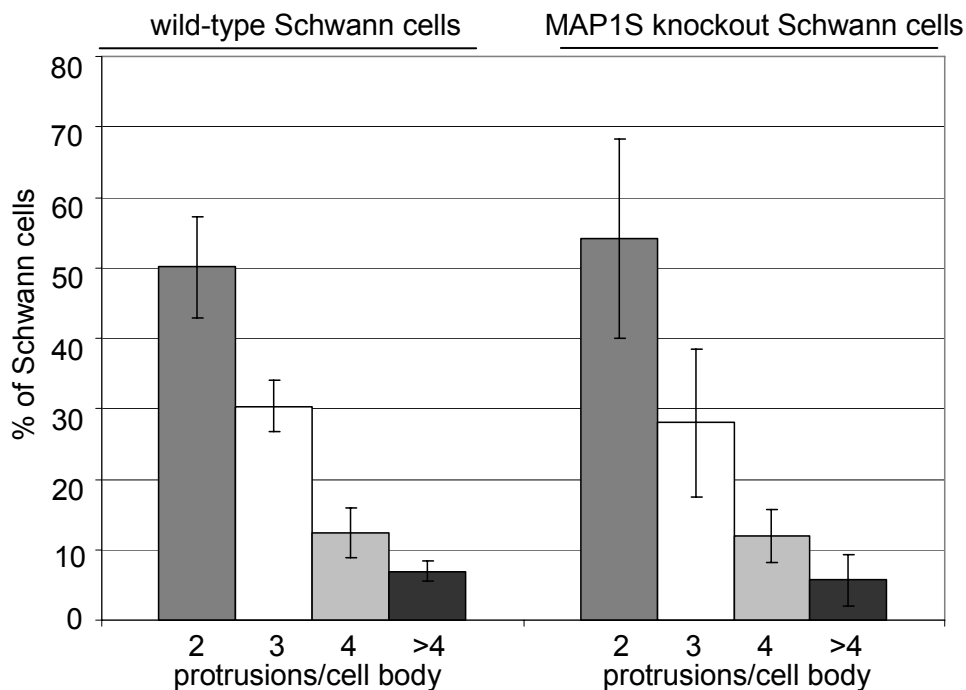


**Figure 35. Schwann cells of MAP1S knockout mice did not differ in the number of protrusions.** Schwann cells from adult wild-type and MAP1S knockout mice were cultured for 48 hours, fixed, and stained for p75 and analysed by confocal fluorescence microscopy. (A) Representative immunofluorescence pictures were taken from Schwann cells showing cell bodies with 2, 3, 4 or 6 protrusions per cell body. All processes, which were longer than one diameter of the associated cell body, were



counted as protrusions. (B) From each genotype at least 100 cells were counted in three independent experiments and presented as mean values with error bars representing standard deviations.

Schwann cells from adult MAP1S knockout mice and their wild-type littermates were isolated, cultured, fixed, stained for the Schwann cell marker p75 and analysed by confocal microscopy. All protrusions longer than one diameter of the associated cell body were counted as protrusions. The number of protrusions per cell did not differ between MAP1S knockout and wild-type mice (figure 35).

### MAP1S knockout fibroblasts

To analyse the role of MAP1S during cell cycle, and in cell migration, fibroblasts of adult wild-type and MAP1S knockout mice were isolated and cultured. Immunoblot analysis confirmed that MAP1S is expressed in fibroblasts of wild-type, but not in fibroblasts of MAP1S knockout mice (figure 36).

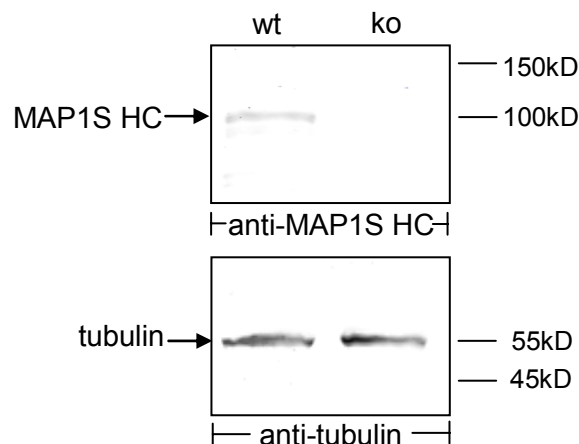


**Figure 36. Immunoblot analysis of the expression of MAP1S in fibroblasts of wild-type and MAP1S knockout mice.** 80µg of protein (total lysate) extracted from fibroblasts from adult wild-type (wt) and MAP1S knockout (ko) mice were analysed by SDS-PAGE and immunoblotting with antibodies against MAP1S heavy chain (anti-MAP1S HC) and against tubulin (anti-tubulin). The positions of the respective proteins are indicated. Tubulin staining served as internal control. Protein bands of 100kD correspond to the MAP1S heavy chain (HC). MAP1S was expressed in wild-type, but not in MAP1S knockout fibroblasts.

## Cellcycle phase distribution in MAP1S knockout fibroblasts

To explore the role of MAP1S in the cell cycle, fibroblasts of MAP1S knockout and wild-type mice were isolated, cultured, and cell cycle FACS analysis was performed in the logarithmic growth phase of the cells (figure 37). In wild-type fibroblasts, 50% were found in G0/G1 phase, 33% in S phase and 17% in G2/M phase. In contrast, 82% of MAP1S knockout fibroblasts were found in G0/G1, only 10% in S phase and 9% in G2/M phase. Compared to wild-type fibroblasts, MAP1S knockout fibroblasts are significantly overrepresented in the G0/G1 phase ( $p=0.0007$ , t-test), and significantly underrepresented in S ( $p=0.002$ , t-test) and in G2/M phase ( $p=0.003$ , t-test).

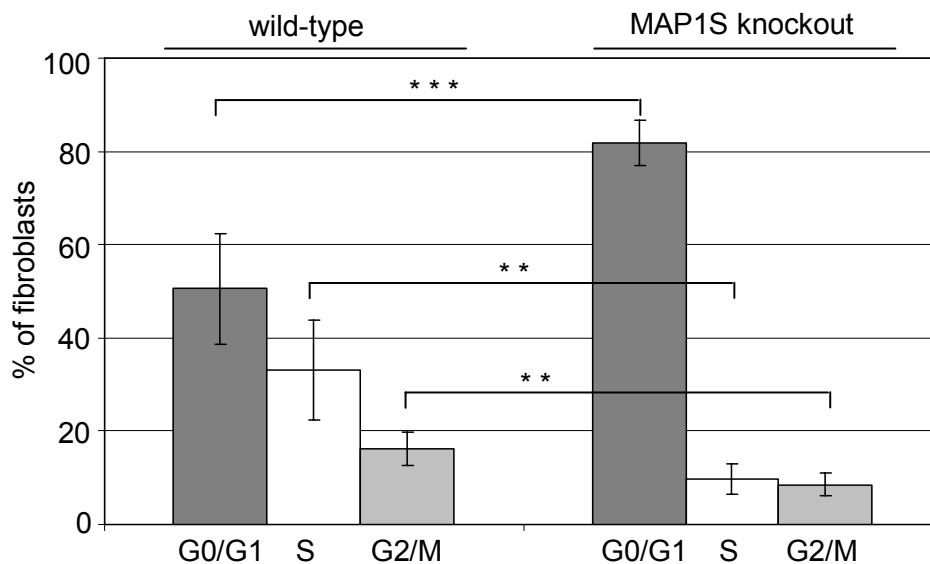


**Figure 37. The cell cycle distribution is altered in MAP1S knockout fibroblasts.**

Fibroblasts isolated from adult wild-type and MAP1S knockout mice were cultured and analysed by cell cycle FACS analysis. Results from three independent experiments, using fibroblasts isolated from two different wild-type and one knockout mice, were calculated and presented as mean values with error bars representing standard deviations. In wild-type fibroblasts, 50% of the cells were found in G0/G1 phase, 33% in S phase and 17% in G2/M phase. In MAP1S knockout fibroblasts, 82% of the cells were found in G0/G1, 10% in S phase and 9% in G2/M phase. MAP1S knockout fibroblasts are significantly overrepresented in the G0/G1 phase ( $p=0.0007$ , t-test), and significantly underrepresented in the S ( $p=0.002$ , t-test) and in the G2/M phase ( $p=0.003$ ).

## Cell migration in MAP1S knockout fibroblasts

As a potential crosslinker protein between microtubules and actin filaments, MAP1S may play a role in random cell movement. Therefore fibroblasts were plated and scattered cells were monitored four hours later by video microscopy. Analysis of this random migration assay was performed with the ImageJ program, tracking single cells and calculating their migration velocity (figure 38). No significant differences in random migration velocity were found.

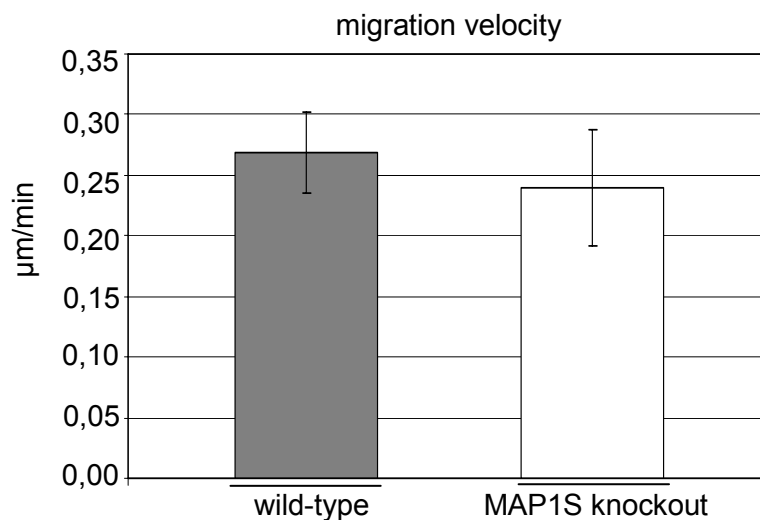


**Figure 38. MAP1S knockout fibroblasts did not migrate significantly slower than wild-type fibroblasts in random migration assay.** Fibroblasts from adult wild-type and MAP1S knockout mice were plated and isolated cells were monitored 4 hours after plating for 5.5 hours. Analysis was performed with the ImageJ program, using manual tracking. Migration velocity in  $\mu\text{m}$  per minute was calculated from three independent experiments using fibroblasts from one wild-type and one knockout mouse and is presented as mean values with error bars representing standard deviations. No significant differences in random migration velocity were found.

And in vitro wound healing assay was performed to analyse directed cell migration. Therefore fibroblasts of MAP1S knockout and wild-type mice were isolated, cultured, grown until they reached near confluency, and a scratch was made within the monolayer (figure 39). The scratched cell free area was monitored and measured at different time points (six to 72 hours after the scratch) and the percentage of free area relative to the free area measured

immediately after scratching was calculated. 24 hours after the scratch, 39% of the scratched area remained cell free in wild-type fibroblasts. In MAP1S knockout fibroblasts, a significantly larger area, 55% of the scratched area ( $p=0.03$ , t-test), remained cell free. 30, 36 and 42 hours after the scratch, the differences were even more significant ( $p=0.01$ ,  $p=0.01$ ,  $p=0.00002$  respectively, t-test).

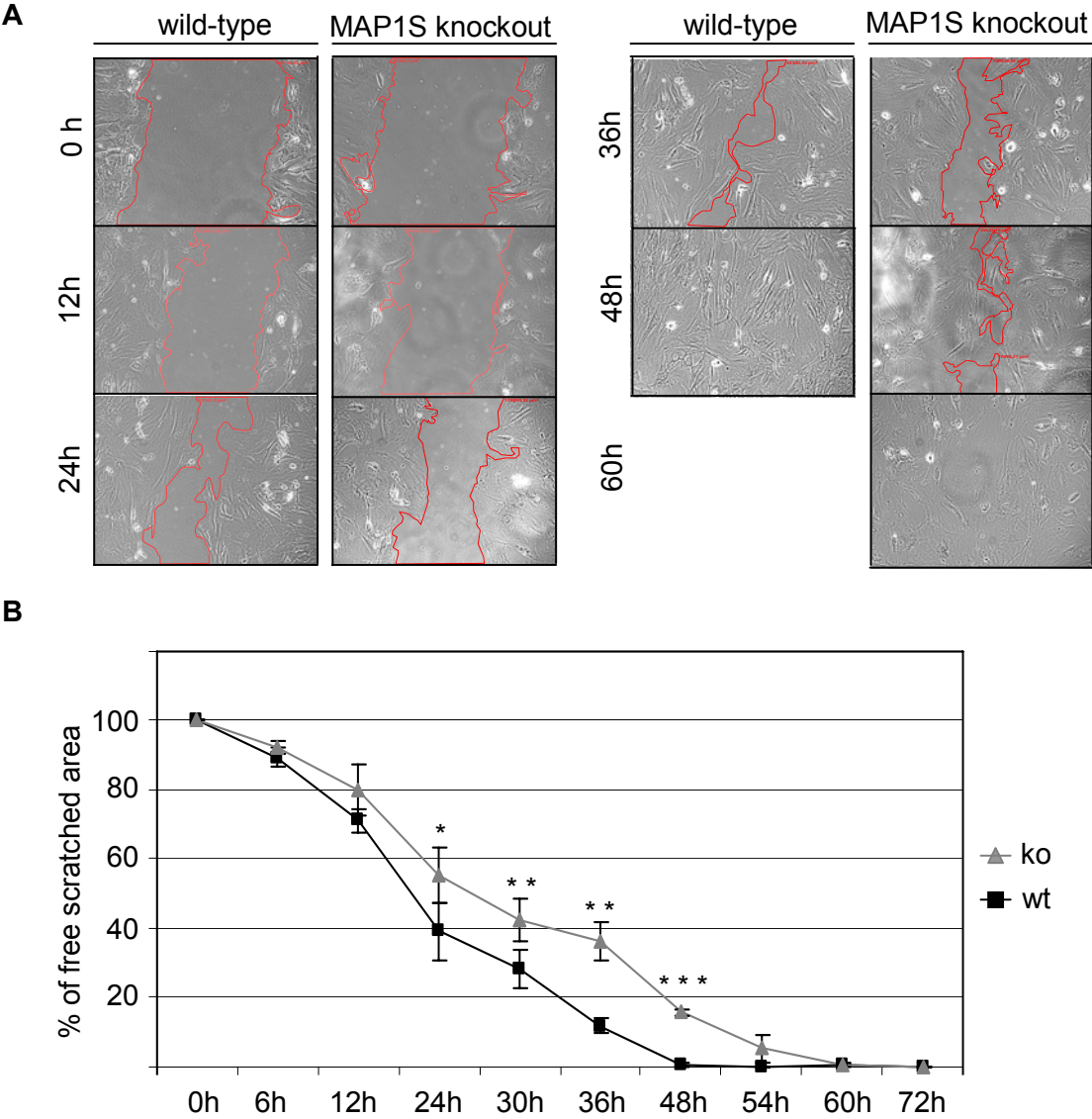


**Figure 39. MAP1S knockout fibroblasts closed the scratched wound slower than wild-type fibroblasts.** Fibroblasts from adult wild-type and MAP1S knockout mice were cultured and grown until they reached near confluence. Then the cell monolayer was scratched and pictures of these scratches were taken every 6 to 12 hours. (A) Representative pictures from scratched fibroblasts show the scratched cell free area from 0 hours (0h) up to 60 hours (60h) after the scratch. Analysis was performed with the AxioVision program, measuring the cell free area of the scratch (surrounded in red). MAP1S knockout fibroblasts migrated slower. Whereas the scratch wound was closed

after 48 hours in wild-type fibroblasts, MAP1S knockout fibroblasts needed 60 hours to close a scratch wound of equal width. **(B)** Cell free areas were measured at different time points and presented as mean values of the percentage of free area relative to the free area measured immediately after scratching (0h) with error bars representing standard deviations (five scratches in two independent experiments, fibroblasts isolated from two wild-type and two knockout mice). MAP1S knockout fibroblasts migrated slower. Whereas the sratch wound was closed after 48 hours in wild-type fibroblasts, MAP1S knockout fibroblast needed 60 hours to close the scratch wound. 24, 30, 36 and 42 hours after the scratch, differences were significant ( $p=0.03$  (\*),  $p=0.01$  (\*\*),  $p=0.01$  (\*\*),  $p=0.00002$  (\*\*\*) respectively, t-test).

MAP1S knockout fibroblasts migrated slower. Whereas the scratched wound was closed after 48 hours in wild-type fibroblasts, MAP1S knockout fibroblast needed 60 hours to close a scratch wound of equal width.

The proper organisation of the cytoskeleton network plays an important role in cell migration. To examine, whether the absence of MAP1S affected the organisation of microtubules and actin filaments, fibroblasts were cultured, fixed, stained for tubulin and actin and analysed by confocal fluorescence microscopy (figure 40). The appearance of microtubules and actin filaments was unaltered compared to wild-type fibroblasts.

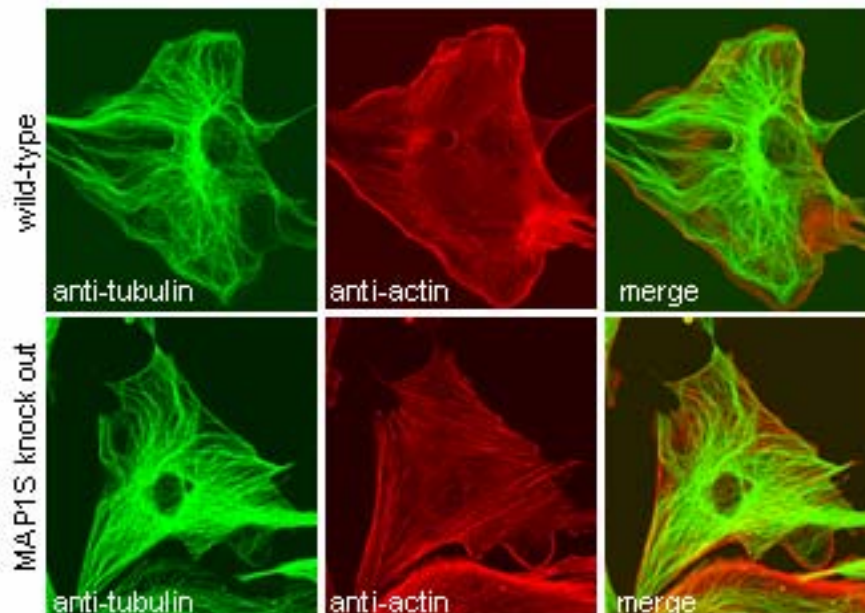


**Figure 40. The appearance of the cytoskeleton was not altered in fibroblasts isolated from MAP1S knockout mice.** Fibroblasts from adult wild-type and MAP1S

knockout mice were cultured, fixed, stained for tubulin and actin, and analysed by confocal fluorescence microscopy. Representative immunofluorescence pictures were taken. No differences were found between MAP1S knockout and wild-type fibroblasts in the appearance of microtubules and actin filaments.

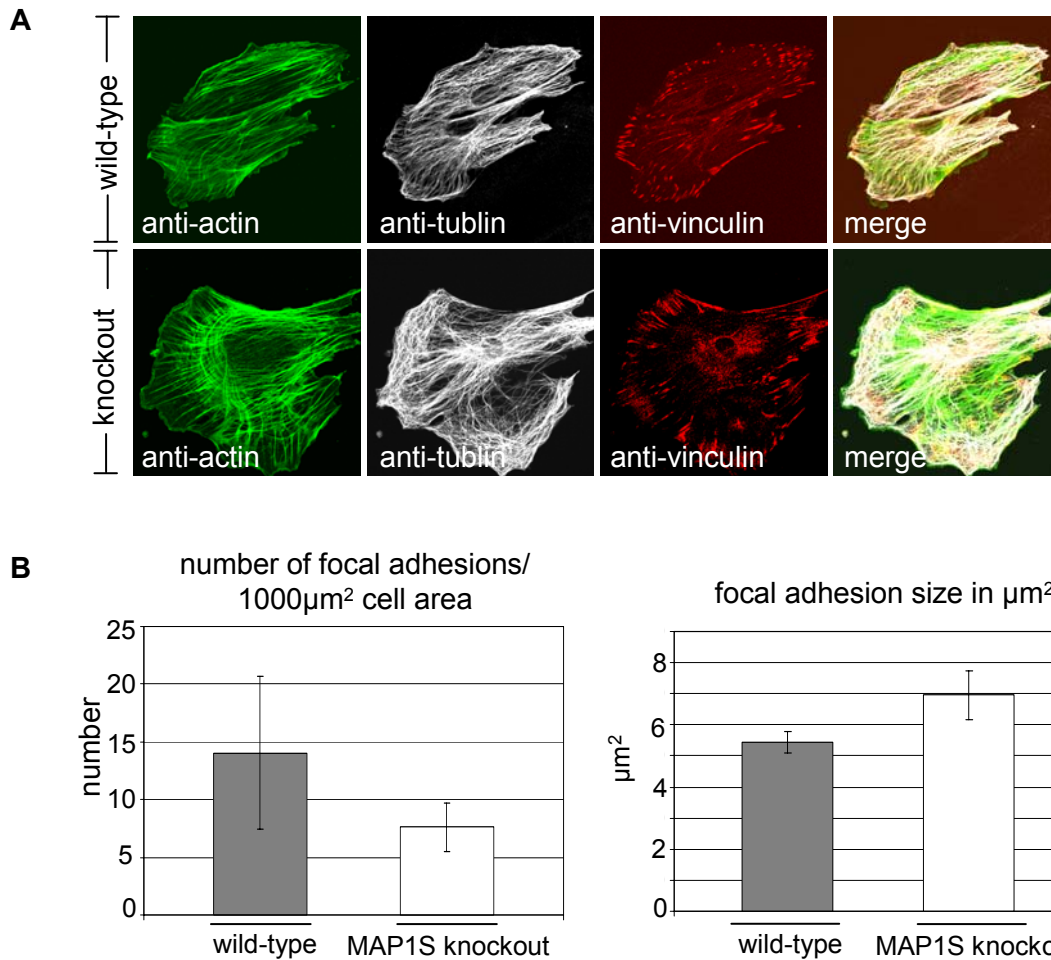


**Figure 41. The number of focal adhesions and their size are not significantly altered in fibroblasts isolated from MAP1S knockout mice.** Fibroblasts from adult wild-type and homozygous knockout mice were cultured for 24 hours, fixed, stained for tubulin, actin, vinculin, and analysed by confocal microscopy. Pictures were analysed by Image J, measuring size and number of particles stained with vinculin. **(A)** Representative immunofluorescence pictures were taken. **(B)** The number of focal adhesions per 1000 $\mu\text{m}^2$  cell area and the size of focal adhesions in  $\mu\text{m}^2$  of three independent experiments of fibroblasts from three wild-type and three knockout mice are presented as mean values with error bars representing standard deviations. The number of focal adhesions per 1000 $\mu\text{m}^2$  cell area is not significantly reduced ( $p=0.23$ , t-test), the size of focal adhesion is not significantly increased ( $p=0.06$ , t-test).

Cell migration is regulated partially by the connection between the substratum and the actin cytoskeleton. Vinculin, a protein in focal adhesion plaques, is one of the proteins involved in this linkage. The dynamic assembly and disassembly of focal adhesions plays a central role in cell migration. To explore the influence of MAP1S on the formation of focal adhesion, fibroblasts of wild-type and MAP1S knockout fibroblasts were isolated, cultured for 24 hours, stained for actin, tubulin and vinculin and analysed by confocal microscopy. Pictures were analysed by Image J, analysing size and number of particles stained with vinculin (figure 41). The number of focal adhesions per 1000 $\mu$ m<sup>2</sup> cell area was not significantly reduced and the size of focal adhesion was not significantly increased.

## DISCUSSION

While several mice with disrupted MAP1B genes have been available for some time (Edelmann et al., 1996; Gonzalez-Billault et al., 2000; Meixner et al., 2000; Takei et al., 1997), mice with disrupted MAP1S genes have not been reported so far. In this thesis, the generation and characterisation of MAP1S knock out mice are described for the first time.

### **General examination and histological analysis of MAP1S knockout mice**

As MAP1S is supposed to play an important role in mitosis by binding to RASSF1A/Cdc20/APC (Dalloi et al., 2007; Song et al., 2005), embryonic lethality after knocking out MAP1S was expected. Surprisingly, I found that homozygous MAP1S knock out mice are viable and fertile without showing any overt phenotype.

Due to its interaction with VCY2, MAP1S was supposed to play an important role in spermatogenesis (Wong et al., 2004). Interestingly, homozygous MAP1S knock out mice are fertile and histological analysis revealed that their testis do not show any abnormalities. Therefore, I can rule out that MAP1S is essential for spermatogenesis.

In brain, like in testis, MAP1S is expressed at a high level. Histological analysis of brains of MAP1S knock out mice showed no differences compared to wild-type mice. According to these results, MAP1S seems to be not essential for the development of the brain. The lack of an obvious phenotype of MAP1S knockout mice may be explained by potential functional redundancies. Developmental plasticity might compensate for the early loss of MAP1S. This may be due to functional redundancies at the single gene levels, the genetic pathway level or it may involve a systemic adaptive mechanism (Muller, 1999). Within the MAP1 family, MAP1A and MAP1B may functionally compensate for deficits associated with the loss of MAP1S. In immunoblot analysis the expression levels of MAP1A LC and MAP1B LC were not altered in the adult MAP1S knockout brain. Nevertheless, a compensatory effect of MAP1A and



MAP1B can not be excluded. On the one hand, MAP1A and MAP1B expression could be elevated during distinct developmental periods. On the other hand, MAP1A and MAP1B could be activated by posttranslational modifications and therefore compensate for MAP1S.

One method to unmask the compensatory effects would be to generate double-knockout mice. The comparison of phenotypes caused by individual and combined gene knockouts would allow the analysis of specific and redundant functions of individual family members (Muller, 1999). MAP1B appears to share some functions with both Tau and MAP2. Double-knockouts of either MAP1B and Tau or MAP1B and MAP2 resulted in more severe phenotypes than those seen in single knockouts (Takei et al., 2000; Teng et al., 2001). If MAP1B and MAP1S would act in a synergistic fashion, the phenotype of double-knockout mice should be more severe than in single-knockout mice. Till now, no MAP1A knockout mice are available to analyse compensation of MAP1A for MAP1S by this approach.

As MAP1S is expressed in all murine organs examined so far, all organs were screened by histological analysis. No abnormalities were found in three mice of different age and sex, apart from altered bile ducts in one liver of a four month old male mouse. The association between the loss of MAP1S and the increased number of interlobular bile ducts aside from portal triads is unclear. The epithelial cells of interlobular bile ducts are called cholangiocytes. Cholangiocytes may develop during fetal development and in the adult liver. During fetal development they emerge from hepatocytes (Cocjin et al., 1996; Lemaigre, 2003). In the adult liver cholangiocytes may originate from proliferation of pre-existing bile duct cells, from activated and differentiated progenitor cells, from cells which entered from the circulation and differentiate to liver cells or from biliary metaplasia of hepatocytes (Roskams et al., 2004). Endotoxins and inflammatory cytokines, such as lipopolysaccharide (LPS), tumour necrosis factor  $\alpha$  (TNF- $\alpha$ ), and interleukin-1 $\beta$  (IL-1 $\beta$ ), lead to stimulated secretion of IL-6 in cholangiocytes. Cholangiocytes themselves respond to IL-6 by enhanced proliferation (Chen et al., 2009; Matsumoto et al., 1994; Park et al., 1999; Van Snick, 1990). LPS additionally induces SOCS3, which negatively regulates IL-6 signalling and the subsequent phosphorylation of STAT3 (Crocker et al., 2003; Zou et al., 2008b). Interestingly, MAP1S depletion experiments by

siRNA suggested that MAP1S plays an important role in the negative regulation of SOCS3 on IL-6 signalling (Zou et al., 2008b). Thus, the increased number of interlobular bile ducts in the liver of the MAP1S knockout mouse may occur due to the disrupted inhibitory mechanism of SOCS3 in IL-6 signalling pathway. Gene targeting studies revealed that SOCS3 and IL-6 are dispensable for normal liver development and function under steady-state conditions, but both proteins are controlling responses to liver damage or disease (Cressman et al., 1996; Croker et al., 2003). Perhaps MAP1S is part of this mechanism and plays a role in response to liver damage or disease. This may explain why the altered liver phenotype was not found in all MAP1S knockout mice. Another reason, why this phenotype was only found in one mouse, may be their different genetic background. MAP1S knockout mice contained DNA from the 129 and C57BL/6 strain. To rule out the influences of the mixed genetic background, backcrossings would have to be performed.

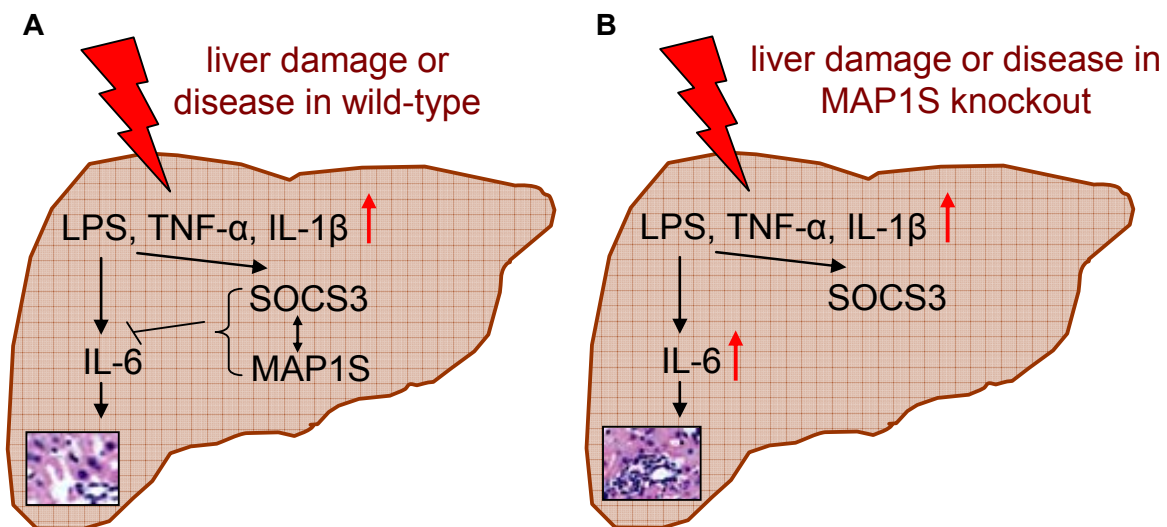


**Figure 42. A model for MAP1S mediated effects in liver damage or disease.** Lipopolysaccharide (LPS), tumour necrosis factor  $\alpha$  (TNF- $\alpha$ ), and interleukin-1 $\beta$  (IL-1 $\beta$ ), lead to stimulated secretion of IL-6 in cholangiocytes, which respond to IL-6 by enhanced proliferation (Chen et al., 2009; Matsumoto et al., 1994; Park et al., 1999; Van Snick, 1990). LPS additionally induces SOCS3, which negatively regulates IL-6 signalling if MAP1S is available (Croker et al., 2003; Zou et al., 2008b). Both, SOCS3 and IL-6 seem to control responses to liver damage or disease (Cressman et al., 1996; Croker et al., 2003). Thus, the increased number of interlobular bile ducts in the liver of the MAP1S knockout mouse may occur in response to liver damage or disease due to the disrupted inhibitory mechanism of SOCS3 in IL-6 signalling pathway.

In mice sent for histological analysis, no tumours were found. MAP1S is suspected to play a role in cancerinogenesis, mainly because MAP1S is interacting with the tumour suppressor protein RASSF1A (Dallol et al., 2004; Song et al., 2005). RASSF1A knockout mice were viable and fertile and were prone to spontaneous tumourigenesis at an advanced age, 18 to 20 months. 13 of 41 RASSF1A knockout mice developed tumours compared to two of 48 wild-type mice (Tommasi et al., 2005). Due to the young age and limited number of mice we analysed, we cannot rule out that MAP1S deficiency effects spontaneous tumourigenesis at an advanced age. To clarify the role of MAP1S in cancerinogenesis, more mice at an advanced age would have to be monitored.

### **MAP1S knockout DRGNs and Schwann cells**

In culture, DRGNs from MAP1S knockout mice displayed a shift towards cells with more than one axon. The mechanism determining where and how many axons form at the neuronal surface of DRGNs is unclear. In general, neurites are thin microtubule-based cell protrusions, which are formed by active outgrowth from the cell body and terminate in a dynamic, actin-rich growth cone of variable size. Several studies show that both microtubules and actin filaments are important in normal neurite initiation. Actin filaments and microtubules probably act not only individually, but in a cooperative fashion. Some findings suggest that actin filaments decelerate, while microtubules promote neurite initiation. Demehlt and Halpain propose that MAPs are a key to neurite initiation by altering microtubule function, for example by stabilising and bundling microtubules, or by mediating the crosstalk between microtubules and F-actin (Dehmelt and Halpain, 2004). MAP1S was shown to stabilise and bundle microtubules and to interact with both, microtubules and actin. Therefore, MAP1S deficiency may alter microtubule stability and interaction with actin filaments and therefore influence neurite initiation.

Caldron et al. described a correlation between axon outgrowth and the position of the centrosome in hippocampal neurons (de Anda et al., 2005; Knoblich, 2005). In cultured hippocampal neurons the axon arises from the neurite that

develops first after mitosis. Opposite the cleavage furrow, centrosomes, the Golgi apparatus and endosomes are clustered together close to the area where the first neurite forms. Interestingly, neurons with more than one centrosome sprout more than one axon (de Anda et al., 2005). The correlation between axon outgrowth and the position of the centrosome is found in rat hippocampal neurons and also in neurons in the developing eye of drosophila (de Anda et al., 2005; Knoblich, 2005). Outgrowth in DRGNs may be determined by a similar mechanism. Interestingly, MAP1S is localised on the centrosome throughout the cell cycle. MAP1S depletion by siRNA causes various mitotic spindle abnormalities including the formation of multipolar spindles (Dallol et al., 2007; Song et al., 2005). Therefore, the shift towards cells with more than one axon in DRGNs from MAP1S knockout mice may be a result of altered centrosomes in DRGNs. Analyses of DRGNs stained for centrosomes would reveal the role of centrosomes in the neurogenesis in DRGNs.

In Schwann cells, the number of processes per cell did not differ between MAP1S knockout and wild-type mice. For this reason, I assume MAP1S is not involved in the initiation of processes in Schwann cells. One can speculate that the initiation of processes in non-neuronal cells differs from the initiation of neurites in neuronal cells like DRGNs.

### **Cell cycle phase distribution in MAP1S knockout fibroblasts**

MAP1S was already suspected to play a crucial role in mitosis through its interaction with RASSF1A, but results obtained in different laboratories appear to contradict each other. Song et al. found that knockdown of MAP1S by short hairpin RNA leads to accelerated mitotic progression and increases the number of abnormal mitosis (Song et al., 2005). In contrast, Dallol et al. showed that the loss of MAP1S mediated by transient treatment with siRNA oligos leads to a delay in mitosis and accumulation in the G2/M phase (Dallol et al., 2007). MAP1S is known to interact with RASSF1A, which regulates mitosis by inhibiting the anaphase-promoting complex (APC)-Cdc20 complex resulting in delay of mitosis (Song and Lim, 2004; Song et al., 2004; van der Weyden and Adams, 2007). This MAP1S-RASSF1A interaction is thought to be required for

the proper control of the APC-Cdc20 complex during mitosis (Song et al., 2004; van der Weyden and Adams, 2007). According to these findings, I would expect that the loss of MAP1S leads to accelerated mitotic progression, as Song et al. found in HeLa cells after down regulating MAP1S by shRNA. Song et al. assumed that the interaction with RASSF1A blocks the ability of Cdc20 to activate the APC and therefore stabilises cyclin A and B and blocks the mitotic progression that usually follows their degradation (Song et al., 2005). My results obtained with fibroblasts from MAP1S null mice suggest that true MAP1S deficient cells spend significantly more time in the G0/G1 phase relative to S and G2/M phases. Therefore, I conclude that the loss of MAP1S results either in a G0/G1 arrest or in a G2/M acceleration. As my cell culture experiments revealed that MAP1S deficient fibroblasts are growing rather slower than wild-type fibroblasts (data not shown), I assume that the loss of MAP1S results more likely in a G0/G1 arrest than in a G2/M acceleration.

Thus, my results neither support those of Song et al. nor those of Dallol et al.. In both knockdown approaches, a low level of MAP1S protein was still detectable (Song et al., 2005), which may explain the discrepancy. My results represent the situation in real MAP1S null fibroblasts. According to my findings, I conclude that MAP1S plays a role in the regulation of the cell cycle. Surprisingly, MAP1S seems to regulate the cell cycle not only via binding to the RASSF1A-APC-Cdc20 complex, but, additionally, via the G1-S checkpoint. Interestingly, beside interacting with the APC-Cdc20 complex, RASSF1A plays also an important role at the G1-S checkpoint. Expression of exogenous RASSF1A induces G1 arrest via inhibiting the accumulation of cyclin D1 protein (Shivakumar et al., 2002; van der Weyden and Adams, 2007). Rong et al. confirmed these findings and found out that the RASSF1A induced G1 arrest is transient. They showed that 72h after transfection with constructs encoding RASSF1A, the proportion of RASSF1A-expressing G1-arrested cells was significantly reduced, but at the same time there was an increase in the population of RASSF1A-expressing cells in G2/M phase (Rong et al., 2004). To sum up, overexpressing RASSF1A seems to induce cell cycle arrest in both G1 and G2/M phase. It is still unknown whether the expression level of MAP1S influences the expression level of RASSF1A or the other way around. The likely G0/G1 arrest in MAP1S deficient fibroblasts may result from an increased level of RASSF1A.

I presume that MAP1S plays an important role in several phases of the cell cycle. The complete loss of MAP1S leads to a G0/G1 arrest, whereas a mere decrease of the MAP1S level results in accelerated mitotic progression (Song et al., 2005) or in a delay in mitosis and accumulation in the G2/M phase (Dallol et al., 2007). Therefore, I propose that the level of MAP1S is crucial for proper regulation of the cell cycle.

Interestingly, centrosomes seem to be required for several cell cycle transitions, including G1 to S phase, G2 to mitosis and metaphase to anaphase. Doxey et al. propose that the loss of centrosome integrity activates a checkpoint that inhibits G1/S progression (Doxey et al., 2005). As MAP1S is localised on the centrosome throughout the cell cycle and its depletion by siRNA causes various mitotic spindle abnormalities (Dallol et al., 2007; Song et al., 2005), the G0/G1 arrest in MAP1S deficient fibroblasts may also be caused by disturbed centrosome integrity.

### **Cell migration in MAP1S knockout fibroblasts**

In the random migration assay, no significant differences in migration velocity were found within 5.5 hours. A longer time period was monitored in the in vitro wound healing assay. Whereas wild-type fibroblasts could close the scratched wound after 48 hours, MAP1S knockout fibroblast needed 60 hours to close a scratch wound of equal width. 24, 30, 36 and 42 hours after the scratch, the width of the remaining free scratch area was different for wild-type and MAP1S knockout fibroblasts. These results show that the loss of MAP1S leads to slower migration of fibroblasts. The migration of cells plays a central role in many normal and pathological processes, like embryonic development, wound healing, inflammation and tumour metastasis (Huttenlocher et al., 1995). Fibroblasts are especially responsible for wound contraction and scar tissue formation. The results obtained in the in vitro wound healing assay revealed a novel role of MAP1S. The loss of MAP1S seems to impair wound healing.

During migration a cell polarises, extends protrusions at its front, pulls itself forward, and retracts its trailing end cyclically. Therefore the organisation of the cytoskeleton constantly changes. The regulated and polarised turn over of the

actin cytoskeleton and of the adhesion complexes that link it to the extracellular matrix drive cell movement (Small et al., 1996; Small et al., 1998). Fibroblasts lacking plectin or vimentin, which are delayed in migration, showed altered formation of the actin network and focal contacts (Andrä et al., 1998; Eckes et al., 1998). Microtubules themselves (Kaverina et al., 2000; Kaverina et al., 1998; Small et al., 2002; Small and Kaverina, 2003) and the interplay between microtubules and actin filaments are essential for cell motility (Waterman-Storer and Salmon, 1999; Rodriguez et al., 2003). Moreover, migrating cells usually exhibit a reorganised microtubule cytoskeleton with centrosomes and most microtubules orientated towards the leading edge. This reorientation of the microtubule-organising center (MTOC) seems to be essential for cell migration (Gotlieb et al., 1981; Gundersen and Bulinski, 1988; Kupfer et al., 1982; Palazzo et al., 2001). It remains to be seen whether reorientation of the microtubule network is impaired in MAP1S deficient fibroblasts.

MAP1S is known to bind to microtubules and actin filaments and to stabilise microtubules (Andrä et al., 1998; Eckes et al., 1998; Orban-Nemeth et al., 2005). Therefore, we expected to find altered formation of the cytoskeleton in MAP1S deficient fibroblasts. Surprisingly, no changes in microtubule and actin filament appearance were detectable in immunofluorescence analyses of MAP1S knockout dermal fibroblasts. MAP1S was shown to localise on centrosomes (Dallol et al., 2007; Song et al., 2005), and the knockdown of MAP1S by siRNA resulted in disrupted MTOCs. Therefore, the loss of MAP1S may disturb the positioning of the MTOC. The exact function of the reorientation of the MTOC toward the leading edge in migrating fibroblasts remains unclear. MAP1S could play an important role in this mechanism.

For migration, the cell adheres to a substrate and exerts traction. Adhesion occurs at specific foci, the focal adhesions. I looked at the formation of focal adhesions by staining for vinculin, a focal adhesion component. Although I could find a tendency towards less frequent, but enlarged focal adhesions, these differences were not significant. Therefore, I can not conclude that the loss of MAP1S alters focal adhesions. Beside their size and number, the dynamic of assembly and disassembly of focal adhesions plays a central role in cell migration. They have to assemble at the cell front and disassemble at the cell rear. As already mentioned, the cell has to exert traction to move. This force

is generated by contractile actin bundles pulling on focal adhesions. Microtubules specifically target focal adhesions and the targeting frequency is inversely proportional to the lifetime of a focal adhesion (Kaverina et al., 1999; Kaverina et al., 1998; Krylyshkina et al., 2003; Rodriguez et al., 2003). It is conceivable that MAP1S plays a role in the dynamic of assembly and disassembly of focal adhesions. More experiments need to be done to clarify this open question.

Rodriguez et al. suggest that microtubules are likely to be linked to focal adhesion associated actin filaments by static crosslinkers and grow along actin bundles (Krylyshkina et al., 2003; Rodriguez et al., 2003; Salmon et al., 2005). MAP1S is a potential crosslinker between microtubules and actin filaments. Its loss might restrict the linkage between microtubules and focal adhesion associated actin filaments and therefore impair cell migration.

Interestingly, Dallol et al. showed that overexpression of RASSF1A in various cell lines causes the formation of stable circular and acetylated microtubules and inhibits cell migration. RASSF1A deficient fibroblasts showed increased motility and migration potential (Dallol et al., 2005). MAP1S is interacting with RASSF1A (Dallol et al., 2004; Liu et al., 2002; Liu and McKeehan, 2002; Wong et al., 2004), but the function of this interaction is unclear. The loss of MAP1S may influence the expression level of RASSF1A. The impaired migration in MAP1S knockout fibroblasts may result from an increased level of active RASSF1A. The exact mechanism by which MAP1S can influence cell migration remains to be elucidated in further studies.



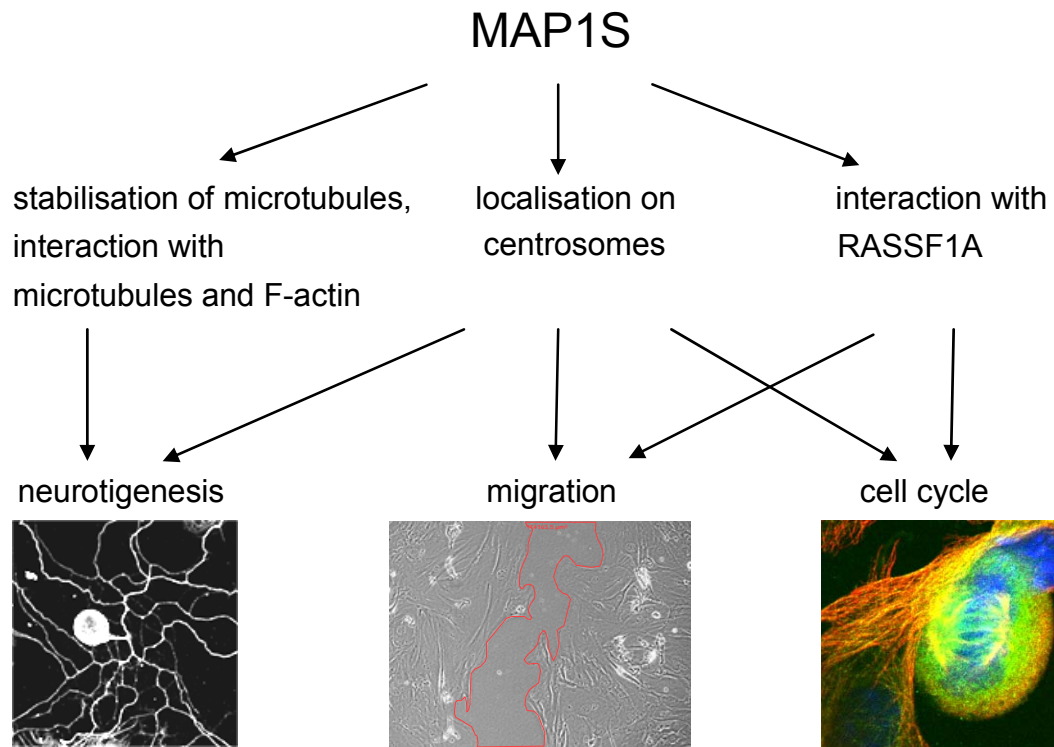


**Figure 43. A summary of potential functions of MAP1S in vivo.** MAP1S is known to bind to and stabilise microtubules, to bind to F-actin (Orban-Nemeth et al., 2005), to localise to centrosomes (Dallol et al., 2007; Song et al., 2005), and to interact with RASSF1A (Dallol et al., 2004; Liu et al., 2002; Liu and McKeehan, 2002; Wong et al., 2004). MAP1S deficiency leads to a shift towards cells with more than one axon in DRGNs. Therefore, MAP1S seems to be necessary in neurotogenesis. MAP1S acts probably due to its capacity to alter microtubule stability and to interact with actin filament, which seems to be essential for neurite initiation (Dehmelt and Halpain, 2004). As axon outgrowth correlates with the position of centrosomes (de Anda et al., 2005; Knoblich, 2005), MAP1S may influence neurotogenesis through its putative function on centrosomes. Moreover, MAP1S deficient fibroblasts migrate slower. Thus, MAP1S influences cell migration. As the cytoskeleton formation was not altered in MAP1S deficient fibroblasts, MAP1S seems to impair cell migration via another mechanism. I propose that the loss of MAP1S may disturb the positioning or functions of reorientated centrosomes, which were found to be essential for cell migration (Gotlieb et al., 1981; Gundersen and Bulinski, 1988; Kupfer et al., 1982; Palazzo et al., 2001). Since the overexpression of RASSF1A inhibits cell migration (Dallol et al., 2005), MAP1S may also regulate the level of active RASSF1A by binding to it and therefore accelerating cell migration. The regulation of the level of active RASSF1A may also explain the role of MAP1S in the G1/S progression, as the loss of MAP1S results in a G0/G1 arrest in fibroblasts, what was also found in RASSF1A overexpressing cells (Rong et al., 2004;

Shivakumar et al., 2002; van der Weyden and Adams, 2007). Additionally, the localisation of MAP1S on centrosomes may be necessary for their integrity, which is needed for G1/S progression (Doxsey et al., 2005).

# **MATERIALS AND METHODS**

## **Commonly used buffers**

1xPBS (phosphate buffered saline) 10mM  $\text{KH}_2\text{PO}_4/\text{Na}_2\text{HPO}_4$  pH 7.5, 150mM NaCl

1xSSC (sodium chloride/ sodium citrate): 150mM NaCl, 15mM Na-citrat, pH 7.0

1xTAE (Tris-acetate-EDTA): 400mM Tris-acetate pH 8.2, 20mM EDTA

1xTE (Tris-EDTA): 10mM Tris/HCl pH 8.0, 1mM EDTA

## **DNA METHODS**

### **DNA manipulation and preparation**

Basic cloning techniques like DNA restriction digests, ligation of DNA fragments and small scale preparation of plasmid DNA from bacteria were performed as described by Sambrook (Sambrook et al., 2001). For large scale preparation of plasmid DNA JetStar 2.0 Midi columns (Genomed) were used according to the manufacturer's instructions. DNA fragments for cloning or labeling were isolated by using the QuiaexII gel extraction kit (Qiagen) or the NucleoSpin ExtractII kit (Macherey-Nagel). Dephosphorylation of 5'-ends of vector DNA was carried out using the shrimp alkaline phosphatase (SAP) according to the manufacturer's protocol (Boeringer Mannheim GmbH).

Concentrations of the DNA were measured spectrophotometrically at 260nm.

### **Agarose gel**

0.7-2g of agarose powder was dissolved in 100ml of electrophoresis TAE buffer, heated in the microwave oven and cooled down to 60°C. After adding ethidium 0.5µg/ml bromide it was poured into a casting tray.

## **Preparation of rubidium chloride competent bacteria and transformation**

Appropriate bacteria (DH5 $\alpha$ , JM109, BL21) were inoculated and grown overnight. 5ml of this fresh overnight culture were inoculated into 500ml LB-medium (Luria Bertani Medium: 10g Bacto-Trypton, 5g Bacto-Yeast extract, 10g NaCl per 1000ml, pH 7.5) and shaken at 37°C until an OD<sub>600</sub> of 0.5 was obtained. The bacterial cells were incubated on ice for 15 minutes, pelleted for 5 minutes at 5000rpm (GSA rotor, 4°C) and resuspended in 200ml TfbI buffer (30mM potassium acetate, 100mM rubidium chloride, 10mM calcium chloride, 50mM manganese chloride, 15% v/v glycerol, pH 5.8 adjusted with acetic acid). The bacterial resuspension was placed again on ice for 15 minutes and centrifuged afterwards for 5 minutes at 5000rpm (GSA rotor, 4°C). The pelleted cells were resuspended in 20ml TfbII buffer (10mM MOPS, 75mM calcium chloride, 10mM rubidium chloride, 15% v/v glycerol, pH 6.5 adjusted with NaOH) put on ice for 15 minutes and aliquoted. The aliquots of competent cells were stored at -80°C.

For bacteria transformation an aliquot was thawed on ice, mixed with around 1 $\mu$ g of plasmid DNA or ligation mixture and placed on ice for 20 minutes. Then the mixture was incubated for 90 seconds at 42°C and afterwards for 90 seconds on ice. LB-medium was added and the cells were incubated for 1 hour at 37°C while gently shaking. Finally bacteria were plated on solid medium with appropriate antibiotics.

## **Isolation of genomic DNA from cells and mouse tails**

ES cell clones or 0.5 to 1cm of mouse tails were incubated with 500 $\mu$ l or 750 $\mu$ l, respectively, of lysis buffer (50mM Tris pH 8.0, 25mM EDTA pH 8.0, 100mM NaCl, 1% SDS, 300 $\mu$ g/ml Proteinase K added fresh) at 37°C overnight. On the next day, the lysates were extracted with phenol, phenol/chloroform and chloroform. Next, two times volume of EtOH was added and the precipitated DNA was spooled out with a sealed Pasteur pipette, put shortly to 70% EtOH for washing and resuspended in 100ml of TE and heated for 1 hour at 65°C.

## Polymerase chain reaction (PCR)

All PCR reactions were performed using the Gene Amp<sup>®</sup> PCR System 9700 (Applied Biosystems, Austria). For cloning the PCR were carried out in a final volume of 50µl containing 39µl ddH<sub>2</sub>O, 5µl 10X buffer (Invitrogen), 1µl dNTPs (10mM each dNTP), 0.5µl of each primer, 1.5µl of MgCl<sub>2</sub>, 0.5µl of Taq polymerase (Invitrogen) and 2µl of template DNA. For genotyping mice the PCR reactions were carried out in a final volume of 25µl containing 16.5µl ddH<sub>2</sub>O, 5µl 5xGreen GoTaq<sup>®</sup> Reaction Buffer (Promega), 0.5µl dNTPs (10mM each dNTP), 0.5µl of each primer, 0.25µl GoTaq<sup>®</sup> Polymerase (Promega) and 2µl of template DNA. Primer sequences and PCR programs used are listed in table 2. The PCR reaction products were analysed on 1-2 % agarose gels.

Primer sequence 5' -3'	PCR program	PCR product
probe U pA: CTCCAGGCCAGAGACCAGATAATG	5 min 94°C; 40x 60 sec 94°C, 60 sec 65°C, 3 min 72°C; 7 min 72°C	probe U: 316bp
probe U pB: GGAGGCTTGAGGGTTCTGCACAATG		
probe D pC: GGTTGCTGTCCTTGGGTCCTATAC	5 min 94°C; 40x 60 sec 94°C, 60 sec 65°C, 3 min 72°C; 7 min 72°C	probe D: 349bp
probe D pD: CCAGTTCATGCTGGCTCAACTCTC		
MAP1S E6/7 fw TGTATACCTGGACCTGGCCTACCTG	5 min 94°C; 40x 60 sec 94°C, 60 sec 65°C, 2 min 72°C; 7 min 72°C	MAP1S (Exon 6- Exon 7): 792bp
MAP1S E6/7 rev AAGGCCTCGTCCTGCATGGACAC		
loxPCR fw: GATCACATGCATGCTAGCATAACTTCGTA TAGCATAATTATACGAAGTTATAAGCTTT ACATGTGCATACAGAAAATCTC	5 min 94°C; 30x 60 sec 94°C, 60 sec 56°C, 6 min 72°C; 7 min 72°C	loxP PCR product: 2.155bp (Pfu polymerase was used)
loxPCR rev: GGGTCTCTGGTGGAGTTGCCTTCCTAGC		
PG1: GATTGGCTGGATGGTCAGGGACTTG		genotyping mice

PG2: TCTGGCCATCCGCTTCACATCTCTG	5 min 94°C; 45x 45 sec 94°C, 45 sec 65°C, 2 min 72°C; 7 min 72°C	
PG3: GATTGGCTGGATGGTCAGGGACTTG		
PG4: TGGGATCCGATGGTGTGTCTAACG		
PG5: GGCCACACGCGTCACCTTAATATGC		
Cre sense: CCAATTTACTGACCGTACACC	5 min 94°C; 45x 45 sec 94°C, 45 sec 65°C, 2 min 72°C; 7 min 72°C	cre: 1029bp
Cre antisense: TAATCGCCATCTTCCAGCAGG		
Flp sense: GTGGATCGATCCTACCCCTTGCG	5 min 94°C; 45x 45 sec 94°C, 45 sec 65°C, 2 min 72°C; 7 min 72°C	flip: 650bp
Flp antisense: GGTCCCAACCTGCAGCCCAAGCTTCC		

**Table 2. Primers and PCR programs used to amplify the described PCR products.**

## Southern Blot analysis

24-32µl of genomic DNA (10-15µg) were digested with 30-40 units of the appropriate restriction enzyme and separated on a 0.8% agarose gel. The DNA was depurinated by soaking the gel once in 500ml of 0.25M HCl for 15 minutes and denaturated twice for 15 minutes in 500ml of denaturation buffer (0.5N NaOH, 1.5M NaCl). To transfer the DNA to a nylon membrane (PALL Biotyne<sup>®</sup>B, pore size 0.45 µm, rinsed with dH<sub>2</sub>O before use) semi-dry alkaline blotting was performed overnight. On the next day the membrane was neutralized for 1 minute in 0.2M Tris/HCl pH 7.5, 1xSSC and the DNA was fixed to the membrane with crosslinking using the UV Stratalinker 2400 (Stratagene, 120mJ/cm<sup>2</sup>). Prehybridisation was done at 65°C in Church buffer (0.5M sodium phosphate pH 7.2, 1mM EDTA, 7% SDS) for 2 to 3 hours. Probes were radioactively labeled ( $\alpha$ -<sup>32</sup>P dCTP) with Prime-it II random labelling kit (Stratagene). Purification of the labeled probes was done with ProbeQuant<sup>™</sup> G-50 Micro columns (Amersham Pharmacia Biotech). Then the labeled probe was

denaturated for 5 minutes at 95°C and cooled down in ice for 3 minutes. For hybridisation the probe was diluted in 15ml of Church buffer, added to the membrane and shacked overnight at 65°C. Afterwards the membrane was washed once for 10 minutes and three times for 30 minutes with Church wash buffer (12mM sodium phosphate pH 7.2, 1% SDS) at 65°C and exposed to a X-ray sensitive film (Fuji medical X-ray film HR-E30) at -80°C for 1 to 5 days using an intensifying screen.

## **Cloning of the MAP1S conditional knockout targeting vector**

First, genomic mouse DNA was isolated from the RPCI-23\_374C22 BAC clone (DOE Joint Genome Institute). This BAC clone contained a region about 300kb from the C57BL/6J mouse chromosome 8, encoding the MAP1S gene amongst others. Bacteria were grown overnight at 37 °C in 150ml LB-medium containing 20µg/ml chloramphenicol, pelleted and resuspended in 6ml buffer E1 (50mM Tris, 10mM EDTA, pH 8.0 adjusted with HCl). 6ml of buffer E2 (200mM NaOH, 1.0% SDS) were added, gently agitated and incubated for 5 minutes at room temperature. Additionally, 6ml of buffer E3 (3.1M potassium acetate, pH 5.5 adjusted with acetic acid) were added, shacked and incubated for 10 minutes at 4°C. The lysate was centrifuged for 15 minutes at 6000rpm (GSA rotor, 4°C). Then, the supernatant was poured through a filter, mixed with 10ml isopropanol and centrifuged for 20 minutes at 10000rpm (HB4 rotor). The dried pellet was dissolved in 1.5ml ddH<sub>2</sub>O and extracted with phenol, phenol/chloroform and chloroform. To precipitate the DNA, 100µl of 3M NaAc pH 5.2 and 1ml of 96% EtOH were added, mixed and centrifuged for 5 minutes at 12000rpm. The DNA pellet was washed twice with 70% EtOH and resolved in 20µl TE.

After digestion with XhoI, a 13221bp fragment encoding exon 2 to exon 7 from MAP1S, was dephosphorylated and cloned into the pAM31 vector, creating the plasmid pK1. Then, one part of the MAP1S gene (including exon 2 and exon 3) was synthesised by PCR with loxPCR fw and loxPCR rev primers as described in table 2 to add the upstream loxPsite including appropriate restriction sites. The PCR product was analysed by sequencing, cloned into a pGEMTeasy vector and cut with NsiI. This fragment was then used to replace

the NsiI terminated part of the plasmid pK1 resulting in the plasmid pK4. To insert the second loxP site and the neo selection marker several cloning steps were needed. First, the oligo Mun was cloned into the SacI and KpnI sites of the pBlueIIKS+ vector resulting in the plasmid pK2. Second, the pRA11 plasmid was cut with NotI and KpnI and cloned into the NotI and KpnI sites of the plasmid pK2 creating the vector pK5. Then, the pK5 was cut with MunI and the 1246bp fragment was cloned into the EcoRI site of pK4 resulting in the targeting vector. Finally, the targeting vector contained exon 2 to exon 7 from MAP1S floxed with loxP sites and downstream a neo resistance flanked with frt sites.

Cloning vector/oligo	Used for	Source
pBlueIIKS+	cloning vector	Stratagene
pAM31	cloning vector	A.Meixner
pGEMTeasy	cloning vector (T/A)	Promega
oligo Mun fw: (5'-3') CAATTGCGGCCGCGGTACCGC TAGCAATTGTGTAC	synthetic oligonucleotides were annealed to oligo Mun and used for cloning	VBC Biotech
oligo Mun rev: (5'-3') ACAATTGCTAGCGGTACCGCG GCCGCAATTGAGCT		
pRA11	source for a loxP site and a frt flanked neo resistance	R. Ackerl

**Table 3. Plasmids and oligos used for cloning the MAP1S conditional knockout targeting vector.**

## PROTEIN METHODS

### Preparation of cell extracts

Cells grown on 6 or 10cm dishes were washed with PBS and 100µl to 250µl of SDS sample buffer (100mM Tris/HCl pH 6.8, 4% SDS, 20% v/v glycerol, 12mM EDTA, 0.2% bromphenol blue, 0.3% DTT and complete Mini protease inhibitor tablets (Roche Diagnostics)) were added. Then, the cells were scraped with a



cell scraper, transferred to an eppendorfer tube and sonicated 3 times 20 seconds at 50% of intensity. Samples were heated at 80°C for 5 minutes and used immediately or stored at -20°C.

### **Preparation of tissue extracts**

Mouse tissues were homogenized in 100µl/10mg SDS sample buffer (100mM Tris/HCl pH 6.8, 4% SDS, 20% v/v glycerol, 12mM EDTA, 0.2% bromphenol blue, 0.3% DTT and complete Mini protease inhibitor tablets (Roche Diagnostics)) and sonicated 3 times 20 seconds at 50% of intensity. Samples were heated at 80°C for 5 minutes and used immediately or stored at -20°C. Approximately 10-20µl of the protein extracts were subjected to SDS-PAGE.

### **Purification of microtubule proteins**

Brains from 1 to 4 day old mice were homogenised with a glass-teflon homogeniser in 100µl of ice cold polymerisation buffer (0,1M Pipes, 2mM EGTA, 1mM MgCl<sub>2</sub>, 1mM GTP, pH 6.8) per 100mg of tissue. Homogenates were centrifuged at 30000rpm (TLA-45, Beckman) for 15 minutes at 4°C and the supernatant was centrifuged again at 44000 rpm (TLA-45, Beckman) for 30 minutes at 4°C. In the next step the clear supernatant was mixed with an equal volume of 8M glycerol in polymerisation buffer. The mixture was incubated at 37°C for 30 minutes and then centrifuged at 44000rpm (TLA-45, Beckman) for 30 minutes at 35°C. The pellet was resuspended in ice cold polymerisation buffer, incubated on ice for 30 minutes and centrifuged at 44000 rpm (TLA-45, Beckman) for 30 minutes at 4°C. The supernatant was mixed with the same amount of 8M glycerol in polymerisation buffer and the sample was heated to 37°C for 30 minutes. After additional centrifugation at 44000rpm (TLA-45, Beckman) for 30 minutes at 35°C the supernatant was harvested. The obtained pellet contained microtubules and microtubule associated proteins. It was resuspended in polymerisation buffer and used immediately or stored at -80°C.

When this procedure was used to test acetylation of microtubule associated proteins, 1mM to 10mM sodium putyrat were added in all buffers to stabilize acetylation.

## **Determination of protein concentration**

Protein concentration was measured according to the Bradford method (Bradford, 1976). 100mg Coomassie Brilliant Blue G-250 was dissolved in 50ml 95% EtOH, 100ml 85% phosphoric acid were adjusted to 1000ml with ddH<sub>2</sub>O. This solution was filtered and stored at 4°C. To 1ml of this Coomassie solution 100µl of (diluted) protein sample was added. After short mixing and incubation at room temperature, the absorbance was measured at 595nm using a spectrophotometer. Dilutions of a BSA stock solution were used to produce a calibration curve.

## **Pulse-chase labeling of adherent cells with <sup>35</sup>S methionine and <sup>35</sup>S cysteine**

To determine the cleavage time of MAP1S, N2a cells were pulse chase labeled and analysed by immunoprecipitating.

5x10<sup>6</sup> N2a cells were seeded on 10 cm dishes. After washing twice with -Meth/-Cys media (DMEM -Meth/-Cys (Invitrogen), 10% dialysed FCS, 10mM HEPES) and incubated with DMEM -Meth/-Cys for 15 min. Then the media was replaced to prewarmed 10ml pulse-labeling media (DMEM -Meth/-Cys, 2mCi <sup>35</sup>S meth/cys) and incubated for 5 to 30 minutes. After removing the pulse-labeling media, cells were washed twice with growth media (DMEM, 10% FCS, 2mM L-glutamate and 50U/ml penicillin/streptomycin) containing 0.5mM Cyclohexamide and incubated in this media for 1 to 48 hours.

Then, cells were analysed by immunoprecipitating as described under co-immunoprecipitating by additionally taking radioactivity related security measures.

## **Immunoblotting**

Analysis of protein samples were carried out on 4-12% SDS-PAGE according to the protein size as described by Sambrook (Sambrook et al., 2001). Proteins were transferred to a nitrocellulose membrane (0.2 $\mu$ M, Schleicher Schuell) in transfer buffer (48mM Tris, 40mM glycine, 20% methanol) using BioRad Semi-Dry Electrophoretic Transfer Cell (Biorad) for 15-30 minutes at 15V. The efficiency of the transfer was controlled by reversibly staining with Amidoblack solution (0.1% Amidoblack, 45% EtOH, 10% Acetic Acid). Then the membrane was blocked in 2% BSA in PBS/0.25% Tween 20 for 1 hour at room temperature, washed three times with PBS/0.25% Tween 20 and incubated for 2 hours with primary antibodies suitably diluted in 1% BSA/PBS/0.25% Tween 20. The washing steps were repeated and the antibodies were visualized either using the appropriate horse radish peroxidase (HRP)-conjugated antibodies and the ECL-detection system (Pierce) or alkaline phosphatase (AP)-conjugated antibodies (Promega, Germany) and incubating the membrane in AP- buffer (100mM Tris/HCl pH 9.6, 100mM NaCl, 5mM MgCl<sub>2</sub>; 90 $\mu$ lNBT (nitroblue tetrazolium chloride, 50mg/ml in 70% DMF) and 45 $\mu$ l BCIP (5-bromo-4-chloro-3-indolyl phosphate, 50mg/ml in 100% DMF) were added per 10ml AP-buffer). Primary and secondary antibodies are listed in table 5 and table 6.

## **Co-Immunoprecipitation**

Cell extracts or mouse brain lysates were homogenized in 1ml of ice cold TEN buffer (100mM Tris/HCl pH 7.5, 100mM NaCl, 10mM EDTA, 0.1mM DTT and Complete Mini protease inhibitors tablets (Roche Diagnostics)) at 4°C with motor driven glass-teflon homogenizer. Homogenates were centrifuged at 14000rpm at 4°C and the supernatants were precleared with 1/5 volume of Protein A sepharose beads (Amersham Pharmacia Biotech, USA) pre-treated with 2% BSA for 3 hours at 4°C. Unspecific bound proteins were removed by centrifugation at 1500rpm for 5 minutes at 4°C. All supernatants were then incubated overnight at 4°C with 1 $\mu$ g/ ml if indicated antibodies followed by an additional incubation with 1/5 volume of Protein A sepharose beads for 3 hours.

Immune complexes were collected by centrifugation at 1500rpm, washed 3 times with TEN buffer containing protease inhibitors and eluted from beads by heating in 50µl SDS sample buffer (100mM Tris/HCl pH 6.8, 4% SDS, 20% v/v glycerol, 12mM EDTA, 0.2% bromphenol blue) containing 5% 2-mercaptoethanol. Finally samples were analysed via immunoblotting.

## **Blot overlay assay**

0.5-1µg of recombinant proteins were loaded on 4-12% SDS-PAGE according to the protein size as described by Sambrook (Sambrook et al., 2001), separated and transferred to a nitrocellulose membrane (0.2µM, Schleicher Schuell, Germany) in transfer buffer (48mM Tris, 40mM glycine, 20% methanol) using BioRad Semi-Dry Electrophoretic Transfer Cell (Biorad) for 15- 30 minutes at 15V. After staining with amidoblack to control the protein transfer, the membranes were destained and blocked for 1 hour at room temperature in 2% BSA in overlay buffer (1xPBS, 0.1% Tween 20, 150mM NaCl). After washing three times for 5 minutes in overlay buffer, the blots were incubated for 2 hours with 0.1µg/ml recombinant protein in 1% BSA in overlay buffer at room temperature. After repeated washing in overlay buffer the membrane was incubated with suitable diluted primary antibody in overlay buffer for 1.5 hours at room temperature. The immune complexes were detected using appropriate alkaline phosphatase (AP)-conjugated (Promega) or horse radish peroxidase (HRP) conjugated antibodies (Pierce).

## **CELL CULTURE, IMMUNOFLUORESCENCE MICROSCOPY**

### **Maintenance of cell lines**

Frozen cells stored in liquid nitrogen were thawed in a 37°C water-bath, diluted in 10ml of growth medium (DMEM, 10% FCS (Fetal Calf Serum), 2mM L-glutamate and 50U/ml penicillin/streptomycin), centrifuged at 1000 rpm (Heraeus Megafuge) for 3 minutes at room temperature and resuspended in growth medium. Ptk2, NIH3T3 and N2a cells were cultured on plastic dishes in

growth medium at 37°C in a humidified atmosphere containing 5%-8.5% CO<sub>2</sub>. When cell reached confluence, they were washed with PBS and incubated with trypsin (0.05% trypsin, 0.2% EDTA) for 5 minutes at 37°C. The trypsinisation was inhibited by adding the double amount of growth medium. Cells were centrifuged, resuspended in growth medium and splitted into new culture dishes. For freezing, cells were trypsinised, pelleted, resuspended in freezing medium (growth medium containing 10% DMSO) and aliquoted into cryotubes (Nunc). The cryotubes were stored at -80°C for 1 day and then put into a liquid nitrogen tank.

### **Transfection of mammalian cells using FuGENE6**

The FuGENE6 (Roche Diagnostic) is a lipid based transfection reagent used for transfection of a wide range of eukaryotic cells because of its high efficiency and minimal cytotoxicity. 12 to 24 hours prior to transfection, cells were seeded on glass coverslips in the wells of a standard 24-well plate (for immunofluorescence analysis) or on 10cm plastic dishes (for protein analysis). Tet-transactivator dependent expression constructs were cotransfected with pTetTA in ration 1:6 Tet responsive expression vector: Tet transactivator pTetTA. The DNA-FuGENE6 complex was prepared in polypropylene tubes. Before use, the FuGENE6 was warmed to room temperature and mixed well. For each well for immunofluorescence analysis, 0.5µg of DNA mixture in 25µl DMEM was mixed with 1.5µl FuGENE6 and incubated for 30 minutes at room temperature. Then solution was diluted in 75µl of Optimem (Invitrogen) and added drop- wise to the middle of the well. For protein analysis 4µg of DNA and 9µl of FuGENE6 in 75µl DMEM were required. After 30 minutes incubation at room temperature, 225µl of DMEM was added and the mixture was transferred to the middle of the culture dish. After gentle mixing the plates were incubated under appropriate conditions for the cell line used.

<b>Construct</b>	<b>Encoding for</b>	<b>Source</b>
pHS1	C-myc tagged mouse MAP1S FL (aa 1-973)	Z. Orban-Nemeth
pHS9	C-myc tagged mouse MAP1S LC (aa 755-973)	Z. Orban-Nemeth
pAT11	C-myc tagged mouse MAP1S HC (aa 1-755)	A. Trancikova
pMT5	C-myc tagged rat MAP1B FL (aa 1-2459)	M. Tögel
pMT7	C-HA tagged rat MAP1B N-terminus (aa 1-508)	M. Tögel
pMT22	C-myc tagged rat MAP1B LC (aa 2210-2459)	M. Tögel
pMT11	C-HA tagged rat MAP1B LC C-terminus (aa 2336-2459)	M. Tögel
pMT11 C2354S	C-HA tagged rat MAP1B LC mutated C-terminus (aa 2336-2459)	A. Trancikova
pMT11 C2457S	C-HA tagged rat MAP1B LC mutated C-terminus (aa 2336-2459)	A. Trancikova
pMT19	C-myc tagged uncleavable rat MAP1B FL (aa 1-2459)	F. Propst
pAH1	C-HA tagged rat MAP1A LC (aa 2554-2774)	F. Propst
nNOS	N-HA tagged human nNOS (aa 3-217)	A. Trancikova

**Table 4. Tet-transactivator dependent expression constructs used for transfection of mammalian cell lines.**

## **Activation and inhibition of nitrosylation in cultured cells**

For the activation of nitrosylation cells were cultured and treated with S-Nitroso-N-acetylpenicillamin (SNAP, Calbiochem) at a final concentration of 100µM for 1 to 4 hours at 37°C in the dark.

The nNOS inhibitor N-ω-propyl-L-arginine (NPA, Tocris) was added at a final concentration of 1mM for 30 minutes to 1 hour.

## **Immunofluorescence microscopy of cells**

PtK2, N2a or NIH3T3 cells were grown on plastic dishes or glass coverslips. When the cells reached the desired density, they were washed with PBS and incubated with 4% PFA in PBS for 20 minutes at room temperature, washes three times with PBS and incubated for 2 minutes with prechilled methanol on a

prechilled (-20°C) metal block for fixation and permeabilizing. Cells were washed again three times with PBS and in the case of cell growth on plastic dishes they were divided into sections with a hydrophobic isolator pen (Lipshaw). For blocking of unspecific binding sites, coverslips or sections of plastic dishes were incubated with 2% BSA in PBS for 1 hour at room temperature. After washing with PBS, primary antibodies diluted in 1% BSA in PBS were added for 1 hour at room temperature. Cells were washed three times with PBS and incubated with fluorescence-labeled secondary antibodies for 1 hour at room temperature under light protection. They were washed again with PBS and additionally with ddH<sub>2</sub>O. 8µl of moviol was added either on the sections and then covered with glass coverslips or the moviol was placed on a glass slide and the coverslip with the cells was put upside down on it. Samples were stored at 4°C.

### **Isolation and cultivation of dissociated adult DRG neurons**

Mice were anesthetized with IsoFlo (Abbott) and killed by decapitation. Skin and muscles beside the vertebra were removed, vertebra was opened and the spinal cord was taken out.

The cultivation of mouse DRG neurons was performed according to the protocol of Tonge (Tonge et al., 1997). DRG neurons were harvested in F-12 medium and cut into small pieces before enzymatic dissociation by collagenase solution (for DRG neurons from 1 mouse: 200µl collagenase (4000U/ml, Sigma), 800µl F-12 medium, 20µl horse serum) for 2 hours at 37°C. Then the solution was removed and DRG neurons were incubated with 1ml trypsin/DNAase solution (500µl Trypsin (0.05% trypsin, 0.2% EDTA), 20µl DNase1 (1µg/µl), 480µl PBS) for 15 minutes at 37°C. The trypsinisation was stopped with 2ml stop solution (1.6ml F-12 medium, 400µl horse serum) and DRG neurons were triturated several times with narrowed Pasteur pipettes. Cells were harvested with centrifugation at 800rpm (Heraeus Megafuge) for 5 minutes and washed twice with F-12 medium. Finally DRG neurons were resuspended in growth medium (F-12 medium supplemented with N3 (Romijn et al., 1981), 5% horse serum, 40% glucose, penicillin/streptomycin (Bottenstein and Sato, 1979) and plated on

poly-L-lysine (10 $\mu$ g/ml, Sigma) and mouse laminin (10 $\mu$ g/ml, Sigma) precoated coverslips with a density of 100 cells/cm<sup>2</sup>. Cells were incubated for 24-48 hours at 37°C in a humidified atmosphere containing 5% CO<sub>2</sub>. For immunofluorescence analysis, DRG neurons were fixed in 4% PFA, 11% sucrose in a PBS: growth medium mixture 1:1 for 45 minutes at room temperature. After washing several times with PBS, cells were permeabilized and blocked with blocking solution (5% BSA in PBS) containing 0.3% TritonX100 for 1 hour at room temperature or overnight at 4°C. Cells were washed with PBS, incubated with primary antibodies diluted in 5% BSA in PBS for 3 hours at room temperature, washed again and incubated with secondary antibodies for 2 hours at room temperature under light protection. The samples were washed with PBS and finally with ddH<sub>2</sub>O and the coverslips were mounted on glass slides with moviol. Samples were stored at 4°C.

### **Isolation and cultivation of adult Schwann cells**

Mice were anesthetized with IsoFlo (Abbott) and killed by decapitation. Then sciatic and trigeminal nerves were removed from mice and used immediately or frozen in 10% DMSO in FCS. Nerves were washed in DMEM-F12 and placed in degeneration media (DMEM with high glucose, 10% FCS, 50 $\mu$ g/ml gentamycin, 2.5 $\mu$ g/ml fungizone, 2 $\mu$ M forskolin, 10ng/ml heregulin- $\beta$ 1). Half of the media was changed every third day for two weeks. Then the nerves were rinsed three times in PBS-/- and transferred to a 80cm<sup>2</sup> flask with 10ml dissociation media (L-15 (Gibco), 130U/ml collagenase type I, 2.5mg/ml dispase I, 50 $\mu$ g/ml gentamycin, 2.5 $\mu$ g/ml fungizone, 50U/ml penicillin/streptomycin) for 3.5 hours at 37°C, agitating every hour. Then 20ml stop solution (DMEM, 10% FCS) were added and nerves were dissociated by pipetting with a narrowed Pasteur pipette. Cells were centrifuged, resuspended in N2-HRG media (DMEM F-12, 1ml/100ml N2 supplement (Gibco), 50 $\mu$ g/ml gentamycin, 2.5 $\mu$ g/ml fungizone, 2 $\mu$ M forskolin, 10ng/ml heregulin- $\beta$ 1) and plated on poly-L-lysine (10 $\mu$ g/ml, Sigma) and mouse laminin (10 $\mu$ g/ml, Sigma) precoated 6cm dishes. On the next day the supernatant was plated on precoated coverslips. The adherent



cells were trypsinised and plated on precoated coverslips for further immunofluorescence analysis.

### **Isolation and cultivation of adult fibroblasts**

Mice were anesthetized with IsoFlo (Abbott) and killed by decapitation. The back of the mouse was shaved and rinsed with 70% of EtOH to remove all hairs. Skin samples with a size around 2-3cm<sup>2</sup> were excised and incubated in 0.3% trypsin in PBS for 20 hours at 4°C. On the next day the epidermis was scraped off, the dermis was washed in PBS and cut into small pieces with surgical scalpels. The small pieces were incubated for 2 hours with 3ml of collagenase (1000U/ml, Sigma) at 37°C, agitating every 20 to 30 minutes. 3ml of cold growth medium (DMEM, 10 % FCS and 50U/ml penicillin/streptomycin) were added to stop the reaction and the cells were vortexed vigorously to release the fibroblasts from collagen fibres. The suspension was passed through a 100µm nylon mesh to remove dermal debris, centrifuged with 800rpm (Hereaus Megafuge) for 10 minutes at 4°C and resuspended in growth medium. The fibroblast suspension was then plated in a 5cm dish. For cultivation the growth medium was changed every second day and the cells were splitted, frozen around passage 4 and thawed as described above.

### **In vitro wound healing assay**

Primary adult fibroblasts were seeded and grown till near confluency. With a sterile pipette tip a scratch was made with in the monolayer. Then, the migration of cell swas measured over a time of 72 hours with the scratch serving as a reference point. The same spot was photographed every 6 hours. Analysis was performed with the AxioVision program, measuring the cell free area of the scratch.

## **Maintenance of embryonic stem (ES) cells**

ES cells were cultured at 37°C in a humidified atmosphere containing 8.8% CO<sub>2</sub> in ES cell medium (high glucose DMEM, 10% FCS (Gibco), 1xNon Essential Amino Acids, 1mM Sodium pyruvate, 2mM L-glutamin, 1xpenicillin/streptomycin solution, 0.05mM mercaptoethanol and 1000U/ml ESGRO LIF (Chemicon)). The medium was changed every day. Cells were maintained as described previously for cell lines with the difference that they were grown on confluent layer of mitomycin C treated G418-resistant primary embryonic fibroblasts. Therefore MEFs were seeded onto the appropriate culture dish, grown up to confluence and treated with MEF medium (DMEM, 10% FCS, 2mM L-glutamin, 1xpenicillin/streptomycin solution) and 10µg/ml mitomycin C for 2 hours before ES cells were split. ES cells were trypsinised for 3 to 5 minutes at 37°C, resuspended with ES cell medium to get a single cell suspension and split 1:3 to 1:5.

## **Electroporation of ES cells with targeting vector**

DNA of the targeting vector was prepared following Qiagen EndoFree Plasmid Maxi (Qiagen) protocol and redissolved in 100µl endotoxin-free TE under sterile conditions. 100µg of the targeting vector was digested in a final volume of 100µl overnight at 37°C. The DNA was extracted with phenol chloroform as described above and precipitated with 1/10 volume of 3M Na-acetate pH 5.0 and two volumes of ethanol. The precipitated DNA was washed with 70% ethanol, air dried and dissolved in 40µl PBS for 10 minutes at 37°C.

For one electroporation 10<sup>7</sup> ES cells or around five 10cm dishes of exponentially growing ES cells were needed. Cells were washed with PBS, trypsinised, centrifuged at 1000rpm for 5 minutes, washed twice with PBS and resuspended in 800µl PBS. 20µg linearised targeting vector was added and the mixture was transferred in a sterile electroporation cuvette (Biorad) and an electric pulse was applied at 260V and 500µF (Biorad Gene Pulser, Biorad). Cell suspension was incubated 10 minutes at room temperature after pulsing, resuspended in ES cell medium and plated at a density of 2x10<sup>6</sup> cells per 10cm dish. 24 hours after

electroporation selection with 300µg/ml G148 was started. Growing ES cell colonies were microscopically inspected and ES cell medium containing 300µg/ml G148 was changed every day. After 7 to 9 days colonies were picked by using a yellow tip of a gilson pipette and transferred to a 96-well microtiter plate. 30µl of 1xtrypsin (Gibco) was added to each well and the plate was incubated for 5 minutes at 37°C. 60µl of ES cell medium was added to stop trypsinisation and cells were transferred into a 24-well plate and grown there for 2-4 days. Almost confluent cultures were trypsinised (300µl 1x trypsin; 750µl ES cell medium). Half of the cell suspension was frozen immediately at -80°C with 500µl of ES freezing medium (ES cell medium containing 20% DMSO and 40% FCS). The rest was transferred onto gelatine coated 24-well-plate. These cells were then used for preparation of genomic DNA and genotypic analysis of the ES clones.

### **Blastocyst injection of ES cells**

The ES cells were thawed and plated on a 6-well-plate before blastocyst injection. For harvesting, cells were washed twice with PBS, trypsinised, centrifuged and resuspended in 2ml of medium. As described by Hogan (Hogan et al., 1986) the blastocysts were isolated and collected from C57BL/6 females at 3.5 days p.c. ES cells were injected into blastocysts and then transferred to female C57BL/6/CBA recipient mice by H. C. Theussl and J. Woitschekowski.

## **ANIMALS**

### **Generation and maintenance of MAP1S (conditional) knockout mice**

ES cell clones were injected into C57BL/6 blastocysts. Chimeric male founder mice were backcrossed to C57BL/6 females to obtain heterozygous mice. Heterozygous offsprings were paired to obtain homozygous conditional knockout mice for further breeding with cre mice lines.

Additionally chimeric male founder mice were paired with cre deleter mice obtain heterozygous knockout mice. These heterozygous offsprings were paired to obtain homozygous conditional knockout mice for further analysis.

All mice were kept under standard housing conditions at the animal facility of the Max F. Perutz Laboratories (University of Vienna).

Offsprings were screened by Southern Blot or PCR analysis (or both) of tail DNA as described in chapter DNA methods.

## ANTIBODIES

All primary and secondary antibodies used for immunoblotting or immunofluorescence are listed in table 5 and table 6. Antibodies used for immunoblotting were diluted in 1%BSA in PBS/0.25% Tween 20, for immunofluorescence antibodies were diluted in 1% BSA in PBS.

Antigen	Name/Clone	Source	Species	IF	WB
$\alpha$ -tubulin	B512	Sigma	mouse	1:2000	1:5000
$\alpha$ -tubulin			rat	1:500	
$\alpha$ - $\beta$ -actin	AC75/15	Sigma	mouse	1:400	1:1000
HA	3F10	BM	rat	1:300	
N-epsil acety lysin	Ab409/11A1	Abcam	mouse		1:1000
nNOS	NOS1 (R20)	Santa Cruz	rabbit	1:500	1:1000
MAP1A HC	HM-1	Biogenesis	rabbit		1:1000
MAP1A LC	892	A.Meixner	rabbit		1:1000
MAP1B HC	891	A.Meixner	rabbit	1:200	1:800
MAP1B LC	LC1A	M.Tögel	rabbit	1:200	1:1000
MAP1S HC		Z.OrbanNemeth	rabbit	5 $\mu$ g/ml	2.5 $\mu$ g/ml
MAP1S LC		Z.OrbanNemeth	rabbit	5 $\mu$ g/ml	2.5 $\mu$ g/ml
myc (IF)	myc 1/2	M.Tögel	rabbit	1:300	
myc (WB)	myc 3/4	M.Tögel	rabbit		1 $\mu$ g/ml
vinculin	vin-11-5	Sigma	mouse	1:400	

**Table 5. List of primary antibodies.**

<b>Antigen</b>	<b>Source</b>	<b>Species</b>	<b>IF</b>	<b>WB</b>
Alexa 488-anti-mouse IgG	Mol. Probes	goat	1:1000	
Alexa 488-anti-rabbit IgG	Mol. Probes	goat	1:1000	
AP-anti-mouse IgG	Jackson lab.	goat		1:5000
AP-anti-rabbit IgG	Jackson lab.	goat		1:5000
Cy5-anti-rat IgG	Mol. Probes	goat	1:1000	
HRP-anti-mouse IgG	Jackson lab.	goat		1:10000
HRP-anti-rabbit IgG	Jackson lab.	goat		1:10000
Texas red-anti mouse IgG	Mol. Probes	goat	1:1000	
Texas red-anti rabbit IgG	Mol. Probes	goat	1:1000	

**Table 6. List of secondary antibodies.**

## References

- Alberts B., J. A., Lewis J., Raff M., Roberts K., Walter P. (2008). *Molecular Biology of the cell*, 5th edition edn).
- Allen, E., Ding, J., Wang, W., Pramanik, S., Chou, J., Yau, V., and Yang, Y. (2005). Gigaxonin-controlled degradation of MAP1B light chain is critical to neuronal survival. *Nature* 438, 224-228.
- Andrä, K., Nikolic, B., Stocher, M., Drenckhahn, D., and Wiche, G. (1998). Not just scaffolding: plectin regulates actin dynamics in cultured cells. *Genes Dev* 12, 3442-3451.
- Avila, J., Dominguez, J., and Diaz-Nido, J. (1994a). Regulation of microtubule dynamics by microtubule-associated protein expression and phosphorylation during neuronal development. *Int J Dev Biol* 38, 13-25.
- Avila, J., Ulloa, L., Gonzalez, J., Moreno, F., and Diaz-Nido, J. (1994b). Phosphorylation of microtubule-associated proteins by protein kinase CK2 in neuritogenesis. *Cell Mol Biol Res* 40, 573-579.
- Bates, C. A., Trinh, N., and Meyer, R. L. (1993). Distribution of microtubule-associated proteins (MAPs) in adult and embryonic mouse retinal explants: presence of the embryonic map, MAP5/1B, in regenerating adult retinal axons. *Dev Biol* 155, 533-544.
- Bettencourt da Cruz, A., Schwarzel, M., Schulze, S., Niyiyati, M., Heisenberg, M., and Kretschmar, D. (2005). Disruption of the MAP1B-related protein FUTSCH leads to changes in the neuronal cytoskeleton, axonal transport defects, and progressive neurodegeneration in *Drosophila*. *Mol Biol Cell* 16, 2433-2442.
- Bomont, P., and Koenig, M. (2003). Intermediate filament aggregation in fibroblasts of giant axonal neuropathy patients is aggravated in non dividing cells and by microtubule destabilization. *Hum Mol Genet* 12, 813-822.
- Bottenstein, J. E., and Sato, G. H. (1979). Growth of a rat neuroblastoma cell line in serum-free supplemented medium. *Proc Natl Acad Sci U S A* 76, 514-517.
- Bouquet, C., Ravaille-Veron, M., Propst, F., and Nothias, F. (2007). MAP1B coordinates microtubule and actin filament remodeling in adult mouse Schwann cell tips and DRG neuron growth cones. *Mol Cell Neurosci* 36, 235-247.
- Bouquet, C., Soares, S., von Boxberg, Y., Ravaille-Veron, M., Propst, F., and Nothias, F. (2004). Microtubule-associated protein 1B controls directionality of growth cone migration and axonal branching in regeneration of adult dorsal root ganglia neurons. *J Neurosci* 24, 7204-7213.

- Bradford, M. M. (1976). A rapid and sensitive method for the quantitation of microgram quantities of protein utilizing the principle of protein-dye binding. *Anal Biochem* 72, 248-254.
- Chang, L., Jones, Y., Ellisman, M. H., Goldstein, L. S., and Karin, M. (2003). JNK1 is required for maintenance of neuronal microtubules and controls phosphorylation of microtubule-associated proteins. *Dev Cell* 4, 521-533.
- Chen, L. P., Cai, M., Zhang, Q. H., Li, Z. L., Qian, Y. Y., Bai, H. W., Wei, X., Shi, B. Y., and Dong, J. H. (2009). Activation of interleukin-6/STAT3 in rat cholangiocyte proliferation induced by lipopolysaccharide. *Dig Dis Sci* 54, 547-554.
- Chowdhury, K., Bonaldo, P., Torres, M., Stoykova, A., and Gruss, P. (1997). Evidence for the stochastic integration of gene trap vectors into the mouse germline. *Nucleic Acids Res* 25, 1531-1536.
- Cocjin, J., Rosenthal, P., Buslon, V., Luk, L., Jr., Barajas, L., Geller, S. A., Ruebner, B., and French, S. (1996). Bile ductule formation in fetal, neonatal, and infant livers compared with extrahepatic biliary atresia. *Hepatology* 24, 568-574.
- Cravchik, A., Reddy, D., and Matus, A. (1994). Identification of a novel microtubule-binding domain in microtubule-associated protein 1A (MAP1A). *J Cell Sci* 107 (Pt 3), 661-672.
- Cressman, D. E., Greenbaum, L. E., DeAngelis, R. A., Ciliberto, G., Furth, E. E., Poli, V., and Taub, R. (1996). Liver failure and defective hepatocyte regeneration in interleukin-6-deficient mice. *Science* 274, 1379-1383.
- Crocker, B. A., Krebs, D. L., Zhang, J. G., Wormald, S., Willson, T. A., Stanley, E. G., Robb, L., Greenhalgh, C. J., Forster, I., Clausen, B. E., *et al.* (2003). SOCS3 negatively regulates IL-6 signaling in vivo. *Nat Immunol* 4, 540-545.
- Dallol, A., Agathangelou, A., Fenton, S. L., Ahmed-Choudhury, J., Hesson, L., Vos, M. D., Clark, G. J., Downward, J., Maher, E. R., and Latif, F. (2004). RASSF1A interacts with microtubule-associated proteins and modulates microtubule dynamics. *Cancer Res* 64, 4112-4116.
- Dallol, A., Agathangelou, A., Tommasi, S., Pfeifer, G. P., Maher, E. R., and Latif, F. (2005). Involvement of the RASSF1A tumor suppressor gene in controlling cell migration. *Cancer Res* 65, 7653-7659.
- Dallol, A., Cooper, W. N., Al-Mulla, F., Agathangelou, A., Maher, E. R., and Latif, F. (2007). Depletion of the Ras association domain family 1, isoform A-associated novel microtubule-associated protein, C19ORF5/MAP1S, causes mitotic abnormalities. *Cancer Res* 67, 492-500.
- Dammann, R., Schagdarsurengin, U., Strunnikova, M., Rastetter, M., Seidel, C., Liu, L., Tommasi, S., and Pfeifer, G. P. (2003). Epigenetic inactivation of the Ras-association domain family 1 (RASSF1A) gene and its function in human carcinogenesis. *Histol Histopathol* 18, 665-677.

de Anda, F. C., Pollarolo, G., Da Silva, J. S., Camoletto, P. G., Feiguin, F., and Dotti, C. G. (2005). Centrosome localization determines neuronal polarity. *Nature* 436, 704-708.

Dehmelt, L., and Halpain, S. (2004). Actin and microtubules in neurite initiation: Are MAPs the missing link? *J Neurobiol* 58, 18-33.

Dehmelt, L., and Halpain, S. (2005). The MAP2/Tau family of microtubule-associated proteins. *Genome Biol* 6, 204.

Del Rio, J. A., Gonzalez-Billault, C., Urena, J. M., Jimenez, E. M., Barallobre, M. J., Pascual, M., Pujadas, L., Simo, S., La Torre, A., Wandosell, F., *et al.* (2004). MAP1B is required for Netrin 1 signaling in neuronal migration and axonal guidance. *Curr Biol* 14, 840-850.

Diaz-Nido, J., Serrano, L., Mendez, E., and Avila, J. (1988). A casein kinase II-related activity is involved in phosphorylation of microtubule-associated protein MAP-1B during neuroblastoma cell differentiation. *J Cell Biol* 106, 2057-2065.

Ding, J., Allen, E., Wang, W., Valle, A., Wu, C., Nardine, T., Cui, B., Yi, J., Taylor, A., Jeon, N. L., *et al.* (2006a). Gene targeting of GAN in mouse causes a toxic accumulation of microtubule-associated protein 8 and impaired retrograde axonal transport. *Hum Mol Genet* 15, 1451-1463.

Ding, J., Liu, J. J., Kowal, A. S., Nardine, T., Bhattacharya, P., Lee, A., and Yang, Y. (2002). Microtubule-associated protein 1B: a neuronal binding partner for gigaxonin. *J Cell Biol* 158, 427-433.

Ding, J., Valle, A., Allen, E., Wang, W., Nardine, T., Zhang, Y., Peng, L., and Yang, Y. (2006b). Microtubule-associated protein 8 contains two microtubule binding sites. *Biochem Biophys Res Commun* 339, 172-179.

Doxsey, S., Zimmerman, W., and Mikule, K. (2005). Centrosome control of the cell cycle. *Trends Cell Biol* 15, 303-311.

Drewes, G., Ebner, A., and Mandelkow, E.-M. (1998). MAPs, MARKs and microtubule dynamics. *Trends Biochem Sci* 23, 307-311.

Dymecki, S. M. (1996). Flp recombinase promotes site-specific DNA recombination in embryonic stem cells and transgenic mice. *Proc Natl Acad Sci U S A* 93, 6191-6196.

Eckes, B., Dogic, D., Colucci-Guyon, E., Wang, N., Maniotis, A., Ingber, D., Merckling, A., Langa, F., Aumailley, M., Delouee, A., *et al.* (1998). Impaired mechanical stability, migration and contractile capacity in vimentin-deficient fibroblasts. *J Cell Sci* 111 (Pt 13), 1897-1907.

Edelmann, W., Zervas, M., Costello, P., Roback, L., Fischer, I., Hammarback, J. A., Cowan, N., Davies, P., Wainer, B., and Kucherlapati, R. (1996). Neuronal abnormalities in microtubule-associated protein 1B mutant mice. *Proc Natl Acad Sci U S A* 93, 1270-1275.



- Eriksson, M., Samuelsson, H., Samuelsson, E. B., Liu, L., McKeehan, W. L., Benedikz, E., and Sundstrom, E. (2007). The NMDAR subunit NR3A interacts with microtubule-associated protein 1S in the brain. *Biochem Biophys Res Commun* 361, 127-132.
- Fifre, A., Spohne, I., Koziel, V., Kriem, B., Yen Potin, F. T., Bihain, B. E., Olivier, J. L., Oster, T., and Pillot, T. (2006). Microtubule-associated protein MAP1A, MAP1B, and MAP2 proteolysis during soluble amyloid beta-peptide-induced neuronal apoptosis. Synergistic involvement of calpain and caspase-3. *J Biol Chem* 281, 229-240.
- Franzen, R., Tanner, S. L., Dashiell, S. M., Rottkamp, C. A., Hammer, J. A., and Quarles, R. H. (2001). Microtubule-associated protein 1B: a neuronal binding partner for myelin-associated glycoprotein. *J Cell Biol* 155, 893-898.
- Garner, C. C., Garner, A., Huber, G., Kozak, C., and Matus, A. (1990). Molecular cloning of microtubule-associated protein 1 (MAP1A) and microtubule-associated protein 5 (MAP1B): identification of distinct genes and their differential expression in developing brain. *J Neurochem* 55, 146-154.
- Gevorkian, G., Gonzalez-Noriega, A., Acero, G., Ordonez, J., Michalak, C., Munguia, M. E., Govezensky, T., Cribbs, D. H., and Manoutcharian, K. (2008). Amyloid-beta peptide binds to microtubule-associated protein 1B (MAP1B). *Neurochem Int* 52, 1030-1036.
- Glozak, M. A., Sengupta, N., Zhang, X., and Seto, E. (2005). Acetylation and deacetylation of non-histone proteins. *Gene* 363, 15-23.
- Gogel, S., Wakefield, S., Tear, G., Klambt, C., and Gordon-Weeks, P. R. (2006). The *Drosophila* microtubule associated protein Futsch is phosphorylated by Shaggy/Zeste-white 3 at an homologous GSK3beta phosphorylation site in MAP1B. *Mol Cell Neurosci* 33, 188-199.
- Gonzalez-Billault, C., Demandt, E., Wandosell, F., Torres, M., Bonaldo, P., Stoykova, A., Chowdhury, K., Gruss, P., Avila, J., and Sanchez, M. P. (2000). Perinatal lethality of microtubule-associated protein 1B-deficient mice expressing alternative isoforms of the protein at low levels. *Mol Cell Neurosci* 16, 408-421.
- González-Billault, C., Demandt, E., Wandosell, F., Torres, M., Bonaldo, P., Stoykova, A., Chowdhury, K., Gruss, P., Avila, J., and Sánchez, M. P. (2000). Perinatal lethality of microtubule-associated protein 1B-deficient mice expressing alternative isoforms of the protein at low levels. *Mol Cell Neurosci* 16, 408-421.
- Gonzalez-Billault, C., Engelke, M., Jimenez-Mateos, E. M., Wandosell, F., Caceres, A., and Avila, J. (2002). Participation of structural microtubule-associated proteins (MAPs) in the development of neuronal polarity. *J Neurosci Res* 67, 713-719.
- Gonzalez-Billault, C., Jimenez-Mateos, E. M., Caceres, A., Diaz-Nido, J., Wandosell, F., and Avila, J. (2004). Microtubule-associated protein 1B function

during normal development, regeneration, and pathological conditions in the nervous system. *J Neurobiol* 58, 48-59.

Goold, R. G., and Gordon-Weeks, P. R. (2003). NGF activates the phosphorylation of MAP1B by GSK3beta through the TrkA receptor and not the p75(NTR) receptor. *J Neurochem* 87, 935-946.

Goold, R. G., and Gordon-Weeks, P. R. (2005). The MAP kinase pathway is upstream of the activation of GSK3beta that enables it to phosphorylate MAP1B and contributes to the stimulation of axon growth. *Mol Cell Neurosci* 28, 524-534.

Goold, R. G., Owen, R., and Gordon-Weeks, P. R. (1999). Glycogen synthase kinase 3beta phosphorylation of microtubule-associated protein 1B regulates the stability of microtubules in growth cones. *J Cell Sci* 112 (Pt 19), 3373-3384.

Gotlieb, A. I., May, L. M., Subrahmanyam, L., and Kalnins, V. I. (1981). Distribution of microtubule organizing centers in migrating sheets of endothelial cells. *J Cell Biol* 91, 589-594.

Gundersen, G. G., and Bulinski, J. C. (1988). Selective stabilization of microtubules oriented toward the direction of cell migration. *Proc Natl Acad Sci U S A* 85, 5946-5950.

Halpain, S., and Dehmelt, L. (2006). The MAP1 family of microtubule-associated proteins. *Genome Biol* 7, 224.

Harada, A., Oguchi, K., Okabe, S., Kuno, J., Terada, S., Ohshima, T., Sato-Yoshitake, R., Takei, Y., Noda, T., and Hirokawa, N. (1994). Altered microtubule organization in small-calibre axons of mice lacking tau protein. *Nature* 369, 488-491.

He, H., Dang, Y., Dai, F., Guo, Z., Wu, J., She, X., Pei, Y., Chen, Y., Ling, W., Wu, C., *et al.* (2003). Post-translational modifications of three members of the human MAP1LC3 family and detection of a novel type of modification for MAP1LC3B. *J Biol Chem* 278, 29278-29287.

Hogan, B., Costanini, F., and Lacy, E. (1986). *Manipulating the Mouse Embryo - A Laboratory Manual*: Cold Spring Harbor Laboratory).

Huttenlocher, A., Sandborg, R. R., and Horwitz, A. F. (1995). Adhesion in cell migration. *Curr Opin Cell Biol* 7, 697-706.

Ivanov, I., Lo, K. C., Hawthorn, L., Cowell, J. K., and Ionov, Y. (2007). Identifying candidate colon cancer tumor suppressor genes using inhibition of nonsense-mediated mRNA decay in colon cancer cells. *Oncogene* 26, 2873-2884.

Iwabata, H., Yoshida, M., and Komatsu, Y. (2005). Proteomic analysis of organ-specific post-translational lysine-acetylation and -methylation in mice by use of anti-acetyllysine and -methyllysine mouse monoclonal antibodies. *Proteomics* 5, 4653-4664.

- Jaffrey, S. R., and Snyder, S. H. (2001). The biotin switch method for the detection of S-nitrosylated proteins. *Sci STKE* 2001, PL1.
- Jensen, P. H., Islam, K., Kenney, J., Nielsen, M. S., Power, J., and Gai, W. P. (2000). Microtubule-associated protein 1B is a component of cortical Lewy bodies and binds alpha-synuclein filaments. *J Biol Chem* 275, 21500-21507.
- Jimenez-Mateos, E. M., Gonzalez-Billault, C., Dawson, H. N., Vitek, M. P., and Avila, J. (2006). Role of MAP1B in axonal retrograde transport of mitochondria. *Biochem J* 397, 53-59.
- Johnstone, M., Goold, R. G., Bei, D., Fischer, I., and Gordon-Weeks, P. R. (1997). Localisation of microtubule-associated protein 1B phosphorylation sites recognised by monoclonal antibody SMI-31. *J Neurochem* 69, 1417-1424.
- Kabeya, Y., Mizushima, N., Ueno, T., Yamamoto, A., Kirisako, T., Noda, T., Kominami, E., Ohsumi, Y., and Yoshimori, T. (2000). LC3, a mammalian homologue of yeast Apg8p, is localized in autophagosome membranes after processing. *Embo J* 19, 5720-5728.
- Kaverina, I., Krylyshkina, O., Gimona, M., Beningo, K., Wang, Y. L., and Small, J. V. (2000). Enforced polarisation and locomotion of fibroblasts lacking microtubules. *Curr Biol* 10, 739-742.
- Kaverina, I., Krylyshkina, O., and Small, J. V. (1999). Microtubule targeting of substrate contacts promotes their relaxation and dissociation. *J Cell Biol* 146, 1033-1044.
- Kaverina, I., Rottner, K., and Small, J. V. (1998). Targeting, capture, and stabilization of microtubules at early focal adhesions. *J Cell Biol* 142, 181-190.
- Knoblich, J. A. (2005). Neurobiology: getting axons going. *Nature* 436, 632-633.
- Krylyshkina, O., Anderson, K. I., Kaverina, I., Upmann, I., Manstein, D. J., Small, J. V., and Toomre, D. K. (2003). Nanometer targeting of microtubules to focal adhesions. *J Cell Biol* 161, 853-859.
- Kupfer, A., Louvard, D., and Singer, S. J. (1982). Polarization of the Golgi apparatus and the microtubule-organizing center in cultured fibroblasts at the edge of an experimental wound. *Proc Natl Acad Sci U S A* 79, 2603-2607.
- Kutschera, W., Zauner, W., Wiche, G., and Propst, F. (1998). The mouse and rat MAP1B genes: genomic organization and alternative transcription. *Genomics* 49, 430-436.
- Kuznetsov, S. A., Rodionov, V. I., Nadezhdina, E. S., Murphy, D. B., and Gelfand, V. I. (1986). Identification of a 34-kD polypeptide as a light chain of microtubule-associated protein-1 (MAP-1) and its association with a MAP-1 peptide that binds to microtubules. *J Cell Biol* 102, 1060-1066.

- Langkopf, A., Hammarback, J. A., Muller, R., Vallee, R. B., and Garner, C. C. (1992). Microtubule-associated proteins 1A and LC2. Two proteins encoded in one messenger RNA. *J Biol Chem* 267, 16561-16566.
- Lemaigre, F. P. (2003). Development of the biliary tract. *Mech Dev* 120, 81-87.
- Lewandoski, M. (2001). Conditional control of gene expression in the mouse. *Nat Rev Genet* 2, 743-755.
- Lien, L. L., Feener, C. A., Fischbach, N., and Kunkel, L. M. (1994). Cloning of human microtubule-associated protein 1B and the identification of a related gene on chromosome 15. *Genomics* 22, 273-280.
- Liu, L., Amy, V., Liu, G., and McKeegan, W. L. (2002). Novel complex integrating mitochondria and the microtubular cytoskeleton with chromosome remodeling and tumor suppressor RASSF1 deduced by in silico homology analysis, interaction cloning in yeast, and colocalization in cultured cells. *In Vitro Cell Dev Biol Anim* 38, 582-594.
- Liu, L., and McKeegan, W. L. (2002). Sequence analysis of LRPPRC and its SEC1 domain interaction partners suggests roles in cytoskeletal organization, vesicular trafficking, nucleocytoplasmic shuttling, and chromosome activity. *Genomics* 79, 124-136.
- Liu, L., Tommasi, S., Lee, D. H., Dammann, R., and Pfeifer, G. P. (2003). Control of microtubule stability by the RASSF1A tumor suppressor. *Oncogene* 22, 8125-8136.
- Liu, L., Vo, A., Liu, G., and McKeegan, W. L. (2005a). Distinct structural domains within C19ORF5 support association with stabilized microtubules and mitochondrial aggregation and genome destruction. *Cancer Res* 65, 4191-4201.
- Liu, L., Vo, A., Liu, G., and McKeegan, W. L. (2005b). Putative tumor suppressor RASSF1 interactive protein and cell death inducer C19ORF5 is a DNA binding protein. *Biochem Biophys Res Commun* 332, 670-676.
- Lu, R., Wang, H., Liang, Z., Ku, L., O'Donnell W, T., Li, W., Warren, S. T., and Feng, Y. (2004). The fragile X protein controls microtubule-associated protein 1B translation and microtubule stability in brain neuron development. *Proc Natl Acad Sci U S A* 101, 15201-15206.
- Ma, D., Chow, S., Obrocka, M., Connors, T., and Fischer, I. (1999). Induction of microtubule-associated protein 1B expression in Schwann cells during nerve regeneration. *Brain Res* 823, 141-153.
- Ma, D., Himes, B. T., Shea, T. B., and Fischer, I. (2000). Axonal transport of microtubule-associated protein 1B (MAP1B) in the sciatic nerve of adult rat: distinct transport rates of different isoforms. *J Neurosci* 20, 2112-2120.
- Mandelkow, E., and Mandelkow, E. M. (1995). Microtubules and microtubule-associated proteins. *Curr Opin Cell Biol* 7, 72-81.

Mann, S. S., and Hammarback, J. A. (1994). Molecular characterization of light chain 3. A microtubule binding subunit of MAP1A and MAP1B. *J Biol Chem* 269, 11492-11497.

Martinez-Ruiz, A., and Lamas, S. (2004). S-nitrosylation: a potential new paradigm in signal transduction. *Cardiovasc Res* 62, 43-52.

Matsumoto, K., Fujii, H., Michalopoulos, G., Fung, J. J., and Demetris, A. J. (1994). Human biliary epithelial cells secrete and respond to cytokines and hepatocyte growth factors in vitro: interleukin-6, hepatocyte growth factor and epidermal growth factor promote DNA synthesis in vitro. *Hepatology* 20, 376-382.

Matus, A. (1988). Microtubule-associated proteins: their potential role in determining neuronal morphology. *Annu Rev Neurosci* 11, 29-44.

Mei, X., Sweatt, A. J., and Hammarback, J. A. (2000). Microtubule-associated protein 1 subunit expression in primary cultures of rat brain. *Brain Res Bull* 53, 801-806.

Meixner, A., Haverkamp, S., Wassle, H., Fuhrer, S., Thalhammer, J., Kropf, N., Bittner, R. E., Lassmann, H., Wiche, G., and Propst, F. (2000). MAP1B is required for axon guidance and is involved in the development of the central and peripheral nervous system. *J Cell Biol* 151, 1169-1178.

Mili, S., and Pinol-Roma, S. (2003). LRP130, a pentatricopeptide motif protein with a noncanonical RNA-binding domain, is bound in vivo to mitochondrial and nuclear RNAs. *Mol Cell Biol* 23, 4972-4982.

Mootha, V. K., Lepage, P., Miller, K., Bunkenborg, J., Reich, M., Hjerrild, M., Delmonte, T., Villeneuve, A., Sladek, R., Xu, F., *et al.* (2003). Identification of a gene causing human cytochrome c oxidase deficiency by integrative genomics. *Proc Natl Acad Sci U S A* 100, 605-610.

Moshnikova, A., Frye, J., Shay, J. W., Minna, J. D., and Khokhlatchev, A. V. (2006). The growth and tumor suppressor NORE1A is a cytoskeletal protein that suppresses growth by inhibition of the ERK pathway. *J Biol Chem* 281, 8143-8152.

Moshnikova, A., Kuznetsov, S., and Khokhlatchev, A. V. (2008). Interaction of the growth and tumour suppressor NORE1A with microtubules is not required for its growth-suppressive function. *BMC Res Notes* 1, 13.

Muller, U. (1999). Ten years of gene targeting: targeted mouse mutants, from vector design to phenotype analysis. *Mech Dev* 82, 3-21.

Noble, M., Lewis, S. A., and Cowan, N. J. (1989). The microtubule binding domain of microtubule-associated protein MAP1B contains a repeated sequence motif unrelated to that of MAP2 and tau. *J Cell Biol* 109, 3367-3376.

Noiges, R., Eichinger, R., Kutschera, W., Fischer, I., Nemeth, Z., Wiche, G., and Propst, F. (2002). Microtubule-associated protein 1A (MAP1A) and MAP1B: light chains determine distinct functional properties. *J Neurosci* 22, 2106-2114.

Noiges, R., Stroissnigg, H., Trancikova, A., Kalny, I., Eichinger, R., and Propst, F. (2006). Heterotypic complex formation between subunits of microtubule-associated proteins 1A and 1B is due to interaction of conserved domains. *Biochim Biophys Acta* 1763, 1011-1016.

Okabe, S., Shiomura, Y., and Hirokawa, N. (1989). Immunocytochemical localization of microtubule-associated proteins 1A and 2 in the rat retina. *Brain Res* 483, 335-346.

Opal, P., Garcia, J. J., Propst, F., Matilla, A., Orr, H. T., and Zoghbi, H. Y. (2003). Mapmodulin/leucine-rich acidic nuclear protein binds the light chain of microtubule-associated protein 1B and modulates neuritogenesis. *J Biol Chem* 278, 34691-34699.

Orban-Nemeth, Z., Simader, H., Badurek, S., Trancikova, A., and Propst, F. (2005). Microtubule-associated protein 1S, a short and ubiquitously expressed member of the microtubule-associated protein 1 family. *J Biol Chem* 280, 2257-2265.

Palazzo, A. F., Joseph, H. L., Chen, Y. J., Dujardin, D. L., Alberts, A. S., Pfister, K. K., Vallee, R. B., and Gundersen, G. G. (2001). Cdc42, dynein, and dynactin regulate MTOC reorientation independent of Rho-regulated microtubule stabilization. *Curr Biol* 11, 1536-1541.

Pangratz-Fuehrer, S., Bubna-Littitz, H., Propst, F., and Reitsamer, H. (2005). Mice deficient in microtubule-associated protein MAP1B show a distinct behavioral phenotype and altered retina function. *Behav Brain Res* 164, 188-196.

Paoletti, P., and Neyton, J. (2007). NMDA receptor subunits: function and pharmacology. *Curr Opin Pharmacol* 7, 39-47.

Park, J., Gores, G. J., and Patel, T. (1999). Lipopolysaccharide induces cholangiocyte proliferation via an interleukin-6-mediated activation of p44/p42 mitogen-activated protein kinase. *Hepatology* 29, 1037-1043.

Riederer, B. M. (2007). Microtubule-associated protein 1B, a growth-associated and phosphorylated scaffold protein. *Brain Res Bull* 71, 541-558.

Rodriguez, O. C., Schaefer, A. W., Mandato, C. A., Forscher, P., Bement, W. M., and Waterman-Storer, C. M. (2003). Conserved microtubule-actin interactions in cell movement and morphogenesis. *Nat Cell Biol* 5, 599-609.

Romijn, H. J., Habets, A. M., Mud, M. T., and Wolters, P. S. (1981). Nerve outgrowth, synaptogenesis and bioelectric activity in fetal rat cerebral cortex tissue cultured in serum-free, chemically defined medium. *Brain Res* 254, 583-589.

- Rong, R., Jin, W., Zhang, J., Sheikh, M. S., and Huang, Y. (2004). Tumor suppressor RASSF1A is a microtubule-binding protein that stabilizes microtubules and induces G2/M arrest. *Oncogene* 23, 8216-8230.
- Roskams, T. A., Theise, N. D., Balabaud, C., Bhagat, G., Bhathal, P. S., Bioulac-Sage, P., Brunt, E. M., Crawford, J. M., Crosby, H. A., Desmet, V., *et al.* (2004). Nomenclature of the finer branches of the biliary tree: canals, ductules, and ductular reactions in human livers. *Hepatology* 39, 1739-1745.
- Salmon, A. B., Murakami, S., Bartke, A., Kopchick, J., Yasumura, K., and Miller, R. A. (2005). Fibroblast cell lines from young adult mice of long-lived mutant strains are resistant to multiple forms of stress. *Am J Physiol Endocrinol Metab* 289, E23-29.
- Sambrook, J., MacCallum, P., and Russell, D. (2001). *Molecular Cloning: A Laboratory Manual*, Third Edition edn: Cold Spring Harbor Laboratory Press).
- Sauer, B. (1998). Inducible gene targeting in mice using the Cre/lox system. *Methods* 14, 381-392.
- Schoenfeld, T. A., McKerracher, L., Obar, R., and Vallee, R. B. (1989). MAP 1A and MAP 1B are structurally related microtubule associated proteins with distinct developmental patterns in the CNS. *J Neurosci* 9, 1712-1730.
- Schoenfeld, T. A., and Obar, R. A. (1994). Diverse distribution and function of fibrous microtubule-associated proteins in the nervous system. *Int Rev Cytol* 151, 67-137.
- Shivakumar, L., Minna, J., Sakamaki, T., Pestell, R., and White, M. A. (2002). The RASSF1A tumor suppressor blocks cell cycle progression and inhibits cyclin D1 accumulation. *Mol Cell Biol* 22, 4309-4318.
- Small, J. V., Anderson, K., and Rottner, K. (1996). Actin and the coordination of protrusion, attachment and retraction in cell crawling. *Biosci Rep* 16, 351-368.
- Small, J. V., Geiger, B., Kaverina, I., and Bershadsky, A. (2002). How do microtubules guide migrating cells? *Nat Rev Mol Cell Biol* 3, 957-964.
- Small, J. V., and Kaverina, I. (2003). Microtubules meet substrate adhesions to arrange cell polarity. *Curr Opin Cell Biol* 15, 40-47.
- Small, J. V., Rottner, K., Kaverina, I., and Anderson, K. I. (1998). Assembling an actin cytoskeleton for cell attachment and movement. *Biochim Biophys Acta* 1404, 271-281.
- Song, M. S., Chang, J. S., Song, S. J., Yang, T. H., Lee, H., and Lim, D. S. (2005). The centrosomal protein RAS association domain family protein 1A (RASSF1A)-binding protein 1 regulates mitotic progression by recruiting RASSF1A to spindle poles. *J Biol Chem* 280, 3920-3927.
- Song, M. S., and Lim, D. S. (2004). Control of APC-Cdc20 by the tumor suppressor RASSF1A. *Cell Cycle* 3, 574-576.

Song, M. S., Song, S. J., Ayad, N. G., Chang, J. S., Lee, J. H., Hong, H. K., Lee, H., Choi, N., Kim, J., Kim, H., *et al.* (2004). The tumour suppressor RASSF1A regulates mitosis by inhibiting the APC-Cdc20 complex. *Nat Cell Biol* 6, 129-137.

Stamler, J. S., Toone, E. J., Lipton, S. A., and Sucher, N. J. (1997). (S)NO signals: translocation, regulation, and a consensus motif. *Neuron* 18, 691-696.

Stroissnigg, H. (PhD thesis 2005). The Role of Microtubule Associated Protein 1B (MAP1B) in Axon Guidance and Myelination. Vienna University.

Stroissnigg, H., Trancikova, A., Descovich, L., Fuhrmann, J., Kutschera, W., Kostan, J., Meixner, A., Nothias, F., and Propst, F. (2007). S-Nitrosylation of microtubule-associated protein 1B mediates nitric-oxide-induced axon retraction. *Nat Cell Biol* 9, 1035-1045.

Takei, Y., Kondo, S., Harada, A., Inomata, S., Noda, T., and Hirokawa, N. (1997). Delayed development of nervous system in mice homozygous for disrupted microtubule-associated protein 1B (MAP1B) gene. *J Cell Biol* 137, 1615-1626.

Takei, Y., Teng, J., Harada, A., and Hirokawa, N. (2000). Defects in axonal elongation and neuronal migration in mice with disrupted tau and map1b genes. *J Cell Biol* 150, 989-1000.

Takemura, R., Okabe, S., Umeyama, T., Kanai, Y., Cowan, N. J., and Hirokawa, N. (1992). Increased microtubule stability and alpha tubulin acetylation in cells transfected with microtubule-associated proteins MAP1B, MAP2 or tau. *J Cell Sci* 103 (Pt 4), 953-964.

Teng, J., Takei, Y., Harada, A., Nakata, T., Chen, J., and Hirokawa, N. (2001). Synergistic effects of MAP2 and MAP1B knockout in neuronal migration, dendritic outgrowth, and microtubule organization. *J Cell Biol* 155, 65-76.

Tögel, M., Eichinger, R., Wiche, G., and Propst, F. (1999). A 45 amino acid residue domain necessary and sufficient for proteolytic cleavage of the MAP1B polyprotein precursor. *FEBS Lett* 451, 15-18.

Tögel, M., Wiche, G., and Propst, F. (1998). Novel features of the light chain of microtubule-associated protein MAP1B: microtubule stabilization, self interaction, actin filament binding, and regulation by the heavy chain. *J Cell Biol* 143, 695-707.

Tommasi, S., Dammann, R., Zhang, Z., Wang, Y., Liu, L., Tsark, W. M., Wilczynski, S. P., Li, J., You, M., and Pfeifer, G. P. (2005). Tumor susceptibility of Rassf1a knockout mice. *Cancer Res* 65, 92-98.

Tonge, D. A., Golding, J. P., Edbladh, M., Kroon, M., Ekstrom, P. E., and Edstrom, A. (1997). Effects of extracellular matrix components on axonal outgrowth from peripheral nerves of adult animals in vitro. *Exp Neurol* 146, 81-90.



- Trančíková, A. (2007). Regulation of MAP1B microtubule binding. Vienna University.
- Trančíková, A. (PhD thesis 2007). Regulation of MAP1B microtubule binding. Vienna University.
- Trivedi, N., Marsh, P., Goold, R. G., Wood-Kaczmar, A., and Gordon-Weeks, P. R. (2005). Glycogen synthase kinase-3 $\beta$  phosphorylation of MAP1B at Ser1260 and Thr1265 is spatially restricted to growing axons. *J Cell Sci* 118, 993-1005.
- Tse, J. Y., Wong, E. Y., Cheung, A. N., O, W. S., Tam, P. C., and Yeung, W. S. (2003). Specific expression of VCY2 in human male germ cells and its involvement in the pathogenesis of male infertility. *Biol Reprod* 69, 746-751.
- Tucker, R. P., and Matus, A. I. (1988). Microtubule-associated proteins characteristic of embryonic brain are found in the adult mammalian retina. *Dev Biol* 130, 423-434.
- Uchida, Y. (2003). Overexpression of full-length but not N-terminal truncated isoform of microtubule-associated protein (MAP) 1B accelerates apoptosis of cultured cortical neurons. *J Biol Chem* 278, 366-371.
- Ulloa, L., Avila, J., and Diaz-Nido, J. (1993). Heterogeneity in the phosphorylation of microtubule-associated protein MAP1B during rat brain development. *J Neurochem* 61, 961-972.
- Vaillant, A. R., Muller, R., Langkopf, A., and Brown, D. L. (1998). Characterization of the microtubule-binding domain of microtubule-associated protein 1A and its effects on microtubule dynamics. *J Biol Chem* 273, 13973-13981.
- van der Weyden, L., and Adams, D. J. (2007). The Ras-association domain family (RASSF) members and their role in human tumorigenesis. *Biochim Biophys Acta* 1776, 58-85.
- Van Snick, J. (1990). Interleukin-6: an overview. *Annu Rev Immunol* 8, 253-278.
- Vos, M. D., Martinez, A., Elam, C., Dallol, A., Taylor, B. J., Latif, F., and Clark, G. J. (2004). A role for the RASSF1A tumor suppressor in the regulation of tubulin polymerization and genomic stability. *Cancer Res* 64, 4244-4250.
- Wahlsten, D. (1982). Deficiency of corpus callosum varies with strain and supplier of the mice. *Brain Res* 239, 329-347.
- Waterman-Storer, C. M., and Salmon, E. (1999). Positive feedback interactions between microtubule and actin dynamics during cell motility. *Curr Opin Cell Biol* 11, 61-67.
- Wiche, G., Oberkanins, C., and Himmler, A. (1991). Molecular structure and function of microtubule-associated proteins. *Int Rev Cytol* 124, 217-273.

- Wolff, S., Xiao, Z., Wittau, M., Sussner, N., Stoter, M., and Knippschild, U. (2005). Interaction of casein kinase 1 delta (CK1 delta) with the light chain LC2 of microtubule associated protein 1A (MAP1A). *Biochim Biophys Acta* 1745, 196-206.
- Wong, E. Y., Tse, J. Y., Yao, K. M., Lui, V. C., Tam, P. C., and Yeung, W. S. (2004). Identification and characterization of human VCY2-interacting protein: VCY2IP-1, a microtubule-associated protein-like protein. *Biol Reprod* 70, 775-784.
- Yang, X. J., and Seto, E. (2008). Lysine acetylation: codified crosstalk with other posttranslational modifications. *Mol Cell* 31, 449-461.
- Yokota, T., Mishra, M., Akatsu, H., Tani, Y., Miyauchi, T., Yamamoto, T., Kosaka, K., Nagai, Y., Sawada, T., and Heese, K. (2006). Brain site-specific gene expression analysis in Alzheimer's disease patients. *Eur J Clin Invest* 36, 820-830.
- Zauner, W., Kratz, J., Staunton, J., Feick, P., and Wiche, G. (1992). Identification of two distinct microtubule binding domains on recombinant rat MAP 1B. *Eur J Cell Biol* 57, 66-74.
- Zou, B., Yan, H., Kawasaki, F., and Ordway, R. W. (2008a). MAP1 structural organization in *Drosophila*: in vivo analysis of FUTSCH reveals heavy- and light-chain subunits generated by proteolytic processing at a conserved cleavage site. *Biochem J* 414, 63-71.
- Zou, T., Ouyang, L., Chen, L., Dong, W., Qiao, H., Liu, Y., and Qi, Y. (2008b). The role of microtubule-associated protein 1S in SOCS3 regulation of IL-6 signaling. *FEBS Lett* 582, 4015-4022.

# CURRICULUM VITAE

Mag. Ilse Kalny  
Hetzendorferstraße 93/9/1  
1120 Wien  
Tel. 0699/10250656  
E-mail: [ilse.kalny@gmx.at](mailto:ilse.kalny@gmx.at)



Date and place of birth 21.04.1979, Vienna  
Nationality Austria

## Education

since 01/2005	PhD thesis "In vivo and in vitro characterisation of MAP1S function" under the supervision of Prof. Friedrich Propst at the Department of Molecular Cell Biology
08/2004	Master Degree in Biology, passed with distinction
03/2003 - 08/2004	Diploma thesis "12-S-Lipoxygenase und ihr Hauptprodukt 12-S-HETE in der Kolonkarzinogenese" under the supervision of Prof. Brigitte Marian at the Institute of Cancer Research
10/1997-08/2004	study: biology, branch of study: human biology
06/1997	Matura passed with successfulness
09/1985 - 06/1997	primary and secondary school (with emphasis on the modern languages) at St. Ursula, 1230 Vienna

## Working Experience

01/2005-12/2008	scientific employee at the Department of Molecular Cell Biology, Max F. Perutz Laboratories, University of Vienna, 1030 Vienna
01/2008-08/2008	stipendary "Forschungsstipendium der Universität Wien 2008: First characterisation of the Microtubule Associated 1 S (MAP1S) knockout mouse"
03/2003 - 08/2004	diploma student at the Institute of Cancer Research, Medical University of Vienna, 1090 Vienna

## Teaching Experience

03/2008-06/2008	teaching position at the University of Vienna “Molekulare Biologie UE III (Zellbiologie)”
01/2006-10/2007	supervising undergraduate students in the context of their „Wahlbeispiel Molekulare Zellbiologie: Einzelunterweisung zur Anwendung moderner molekularbiologischer und zellbiologischer Techniken“
03/2005-06/2007	tutor at the University of Vienna for „Biochemisches Praktikum B (Molekularbiologie) + Seminar für Chemiker“ and „Molekulare Biologie UE II, Teil A + Biochemisches Praktikum C (Proteinbiochemie) für Chemiker“

## Additional skills

11-12/2008	Writing Scientific English
05/2008	EBC*L European Business Competence* Licence Stufe A exam passed
12/2007	Projektmanagement – Die Anlage von Forschungsprojekten
12/2007	Research Writing – Vom Schreiben wissenschaftlicher Texte
Language skills	German: mother tongue English: fluent in written and spoken English (C2) French and Spanish: basics (A1)
Computer skills	MS Office, Zeiss Confocal microscopy software LSM510, Zeiss Apotome Microscopy software AxioVision, Adobe Photoshop, Prism, SPSS

## Publications

Noiges, R., Stroissnigg, H., Trancikova, A., Kalny, I., Eichinger, R., Propst, F.;  
Heterotypic complex formation between subunits of microtubule-associated  
proteins 1A and 1B is due to interaction of conserved domains. *Biochim  
Biophys Acta* 1763, 1011-6, 2006

Poster: Kalny I., Orban-Nemeth Z., Noiges R., Stroissnigg H., Eichinger R.,  
Trancikova A., Propst F., 2007 „Microtubule-associated protein MAP1S, a short  
and ubiquitously expressed member of the MAP1 family – Heterotypic complex  
formations between MAP1A, MAP1B, MAP1S“, ELSO 2007. Dresden Germany  
01/09/2007-04/09/2007